Research Paper

GEOSPHERE

GEOSPHERE, v. 17, no. 6

https://doi.org/10.1130/GES02307.1

18 figures; 1 plate; 3 tables; 1 set of supplemental files

CORRESPONDENCE: azuza@unr.edu; avz5818@gmail.com

CITATION: Zuza, A.V., Henry, C.D., Dee, S., Thorman, C.H., and Heizler, M.T., 2021, Jurassic–Cenozoic tectonics of the Pequop Mountains, NE Nevada, in the North American Cordillera hinterland: Geosphere, v. 17, no. 6, p. 2078–2122, https://doi.org/10.1130/GES02307.1.

Science Editor: Andrea Hampel
Associate Editor: Francesco Mazzarini

Received 24 June 2020
Revision received 12 January 2021
Accepted 13 April 2021

Published online 27 October 2021

Jurassic–Cenozoic tectonics of the Pequop Mountains, NE Nevada, in the North American Cordillera hinterland

Andrew V. Zuza[1], Christopher D. Henry[1], Seth Dee[1], Charles H. Thorman[2], and Matthew T. Heizler[3]

[1]Nevada Bureau of Mines and Geology, University of Nevada, Reno, Nevada 89557, USA
[2]Scientist Emeritus, U.S. Geological Survey, Denver, Colorado 80215, USA
[3]New Mexico Bureau of Geology and Mineral Resources, New Mexico Tech, 801 Leroy Place, Socorro, New Mexico 87801, USA

ABSTRACT

The Ruby Mountains–East Humboldt Range–Wood Hills–Pequop Mountains (REWP) metamorphic core complex, northeast Nevada, exposes a record of Mesozoic contraction and Cenozoic extension in the hinterland of the North American Cordillera. The timing, magnitude, and style of crustal thickening and succeeding crustal thinning have long been debated. The Pequop Mountains, comprising Neoproterozoic through Triassic strata, are the least deformed part of this composite metamorphic core complex, compared to the migmatitic and mylonitized ranges to the west, and provide the clearest field relationships for the Mesozoic–Cenozoic tectonic evolution. New field, structural, geochronologic, and thermochronological observations based on 1:24,000-scale geologic mapping of the northern Pequop Mountains provide insights into the multi-stage tectonic history of the REWP. Polyphase cooling and reheating of the middle-upper crust was tracked over the range of <100 °C to 450 °C via novel $^{40}Ar/^{39}Ar$ multi-diffusion domain modeling of muscovite and K-feldspar and apatite fission-track dating. Important new observations and interpretations include: (1) crosscutting field relationships show that most of the contractional deformation in this region occurred just prior to, or during, the Middle-Late Jurassic Elko orogeny (ca. 170–157 Ma), with negligible Cretaceous shortening; (2) temperature-depth data rule out deep burial of Paleozoic stratigraphy, thus refuting models that incorporate large cryptic overthrust sheets; (3) Jurassic, Cretaceous, and Eocene intrusions and associated thermal pulses metamorphosed the lower Paleozoic–Proterozoic rocks, and various thermochronometers record conductive cooling near original stratigraphic depths; (4) east-draining paleovalleys with ~1–1.5 km relief incised the region before ca. 41 Ma and were filled by 41–39.5 Ma volcanic rocks; and (5) low-angle normal faulting initiated after the Eocene, possibly as early as the late Oligocene, although basin-generating extension from high-angle normal faulting began in the middle Miocene. Observed Jurassic shortening is coeval with structures in the Luning-Fencemaker thrust belt to the west, and other strain documented across central-east Nevada and Utah, suggesting ~100 km Middle-Late Jurassic shortening across the Sierra Nevada retroarc. This phase of deformation correlates with terrane accretion in the Sierran forearc, increased North American–Farallon convergence rates, and enhanced Jurassic Sierran arc magmatism. Although spatially variable, the Cordilleran hinterland and the high plateau that developed across it (i.e., the hypothesized Nevadaplano) involved a dynamic pulsed evolution with significant phases of both Middle-Late Jurassic and Late Cretaceous contractional deformation. Collapse long postdated all of this contraction. This complex geologic history set the stage for the Carlin-type gold deposit at Long Canyon, located along the eastern flank of the Pequop Mountains, and may provide important clues for future exploration.

Andrew V. Zuza https://orcid.org/0000-0001-6130-5121
Matthew Heizler https://orcid.org/0000-0002-3911-4932

1. INTRODUCTION

The continental margins that bound the Pacific Ocean have been part of the Circum-Pacific orogenic belt since the Mesozoic, with alternating phases of contraction and distributed extension influenced by subduction and relative plate kinematics (e.g., Atwater, 1970; Burchfiel and Davis, 1975; DeCelles, 2004; Dickinson, 2004; Shu et al., 2009; Li et al., 2014, 2018). Knowledge of the ~100 m.y. evolution of the Mesozoic–Cenozoic North American Cordillera orogenic system, which resulted from east-dipping oceanic subduction beneath the western margin of the North American continent (e.g., Burchfiel and Davis, 1975; Oldow et al., 1989; Allmendinger, 1992; Burchfiel et al., 1992; DeCelles, 2004; Dickinson, 2004), is fundamental to our broader understanding of non-collisional (e.g., "Andean-type") orogens and continental tectonics. For example, study of the Jurassic to Paleogene evolution of the North American Cordillera (e.g., Armstrong, 1968; Royse et al., 1975; Villien and Kligfield, 1986; DeCelles and Coogan, 2006; Kelly et al., 2015) has resulted in new insights, such as the potential coupling between arc magmatism and upper-plate shortening as part of the general "Cordilleran cyclicity" models (e.g., Ducea, 2001; DeCelles et al., 2009; DeCelles and Graham, 2015) and a greatly improved understanding of the western Pacific realm (e.g., Li and Li, 2007; Yin, 2010; Li et al., 2014, 2018).

Numerous studies have focused on understanding the deformational history of the later stages of the North American Cordillera orogen, including thin-skinned Cretaceous–Paleogene Sevier fold-and-thrust belt development and the commonly thick-skinned, basement-uplift–involving

Paleogene Laramide deformation (e.g., Dickinson and Snyder, 1978; Jordan, 1981; Livaccari et al., 1981; Allmendinger et al., 1983, 1987; DeCelles et al., 1995; DeCelles and Coogan, 2006; Greene, 2014; Long et al., 2014, 2015; Long, 2015; Copeland et al., 2017; Axen et al., 2018). This deformation is associated with crustal thickening of the Great Basin region as part of the interpreted Late Cretaceous–early Cenozoic Nevadaplano orogenic plateau (e.g., DeCelles, 2004; Snell et al., 2014; Chapman et al., 2015). Cretaceous–Paleogene deformation was preceded by Jurassic plutonism and deformation, which is observed across Nevada-Utah (Riva, 1970; Allmendinger et al., 1984; Ketner, 1984; Oldow, 1984; Coats, 1987; Thorman et al., 1990, 1992; Miller and Hoisch, 1995; Ketner et al., 1998; Wyld et al., 2003; Thorman, 2011a, 2011b; Rhys et al., 2015). However, little consensus exists on the tectonic setting and evolution of a Jurassic phase of Cordilleran retroarc activity (e.g., Thorman et al., 1991, 1992; Miller and Hoisch, 1995; Anderson, 2020). Distributed arc-backarc magmatism and shortening likely started to thicken the crust in the Jurassic (e.g., Miller and Hoisch, 1995; Haschke and Gunther, 2003; Cao et al., 2016), but this phase of activity is rarely considered in models of the hypothesized Nevadaplano. Reconciling widespread observations of Jurassic structures with an integrated tectonic model is required to better understand the initial conditions for the development and full evolution of the proposed plateau (e.g., DeCelles, 2004; Chapman et al., 2015), subsequent collapse of this thickened crust during Cenozoic extension (e.g., Gans and Miller, 1983; Miller et al., 1983; Snoke et al., 1990; Wright and Snoke, 1993; Gébelin et al., 2015), and significant mineralization across the region (e.g., Howard, 2003; Bedell et al., 2010; Rhys et al., 2015).

A longstanding dilemma in Cordilleran tectonics has revolved around the apparent lack, or relative insignificance, of Cretaceous deformation in the hinterland of the Sevier fold and thrust belt across present-day Nevada, including much of the proposed Nevadaplano (e.g., Long, 2012; Long et al., 2014). This has led to debate regarding the evolution of a Cordilleran orogenic plateau. It also remains unclear how the various Cordilleran domains were kinematically and/or dynamically connected, such as the magmatic arc, retroarc thrust belt, and the thrust belt's hinterland (e.g., Dickinson and Snyder, 1978; Bird, 1998; DeCelles, 2004; DeCelles and Graham, 2015; Anderson, 2020). This apparent lack of Cretaceous hinterland deformation may either result from the concentration of deformation at rarely exposed mid-crustal levels (e.g., Miller and Hoisch, 1995; Camilleri et al., 1997) or overprinting by Cenozoic extension that can be documented through systematic field mapping and structural restorations (e.g., Greene, 2014; Long et al., 2014).

To resolve some of these uncertainties, we provide new interpretations on Mesozoic contractional deformation and Cenozoic extension based on field investigations in the Cordillera hinterland in northeastern Nevada. Here, we present updated observations based on detailed geologic mapping from the Pequop Mountains, which expose strongly deformed rocks west of the Sevier fold-thrust belt (Fig. 1A). The range occupies the northern extent of the Pequop synclinorium (Fig. 1A), which may have passively folded above more strongly deformed rocks as inferred for the Confusion synclinorium in western Utah (Gans and Miller, 1983; Long, 2012, 2015; Greene, 2014). The Pequop Mountains are also the least deformed part of the composite Cenozoic Ruby Mountains–East Humboldt Range–Wood Hills–Pequop Mountains (REWP) metamorphic core complex, which formed due to high-magnitude extension (e.g., Snoke, 1980; Wright and Snoke, 1993; Camilleri and Chamberlain, 1997; Mueller et al., 1999; Satarugsa and Johnson, 2000).

We first review the geology of the Pequop Mountains and the greater REWP. We then provide new thermochronology and geochronology (i.e., $^{40}Ar/^{39}Ar$, fission-track, and U-Pb dating), systematic field relationships, and structural observations from the northern Pequop Mountains alongside new 1:24,000-scale geologic mapping (Figs. 1 and 2; Plate 1) (Henry and Thorman, 2015; Zuza et al., 2018, 2019a). This work builds on Zuza et al. (2020a), where we established that a significant phase of contractional deformation occurred in the Middle-Late Jurassic, as constrained by field observations and Late Jurassic $^{40}Ar/^{39}Ar$ ages from crosscutting lamprophyre intrusions emplaced into middle-lower Paleozoic strata. In the present study, we document the evolution of Jurassic contractional deformation and Cenozoic extension, including active normal faulting, and provide a detailed structural reconstruction of this complex overprinting history that supports more regional interpretations. We assert that most of the deformation, including broad shearing, unit attenuation, boudinage development, and brittle thrust faulting occurred in the Late Jurassic (ca. 160–150 Ma). Correlation of this phase of deformation with other Jurassic strain documented across the Cordillera, from the Sierra Nevada across its backarc and retroarc regions, suggests that this deformation contributed significantly to early crustal thickening of the proto-Nevadaplano plateau. Furthermore, nominal evidence for Late Cretaceous shortening and related crustal thickening in the Pequop Mountains impacts broad models for crustal thickening, burial, and more recent exhumation within the greater Ruby–East Humboldt–Wood Hills–Pequop metamorphic core complex. We interpret that post-Eocene, possibly Oligocene–early Miocene(?), low-angle normal faulting in the Pequop Mountains was kinematically linked with the greater REWP metamorphic core complex to the west based on geometric and available timing constraints.

2. REGIONAL GEOLOGY

The Cenozoic Basin and Range extensional province (Hamilton and Myers, 1966; Stewart, 1978, 1980; Allmendinger et al., 1983) consists of north-northeast–trending basins and normal-fault–bounded mountain ranges (Stewart, 1971; Fletcher and Hallet, 1983) (Fig. 1A). Extension was preceded by (1) Neoproterozoic–Paleozoic passive margin sedimentation (Stewart, 1972; Bond et al., 1989; Hadlari et al., 2012), (2) contraction along Laurentia's western margin throughout the Paleozoic (e.g., Antler and Sonoma orogenies) (Roberts et al., 1958; Gehrels et al., 2000; Cashman et al., 2008; Lawton et al., 2017), and (3) development of the Jurassic–Paleogene North American Cordillera (Coney and Harms, 1984; Ketner and Alpha, 1992; DeCelles, 2004; Best et al., 2009; Yonkee and Weil, 2015;

Yonkee et al., 2019). Twelve to 15 km of Neoproterozoic–Paleozoic carbonate and siliciclastic rocks accumulated along the passive margin (Stewart and Poole, 1974). Sedimentation was interrupted by the Mississippian Antler orogeny, which created a north-trending highland in central Nevada and a parallel Mississippian siliciclastic trough to the east (Poole and Sandberg, 1977; Speed and Sleep, 1982; Trexler and Nitchman, 1990; Gehrels et al., 2000; Ketner, 2008; Beranek et al., 2016).

Mesozoic subduction, magmatism, and deformation define the geologic framework in north-central Nevada (latitude of ~41–40°N) (Fig. 1). Triassic subduction initiation along the western margin of North America led to an early pulse of plutonism in the Sierra Nevada arc (e.g., Dickinson, 2004; Schweickert, 2015; Cao and Paterson, 2016; Levy et al., 2021), which was followed by magmatic pulses in the Middle-Late Jurassic and Late Cretaceous (e.g., Paterson and Ducea, 2015; Kirsch et al., 2016). The Triassic magmatic arc was flanked to the east by an extensional backarc basin (Wyld, 2000, 2002) and shallow-marine shelf farther east (e.g., Gehrels and Dickinson, 1995). Major east-vergent crustal shortening (>50% strain) in the Middle Jurassic Luning-Fencemaker thrust belt closed the backarc. This thrust system, well documented across the Blue and Eugene Mountains of west-central Nevada (Fig. 1B) (Wyld, 2000, 2002), propagated in sequence eastward across western Nevada until the Late Jurassic (Wyld, 2002). Jurassic retroarc deformation coincided with the accretion of terranes against the Sierra forearc (e.g., Schweickert et al., 1988; Schweickert, 2015), increased North American–Farallon convergence rates (Yonkee and Weil, 2015), and increased crustal thickness in the Mesozoic Sierran arc (Profeta et al., 2015; Cao et al., 2016).

Luning-Fencemaker activity in west-central Nevada (Oldow, 1984; Wyld et al., 2001, 2003; Wyld, 2002) was approximately coeval with Middle-Late Jurassic deformation in central-eastern Nevada and west-central Utah (Riva, 1970; Allmendinger and Jordan, 1984; Coats, 1987; Hudec, 1992; Miller and Hoisch, 1992, 1995; Thorman and Peterson, 2003; Rhys et al., 2015; Anderson, 2015, 2020) (Fig. 1B). In northeast Nevada and western Utah, the Jurassic deformation is referred to as the Elko orogeny

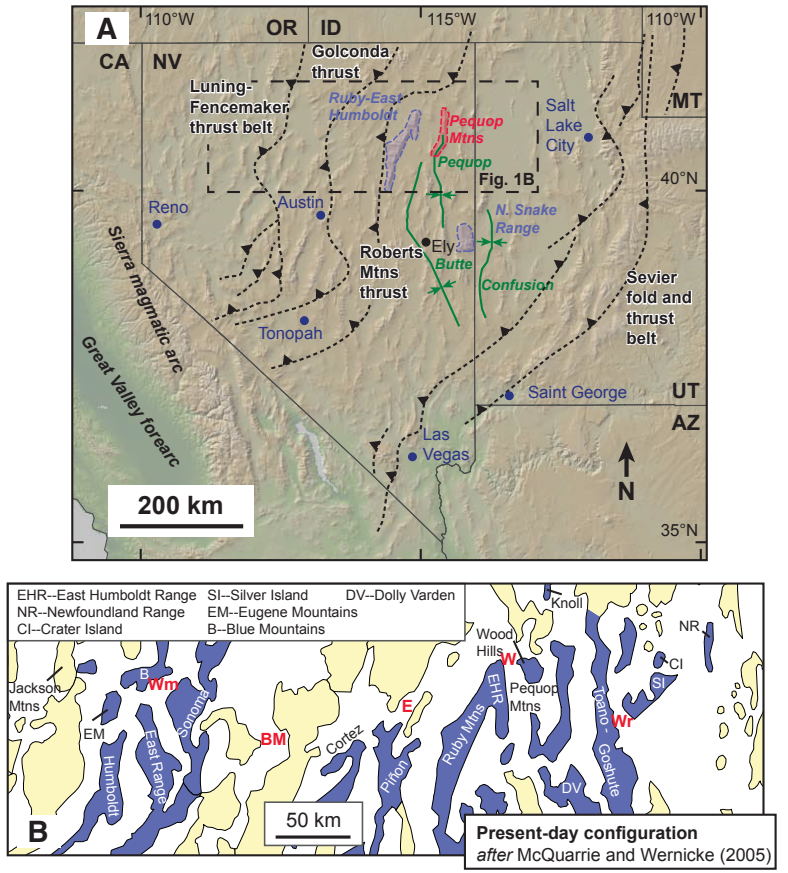

Figure 1. (A) Regional map of the Great Basin schematically showing major Paleozoic–Mesozoic thrust systems (Best et al., 2009; DeCelles, 2004). Also shown are the location of the Butte, Pequop, and Confusion synclinoria in green (Gans and Miller, 1983) and the location of the Pequop Mountains in red. N.—northern. (B) Present-day McQuarrie and Wernicke (2005) base map showing distribution of ranges in northern Nevada. Jurassic deformation has been documented in the blue ranges, although other ranges probably experienced Jurassic deformation that has not yet been confirmed. Middle-Late Jurassic deformation corresponds to Luning-Fencemaker thrusting in the west and Elko orogeny in the east. Cities for spatial reference: BM—Battle Mountain, Nevada; E—Elko, Nevada; W—Wells, Nevada; Wm—Winnemucca, Nevada; Wr—Wendover, Utah.

(Fig. 1B), with a probable foreland basin to the east (Thorman et al., 1990, 1992; the "Utah-Idaho trough" of Bjerrum and Dorsey, 1995). Middle-Late Jurassic deformation is also reported in eastern California (Hoisch et al., 2014), southern Nevada (Giallorenzo et al., 2018), and possibly Utah (Yonkee et al., 2019), generally associated with coeval intrusions (Elison, 1995; Miller and Hoisch, 1995).

Deformation, metamorphism, and magmatism spanned ca. 165–145 Ma in the Toano, Pilot, and Pinon Ranges, and the Ruby, Dolly Varden, Silver Island, Newfoundland, White Horse, Gold Hill, and

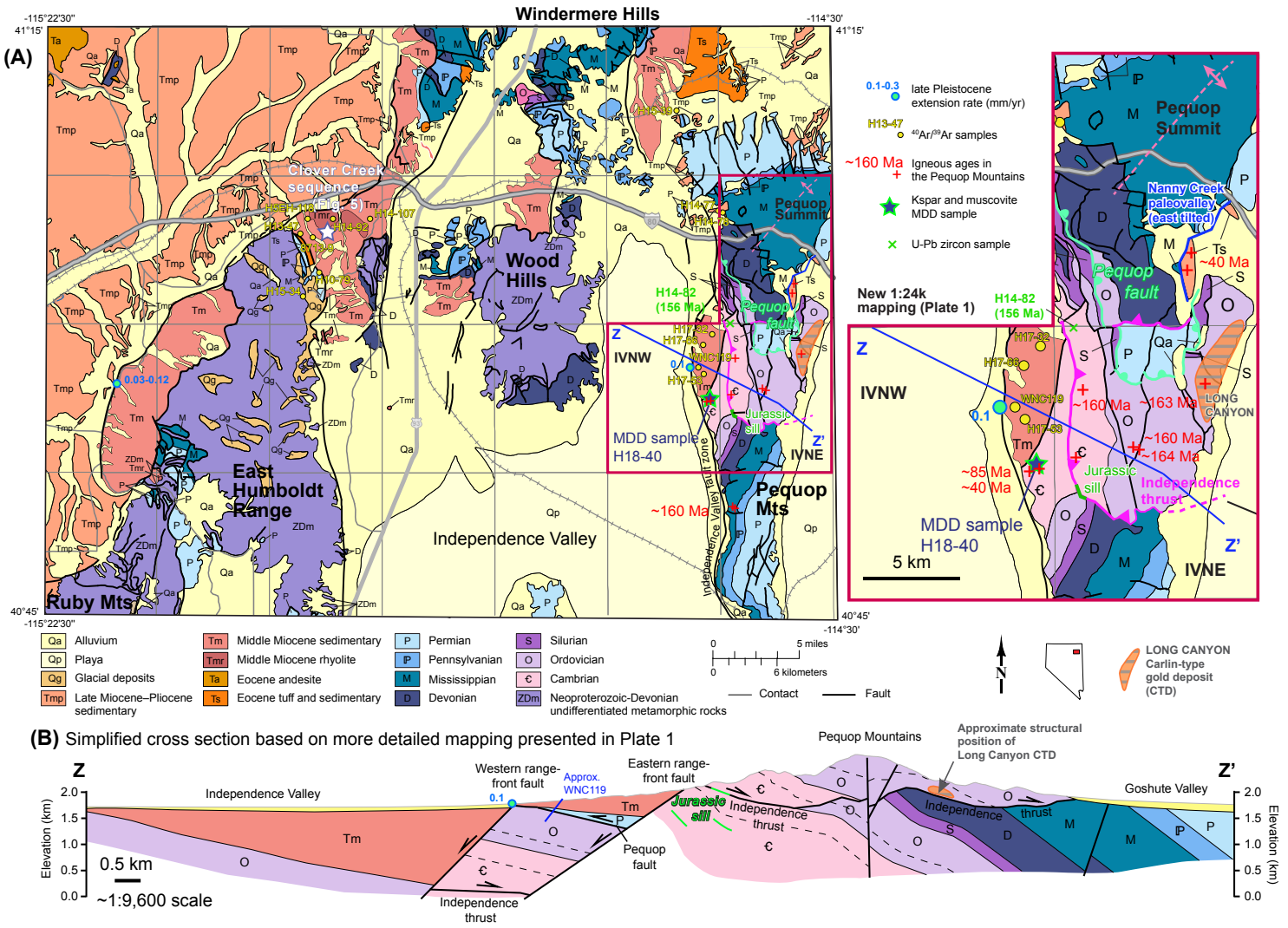

Figure 2. (A) Geologic map of northeastern Nevada, simplified from Crafford (2007), showing the Ruby Mountains, East Humboldt Range, Wood Hills, and Pequop Mountains. Also shown is the location of three new 1:24,000-scale quadrangle maps (red outline, enlarged on right): Pequop Summit (Henry and Thorman, 2015), Independence Valley Northwest (IVNW; Zuza et al., 2019a), and Independence Valley Northeast (IVNE; Zuza et al., 2018). Igneous ages from the Pequop Mountains (red crosses) from Henry and Thorman (2015), Zuza et al. (2020a), and Bedell et al. (2010). Argon sample (i.e., multi-diffusion domain [MDD] and traditional $^{40}Ar/^{39}Ar$ ages), U-Pb zircon, and Carlin-type gold deposit (CTD) locations also shown. Late Pleistocene extension rates in the East Humboldt Range are from Wesnousky and Willoughby (2003), and in the northern Pequops are from this study. Also shown is the Clover Creek sequence along the East Humboldt Range (shown in Fig. 5). (B) Simplified cross section along Z–Z′ (in Fig. 2A). Note that the section is at a different scale than Figure 2A and is based on more detailed geologic mapping presented in Plate 1. Approximate location and orientation of drill hole WNC119 shown. Figure adapted from Zuza et al. (2020a).

To view Plate 1 at full size, please visit https://doi.org/10.1130/GEOS.S.14608005 or access the full-text article on www.gsapubs.org.

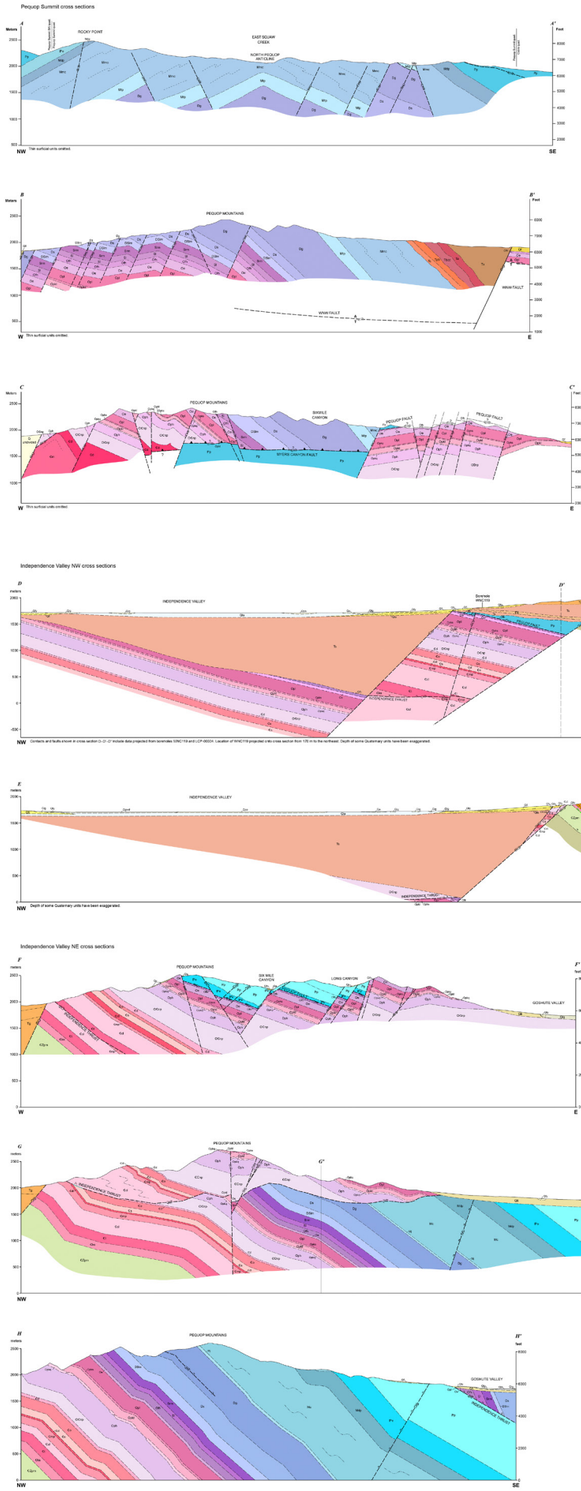

Plate 1. 1:24,000-scale geologic maps and associated cross sections of the Independence Valley NW, Independence Valley NE, and Pequop Summit quadrangles, Elko County, Nevada. Maps from Henry and Thorman (2015), Dee et al. (2017), Zuza et al. (2018), and Zuza et al. (2019a). Note that the quadrangle maps have not been modified, and some artifacts of unit and contact continuity across map boundaries are present. Full maps and accompanying text files can be found on the Nevada Bureau of Mines and Geology's server: https://gisweb.unr.edu/GeologicMaps. To view Plate 1 at full size, please visit https://doi.org/10.1130/GEOS.S.14608005 or access the full-text article on www.gsapubs.org.

Knoll Mountains of northeast Nevada and northwestern Utah (e.g., Allmendinger and Jordan, 1984; Hudec and Wright, 1990; Miller and Hoisch, 1992, 1995; Ketner et al., 1998; Wyld and Wright, 2014, 2015) (Fig. 1B). Hallett and Spear (2015) reported 158–148 Ma monazite ages from paragneiss and schist samples from the East Humboldt Range (Fig. 2), and a phase of deformation preceded the Late Jurassic Dawley Canyon granite in the Ruby Mountains (Hudec, 1992; Jones, 1999). Jurassic plutons and dikes vary from pre-, syn-, to post-kinematic (Elison, 1995; Miller and Hoisch, 1995; Milliard et al., 2015; Rhys et al., 2015). The ca. 157 Ma Silver Zone Pass pluton (Mortensen et al., 2000) crosscuts metamorphic foliations in Cambrian rocks in the Toano Range (Ketner et al., 1998) (Fig. 2).

Following an apparent pause in deformation in the REWP region between Late Jurassic and Late Cretaceous (cf. Kelly et al., 2015), east-directed fold-thrust shortening was well established across Utah by the Late Cretaceous Sevier orogeny (Fig. 1A; e.g., Armstrong, 1968; DeCelles, 2004; DeCelles and Coogan, 2006). REWP geology reflects related hinterland deformation and magmatism (e.g., Camilleri et al., 1997). In the Ruby Mountains–East Humboldt Range (Fig. 1), Cretaceous deformation includes folded thrust faults that have been intruded by Late Cretaceous peraluminuous melts and were thus interpreted as Late Cretaceous structures (e.g., McGrew et al., 2000; McGrew and Snoke, 2015). Late Cretaceous intrusions, mostly leucogranites, compose more than two-thirds of the Ruby Mountains and East Humboldt Range (Lee et al., 2003; Howard et al., 2011) and are interpreted to be crustal melts in thickened crust (McGrew et al., 2000; Lee et al., 2003; Hallet and Spear, 2013). Crustal thickening, presumably during Sevier fold-thrust deformation, is interpreted to have caused the growth of the Nevadaplano orogenic plateau west of the Sevier front (DeCelles, 2004; Chapman et al., 2015). Anatectic melting may have alternatively been driven by westward underthrusting of basement and/or lower Proterozoic–Paleozoic strata from the Sevier thrust front (Best et al., 1974; Gottlieb, 2017). Minor, probably Cretaceous, leucogranites are present in the Wood Hills (Camilleri, 2010a) and Pequop Mountains (Zuza et al., 2018, 2019a).

Thermobarometry on metamorphic rocks exhumed within the REWP indicates that the lower section of the 12–15-km-thick Neoproterozoic–Paleozoic passive-margin sequence experienced pressures of 6–8 kbar at temperatures of 500–700 °C (Hodges et al., 1992; McGrew et al., 2000; Hallett and Spear, 2013), which requires burial to depths >25–30 km. Similar geobarometric pressures in the northern Snake Range, southeast of the REWP (Fig. 1A), suggest burial to >25 km depths (Lewis et al., 1999; Cooper et al., 2010). Monazite and zircon ages in the REWP constrain this burial event to be Late Cretaceous (Hallett and Spear, 2015). A Lu-Hf age of prograde garnet is ca. 83 Ma (Wills, 2014). In contrast, lower pressure estimates of ~3.5 kbar from the East Humboldt Range and ~4.1 kbar from the central Ruby Mountains (i.e., near the Dawley Canyon granite) (Hurlow et al., 1991; Hudec, 1992) suggest burial only several km deeper than predicted stratigraphic depths. Camilleri and Chamberlain (1997) and Lewis et al. (1999) invoked large cryptic thrust sheets to deeply bury these rocks. However, field evidence for these thrust sheet(s) has not been documented in either the REWP or northern Snake Range, which has led to an ongoing debate over the timing and magnitude of Late Cretaceous contraction (e.g., Miller et al., 1983; Miller and Gans, 1989; Thorman et al., 1991; Camilleri and Chamberlain, 1997; Thorman, 2011a, 2011b). Thorman et al. (2019) and Zuza et al. (2020a) presented field relationships and peak-temperature constraints from the Pequop Mountains that indicate the Neoproterozoic–Paleozoic passive margin section was not buried significantly beyond stratigraphic depths.

Regionally, the integrated effects of Mesozoic magmatism and crustal shortening led to crustal thickening associated with the development of the inferred Nevadaplano orogenic plateau (Coney and Harms, 1984; DeCelles, 2004; Chapman et al., 2015; Bahadori et al., 2018). The subsequent collapse of thickened crust and progressive extension of the Basin and Range province started in the Late Cretaceous or Cenozoic (e.g., Camilleri and Chamberlain, 1997; Colgan and Henry, 2009; Wells et al., 2012; Long, 2018). Cenozoic basins that may reflect local extension include the Eocene Elko and Copper, Oligocene(?) Clover Creek, and Miocene Humboldt basins (Henry, 2008; Henry et al., 2012; McGrew and Snoke, 2015; Smith et al., 2017; Canada et al., 2019). The primary driving force for regional extension is debated, with end-member models arguing for control by boundary conditions (i.e., relative plate motion), internal body forces (i.e., gravitational collapse), or a combination of mechanisms (Jones et al., 1998; Colgan and Henry, 2009). The time lag between plateau buildup and subsequent collapse is used to test these models, and thus the timing of peak crustal thickness and extension initiation is critical. Accordingly, evidence for major Late Cretaceous–early Cenozoic extension might favor gravitational collapse models (e.g., Sonder and Jones, 1999), whereas primarily middle Miocene extension would suggest that plate-boundary reorganization during this time drove Basin and Range extension (e.g., Atwater and Stock, 1998). The lack of widely distributed Late Cretaceous to Oligocene basin deposits appears to preclude significant pre-Miocene extension (e.g., Henry et al., 2011).

3. GEOLOGY OF THE PEQUOP MOUNTAINS

The Pequop Mountains are a mostly east-tilted range consisting primarily of Neoproterozoic–Mesozoic strata that are variably metamorphosed and deformed (Figs. 2 and 3; Plate 1). The range is surrounded by Cenozoic basins, with well-exposed Miocene deposits on the western and northern extents (Fig. 2) (e.g., Camilleri et al., 2017). Early mapping by Thorman (1962, 1970) established the range's structural framework, stratigraphic units, and metamorphic facies and identified two major low-angle faults: the Pequop fault and Independence thrust fault (Fig. 2). The lack of detailed constraints on Paleozoic stratigraphy precluded robust interpretations of faults' juxtaposition relationships and kinematics. Subsequent mapping and analysis identified the Pequop fault as a normal fault and better constrained the Independence thrust fault (Camilleri, 1994; Camilleri and Chamberlain, 1997).

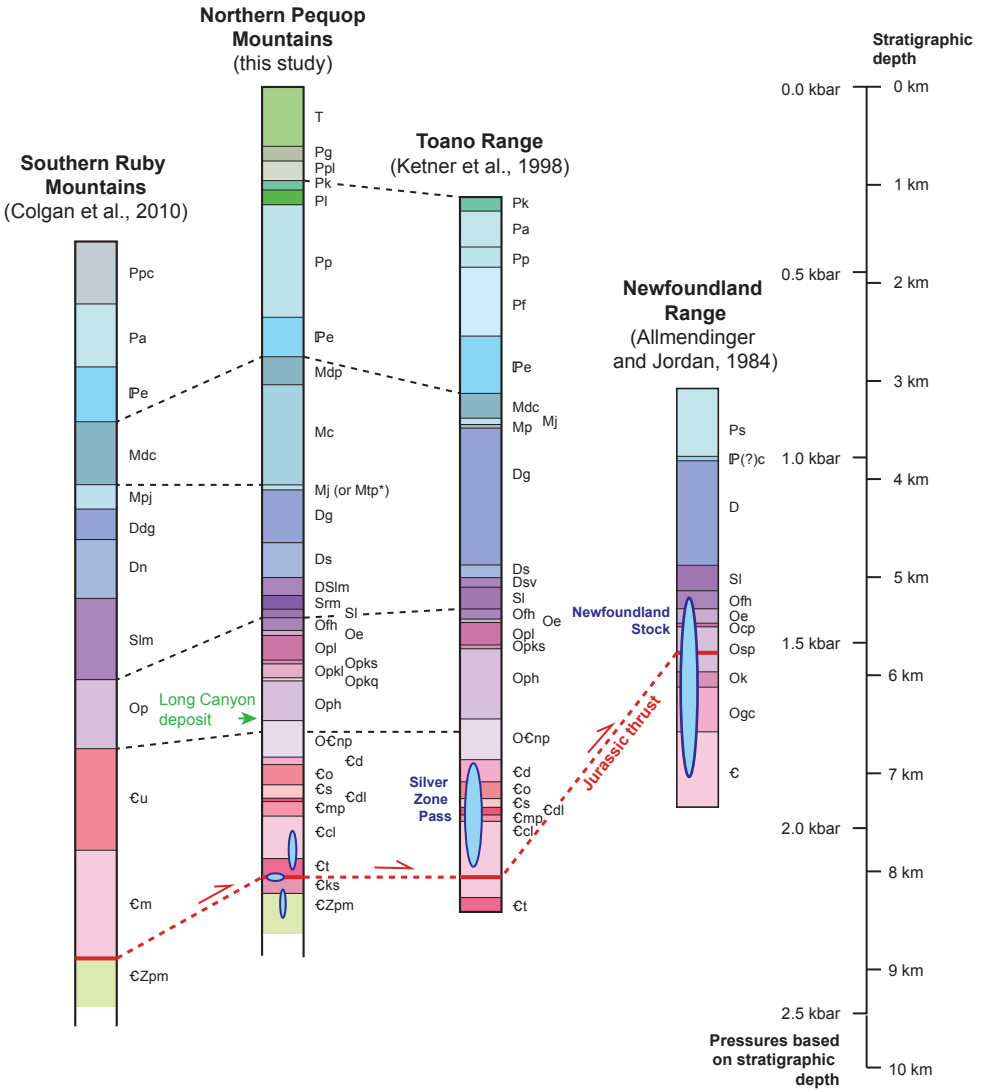

Figure 3. Compilation of schematic stratigraphic columns (with associated references) across the study region in northeastern Nevada, including associated stratigraphic depth and corresponding pressure estimates assuming ρ = 2.7 g/cm³ (e.g., Sharma, 1997). Individual unit names are provided in Table 1. Columns are not hung on a particular datum but were qualitatively aligned for comparison. Blue ellipses show Jurassic intrusions and the stratigraphic location they intrude. Mississippian Tripon Pass (Mtp) and Joana Limestone (Mj) occupy the same stratigraphic position, and their occurrence varies along strike in our mapped geology. Approximate location of Long Canyon gold deposit shown in the Pequop Mountains column.

3.1 Pre-Cenozoic Bedrock Geology

Complete stratigraphic descriptions from the northern Pequop Mountains are provided in Camilleri (2010a), Henry and Thorman (2015), and Zuza et al. (2018). Figure 3 shows the relevant stratigraphy in comparison to nearby ranges, and Table 1 defines the regional stratigraphic nomenclature. The dominantly siliciclastic and carbonate sedimentary units span the Neoproterozoic to Triassic. Neoproterozoic through Ordovician strata are metamorphosed to greenschist-amphibolite facies, and metamorphic grade diminishes upsection (Thorman, 1970; Camilleri and Chamberlain, 1997). The oldest rocks are the Neoproterozoic–Cambrian Prospect Mountain Quartzite (Z€pm), overlain by interbedded meta-carbonate and schist/phyllite including the distinctive dark green-gray Cambrian Dunderberg Shale (€d) (Fig. 3). Ordovician–Cambrian Notch Peak Formation (O€np) overlies the Dunderberg Shale and consists of banded, gray to white dolomite and calcite marbles with chert lenses. A thick, Silurian, dominantly meta-dolomitic section is overlain by Devonian limestones, including the Guilmette Formation (Dg), which is overlain by the Mississippian Tripon Pass (Mtp) or Joana Limestone (Mj), Chainman Shale (Ms), and Diamond Peak Formation (Mdp). Limestone, with numerous cherty lenses, composes the upper Pennsylvanian and Permian section in the northern Pequop Mountains. Overlying Permian–Triassic strata are observed in the southern Pequop Mountains and consist of interbedded carbonate and siliciclastic strata (Snelson, 1955; Fraser et al., 1986; Swenson, 1991). Altogether, the stratigraphy down to Z€pm is ~8.5 km thick, although apparent unit thicknesses vary substantially due to internal bedding-parallel faulting and folding (Zuza et al., 2018). In this sense, the ~8.5 km thickness is a structural thickness, but this thickness of Neoproterozoic–Triassic rocks is similar to stratigraphic thicknesses in adjacent ranges (Fig. 3). The Neoproterozoic McCoy Creek Group, which underlies Z€pm, is 3–5+ km thick (Misch and Hazzard, 1962) but is not shown in these stratigraphic columns (Fig. 3) because these rocks are not exposed in the Pequop Mountains.

Igneous rocks in the northern Pequop Mountains consist of Jurassic dikes and sills, probable Cretaceous leucogranite, and Eocene intrusions

TABLE 1. REGIONAL STRATIGRAPHY IN NORTHEAST NEVADA

Southern Ruby Mountains (Colgan et al., 2010)			Pequop Mountains (this study)			Toano Range (Ketner et al., 1998)			Newfoundland Range (Allmendinger and Jordan, 1984)		
Age	Symbol	Name	Age	Symbol	Name	Age	Symbol	Name	Age	Symbol	Name
P	Ppc	Park City Group	T	T	Triassic undifferentiated	P	Pk	Kaibab Limestone	P	Ps	Permian sandstone
	Pa	Arcturus Group	P	Pg	Gerster Formation		Pa	Arcturus Formation	ℙP	ℙ(?)c	Penn.-Perm. conglomerate
ℙe	Pe	Ely Limestone		Ppl	Plympton Formation		Pp	Pequop Formation	D	D	Devonian undifferentiated
M	Mdc	Diamond Peak Formation & Chainman Shale		Pk	Kaibab Limestone		Pf	Ferguson Mountain Fm	S	Sl	Laketown Dolomite
	Mpj	Pilot Shale and Joana Limestone		Pl	Loray Formation	ℙe	Pe	Ely Limestone	O	Ofh	Fish Haven Dolomite
D	Ddg	Devil's Gate Limestone		Pp	Pequop Formation	M	Mdc	Diamond Peak Formation & Chainman Shale		Oe	Eureka Quartzite
	Dn	Nevada Formation	ℙe	Pe	Ely Limestone		Mj	Joana Limestone		Ocp	Crystal Peak Dolomite
S	Slm	Lone Mountain Dolomite	M	Mdp	Diamond Peak Formation		Mp	Pilot Shale		Osp	Swan Peak Quartzite
O	Op	Pogonip Group		Mc	Chainman Shale	D	Dg	Guilmette Formation		Ok	Pogonip Kanosh Shale
€	€u	Upper Cambrian		Mtp	Tripon Pass Limestone		Ds	Simonson Dolomite		Ogc	Garden City Limestone
	€m	Middle Cambrian		Mj	Joana Limestone		Dsv	Sevy Formation	€	€	Cambrian undifferentiated
€Z	€Zpm	Prospect Mountain Quartzite	D	Dg	Guilmette Formation	S	Sl	Laketown Dolomite			
				Ds	Simonson Dolomite	O	Ofh	Fish Haven Dolomite			
				DSlm	Lone Mountain Formation		Oe	Eureka Quartzite			
			S	Srm	Roberts Mountain Formation		Opl	Pogonip Lehman Fm			
				Sl	Laketown Dolomite		Opks	Pogonip Kanosh Shale			
			O	Ofh	Fish Haven Dolomite		Oph	Pogonip House Formation			
				Oe	Eureka Quartzite	O€	O€np	Notch Peak Formation			
				Opl	Pogonip Lehman Formation	€	€d	Dunderberg Shale			
				Opks	Pogonip Kanosh Shale		€o	Oasis Formation			
				Opkl	Pogonip Kanosh Limestone		€s	Shafter Formation			
				Opkq	Pogonip Kanosh Quartzite		€dl	Decoy Limestone			
				Oph	Pogonip House Formation		€mp	Morgan Pass Formation			
			O€	O€np	Notch Peak Formation		€cl	Clifside Limestone			
			€	€d	Dunderberg Shale		€t	Toano Limestone			
				€o	Oasis Formation						
				€s	Shafter Formation						
				€dl	Decoy Limestone						
				€mp	Morgan Pass Formation						
				€cl	Clifside Limestone						
				€t	Toano Limestone						
				€ks	Kilian Springs Formation						
			€Z	€Zpm	Prospect Mountain Quartzite						

and volcanic rocks (Brooks et al., 1995; Henry, 2008; Bedell et al., 2010; Camilleri, 2010a; Smith et al., 2013; Henry and Thorman, 2015; Zuza et al., 2018). Jurassic intrusions range from granite to gabbro, including numerous, but volumetrically small, distinct lamprophyre dikes. Camilleri and Chamberlain (1997) reported a lower intercept U-Pb zircon age of 154 ± 5 Ma from a boudinaged granitic sill near the western mouth of Meyers Canyon (individual boudins up to ~3 m thick and ~12 m long over a total 100 m southeast-strike length). We re-dated this sill to confirm its age. A foliated granite that intruded the Cambrian Shafter Formation along the western flank of the range gave a U-Pb zircon age of 159.9 ± 1.9 Ma (Fig. 2; Bedell et al., 2010). $^{40}Ar/^{39}Ar$ dating of hornblende from lamprophyre dikes from across the range confirms a Late Jurassic age of ca. 160 Ma (four samples in Henry and Thorman, 2015; Zuza et al., 2018, 2020a). Outcrops of garnet-bearing, two-mica leucogranite on the western flank of the range are interpreted as Cretaceous based on sparse data. Five zircons from one sample yielded $^{206}Pb/^{238}U$ ages between 69 and 87 Ma among many Triassic, early Paleozoic, and Proterozoic inherited grains (Bedell et al., 2010). $^{40}Ar/^{39}Ar$ dating of muscovite yielded climbing spectra with maximum ages of ca. 85 Ma (Zuza et al., 2018).

3.2 Deformation

From oldest to youngest, the deformational phases that affected the Pequop Mountains are Mesozoic contraction, a Late Cretaceous–Cenozoic (?) phase of low-angle normal faulting, and Miocene-to-present high-angle normal faulting. Mesozoic contraction is associated with the Independence thrust fault, which traverses the range (Plate 1) and generally places lower Paleozoic over middle Paleozoic rocks (Thorman, 1970; Camilleri and Chamberlain, 1997; Camilleri, 2010a) and the development of a northeast-trending, ~6-km-wavelength syncline in the southern Pequop Mountains (Snelson, 1955; Coats, 1987; Swenson, 1991) (Fig. 2). The age of this syncline is only constrained to be post-Triassic by the youngest units in the fold (located southeast of the Fig. 2A map extent; Coats, 1987; Swenson, 1991). Additionally, Camilleri and Chamberlain (1997) proposed the emplacement of a hypothesized Windermere thrust sheet between the Middle Jurassic and Late Cretaceous to explain deep burial of the stratigraphy. Surface expression of this fault was subsequently obscured or eliminated by later extension. According to the Camilleri and Chamberlain (1997) model, the Independence thrust was active after Windermere thrusting in the Cretaceous–Paleogene between 84 Ma and 41 Ma.

Camilleri and Chamberlain (1997) suggested that Pequop normal-sense fault motion (Fig. 4) occurred between 84 Ma and 75 Ma on the basis of decompression and/or exhumation recorded by metamorphic rocks in the Ruby Mountains–East Humboldt Range to the west (McGrew and Snee, 1994) and an interpreted crosscutting relationship between the hanging wall rocks and incision of the >41 Ma Nanny Creek paleovalley (Brooks et al., 1995; Henry, 2008; Henry et al., 2011). This episode of faulting was attributed to orogenic collapse and exhumation-related decompression. Most recently, Cenozoic high-angle normal faulting tilted the range eastward and is associated with the development of a Miocene basin on the western flank of the range (e.g., Camilleri, 2010a; Zuza et al., 2019a) (Fig. 2).

3.3 Metamorphism

In the Pequop Mountains and Wood Hills, regional syn-kinematic metamorphism was overgrown by static, post-kinematic, randomly oriented biotite and tremolite grains in the foliation plane of interbedded pelitic marble (e.g., Thorman, 1962, 1970; Camilleri, 1998). The structurally and stratigraphically lowest units exposed along the western flank of the Pequop Mountains exhibit the highest metamorphic grade, with garnet, muscovite, biotite, and tremolite present in the Z€pm through €t units, and biotite and muscovite variably present in most of the Cambrian rocks (Fig. 2). The Cambrian Morgan Pass Formation (€mp) and Dunderburg Shale (€d) commonly consist of biotite-muscovite schist, with foliation-parallel micas crosscut by obliquely oriented post-kinematic micas. This is most commonly observed as syn-kinematic, foliation-parallel biotite crosscut by post-kinematic muscovite, such as observed in the Cambrian Kilian Springs Formation, €mp, and €d schists (e.g., Thorman, 1962; Zuza et al., 2019a). Similar, variably oriented tremolite in the Cambrian stratigraphy was interpreted to represent post-kinematic metamorphism (Thorman, 1962). Retrograde chlorite exists in some rocks. Limestones in Devonian and higher units do not contain any metamorphic minerals, and the Mississippian Chainman Shale is distinctly not metamorphosed.

Argon thermochronology on both foliation-parallel and orthogonal biotite (five samples) and muscovite (eight samples) suggests cooling through their respective closure temperatures in the Late Cretaceous (broadly 70–90 Ma) (Zuza et al., 2019a). Camilleri and Chamberlain (1997) reported a titanite–whole-rock isochron age from the Cambrian Toano Limestone of ca. 84 Ma and a titanite U-Pb age of ca. 75 Ma from the Wood Hills. Titanite has a high closure temperature of 600–700 °C (e.g., Spencer et al., 2013), although its close association with hornblende could suggest that the titanite grew during the same prograde metamorphism that produced the hornblende grains. A Lu-Hf garnet age of ca. 83 Ma in the Cambrian Dunderberg Shale in the Wood Hills (Wills, 2014) suggests Late Cretaceous prograde metamorphism.

Concordant Ar age spectra that provide well-defined Late Jurassic (ca. 160 Ma) plateau ages for hornblende from lamprophyres from the structurally higher eastern part of the range near Long Canyon indicate that these rocks were not heated above 500 °C (e.g., Harrison, 1982) since ca. 157 Ma (Henry and Thorman, 2015; Zuza et al., 2019a, 2020a). Biotite analyses from this same region show disturbed Late Jurassic–Cretaceous spectra (Zuza et al., 2020a), which indicate these rocks probably experienced temperatures close to the biotite closure temperature of ~300 °C (Harrison et al., 1985) in the Late Cretaceous.

3.4 Cenozoic Basin Deposits, Igneous Rocks, and Previous Extension Interpretations

The Cenozoic sedimentary and igneous rock record provides constraints for Cenozoic paleo-relief

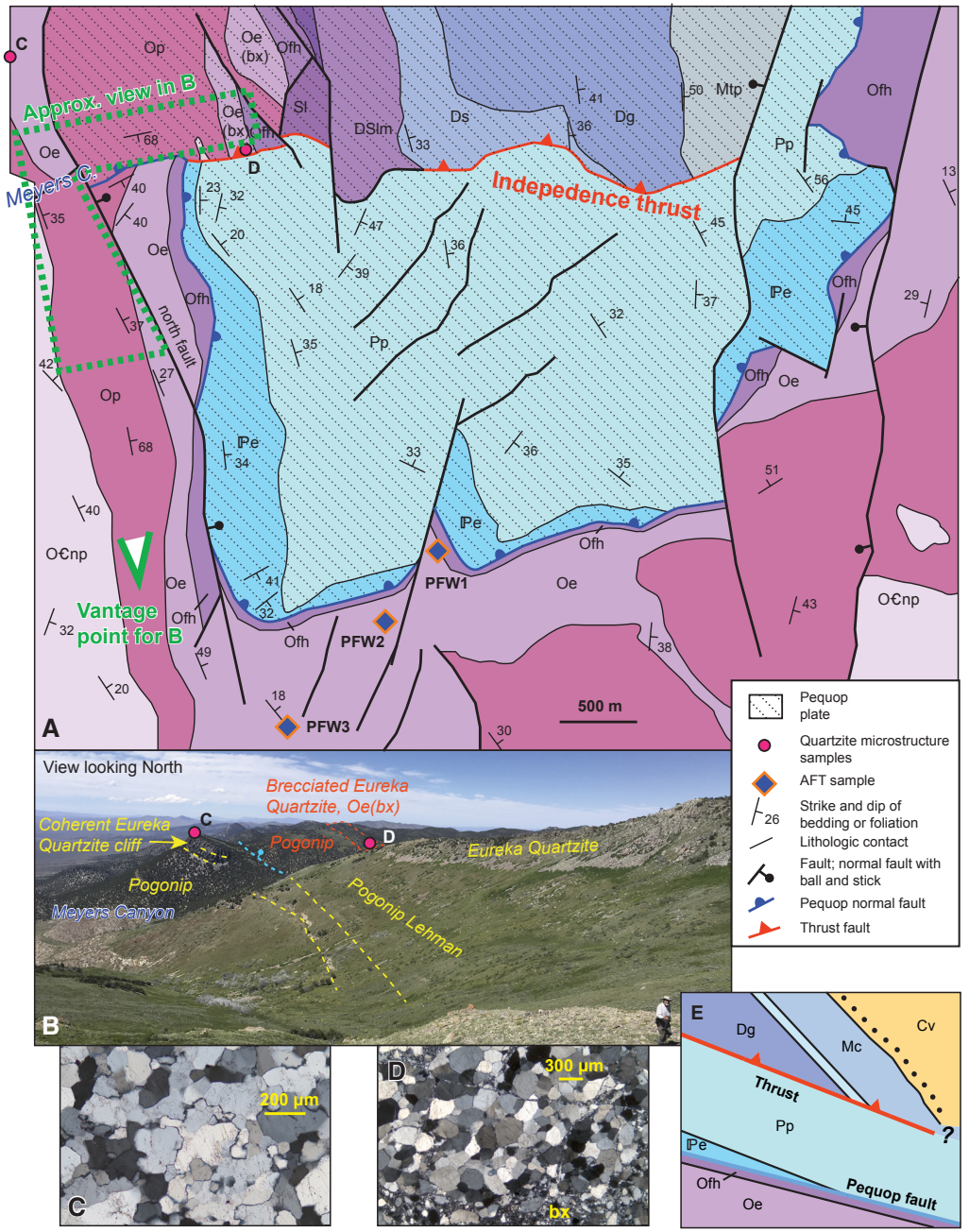

Figure 4. (A) Sketch geologic map showing the Pequop plate, apatite-fission track (AFT), and quartzite samples discussed in this study. Map units and symbology are as in Plate 1. Ordovician Eureka Quartzite (Oe) is present in the hanging wall and footwall of the Pequop plate, but Oe in the Pequop plate is brecciated (bx) whereas it is an intact major-cliff former in the footwall. View in Fig. 4B shows different character of Oe. (B) View looking north across Meyers Canyon, looking at the geology in part of Figure 4A. The Ordovician Eureka Quartzite and Pogonip Group in the foreground (yellow text) is in the footwall of the Pequop plate and the rocks in the background (red-orange text) are in the hanging wall, here separated by a high-angle normal fault that drops upper plate rocks against lower plate rocks. The character of Oe changes from a prominent cliff-forming unit in the lower plate (Oe in Fig. 4A) to a rubbly hill in the upper plate (Oe(bx) in Fig. 4A). Quartz microstructural observations for (C) a strongly lineated sample with interlobate grain boundaries (N41.005619, W114.602907) and (D) brecciated sample with polygonal texture and brecciation (bx) (N41.009524, W114.584972). (E) Sketch of Pequop fault field relationships, including Ordovician footwall rock.

and extension in the REWP region. In the northern Pequop Mountains, the 41.0–39.5 Ma Eocene Nanny Creek volcanic and sedimentary sequence (i.e., basal conglomerate, 40.95 Ma plagioclase-biotite tuff, 40.2 Ma tuff of Big Cottonwood Canyon, and 39.5 Ma dacite-rhyolite lavas) was deposited in an east-trending paleovalley (Brooks et al., 1995; Henry, 2008; Henry et al., 2011; Henry and Thorman, 2015) (Fig. 2). The ~1.5-km-deep, Nanny Creek paleovalley was incised into the Mesozoic Nevadaplano by an eastward-flowing stream system from relatively high topography (Henry, 2008; Henry et al., 2011) (Fig. 2). Although the paleovalley contains volcanic rocks as old as ca. 41 Ma, when it began to form is not well constrained. Other paleovalleys in northeastern Nevada contain tuffs as old as 45 Ma (Henry, 2008). The Nanny Creek paleovalley likely began to incise in the Late Cretaceous or possibly in the Middle-Late Jurassic when regional uplift started.

West of the Pequop Mountains, widely distributed, but generally thin (all ≤1 km) Eocene lacustrine and volcaniclastic sediments are interpreted to record accumulation in the extensional ca. 48–38 Ma Elko Basin (e.g., Solomon et al., 1979; Haynes, 2003; Lund-Snee et al., 2016; Smith et al., 2017). Whether the Elko Basin was a wide lake basin covering most of the REWP region or represented a series of infilled paleovalleys cut by normal faults is debated (Hickey et al., 2005; Henry et al., 2011; Lund Snee et al., 2016), but the distribution and thickness of Eocene deposits favors infilled paleovalleys (Smith et al., 2017; Henry, 2018). Eocene deposits in the Pequop Mountains are all distal ash-flow tuffs and locally derived lavas. The absence of any significant Eocene lacustrine sedimentary deposit in the Pequop Mountains, adjacent Wood Hills to the west, and Windermere Hills to the north (Mueller, 1993; Mueller et al., 1999; Henry, 2008; Camilleri, 2010a, 2010b; Fig. 2A) likely indicates the Elko Basin did not extend into this region.

Mueller et al. (1999) interpreted two pre-middle Miocene episodes of extension in the eastern Windermere Hills and the adjacent northern end of the Pequop Mountains (Fig. 2A), primarily on the basis of the volcanic-sedimentary record: an Eocene (ca. 39–35 Ma) episode based on west-tilted rocks of that age in the Windermere Hills and a south-tilted section dipping into a shallowly north-dipping fault active between ca. 35 and 15 Ma in the northern Pequop Mountains. However, the 39–35 Ma rocks in the Windermere Hills comprise a volcaniclastic sequence that overlies the same 40.95 and 40.2 Ma tuffs found in the Nanny Creek paleovalley in the Pequop Mountains. Overlying middle Miocene deposits are concordant with the west-tilted Eocene rocks. Based on these characteristics, the Eocene sequence has more recently been interpreted to fill a paleovalley and not to indicate contemporaneous extension (Henry, 2008; Henry et al., 2011). The 35–15 Ma episode of extension is interpreted based on an ~900 m, south-dipping sequence of conglomerate, laminated siltstone, and sandstone in the northern Pequop Mountains assigned to the "lower Humboldt formation," which is an informal unit thought to be a lower part of the middle Miocene–and younger Humboldt Formation (Sharp, 1939; Frerichs and Pekarek, 1994; Wallace et al., 2008). These "lower Humboldt formation" rocks were interpreted to be part of the hanging wall of the north-dipping "Holborn" fault (Mueller et al., 1999). However, this sequence is absent between the Eocene and Miocene rocks in the west-dipping section 4 km to the northwest. Two sandstone samples from the south-dipping sequence yielded detrital zircons with ages that ranged continuously between 42 and 27 Ma (Drescher et al., 2019). From these data, Drescher et al. (2019) interpreted deposition of the south-dipping rocks, active faulting on the north-dipping fault, and significant extension at ca. 29–28 Ma. However, the reported ages are maximum depositional ages, and the rocks could be significantly younger. The absence of ca. 29–28 Ma rocks in, and lack of an angular unconformity between, the Eocene and middle Miocene section in the adjacent Windermere Hills (Fig. 2A) limits the magnitude of any extension between Eocene and Miocene.

Camilleri et al. (2017) combined the "lower Humboldt Formation" in the northern Pequop Mountains and the Clover Creek sequence (discussed below) into the east-northeast–trending Holborn basin that formed due to north-directed extension between 38 and 16 Ma. However, north-south extension interpreted by Mueller et al. (1999), Camilleri et al. (2017), and Drescher et al. (2019) would be an anomaly in northeast Nevada, because all other Cenozoic basins formed from west-northwest extension (e.g., Colgan and Henry, 2009; Henry, 2018).

A major phase of extension in the REWP metamorphic core complex has been interpreted to occur in the Oligocene. Crosscutting relationships with intrusions in the Ruby Mountains–East Humboldt Range suggest mylonitization and normal-sense exhumation between ca. 29 Ma and ca. 23 Ma (e.g., Snoke, 1980; Wright and Snoke, 1993). Oligocene–Miocene cooling was reported based on zircon and apatite helium thermochronology (~200–100 °C closure temperatures) in the Ruby Mountains and Wood Hills (Wolfe, 2016; Gonzalez et al., 2019; Metcalf et al., 2019; Mueller, 2019). Argon mica ages suggest initiation of exhumation of the Ruby Mountains at 25–22 Ma (Gifford, 2008), and a $^{40}Ar/^{39}Ar$ compilation in McGrew and Snoke (2015) shows several 21–25 Ma muscovite and biotite cooling ages in the East Humboldt Range. However, basins coeval with this phase of extension are not known in the area, and Oligocene deposits are absent, thin, or equivocal in the broader REWP region (Mueller et al., 1999; Henry et al., 2011; Camilleri et al., 2017).

The best case for Oligocene basin sedimentation is a 3-km-thick sedimentary section in the hanging wall of the detachment fault in the East Humboldt Range that contains Eocene through middle Miocene deposits (Snelson, 1957; McGrew and Snoke, 2015) (Fig. 5). Nearly 1500 m of conglomerate and sedimentary breccia in the middle of the section was initially assigned to the "lower Humboldt formation" and most recently to the late Oligocene(?)–early Miocene sedimentary sequence of Clover Creek (Fig. 5; McGrew and Snoke, 2015). McGrew and Snoke (2015) reasonably interpreted megabreccia consisting of internally brecciated blocks of non-metamorphosed Devonian Guilmette Formation in the middle part of this section to be rock-avalanche deposits from active normal fault scarps. The lower part of the section consists of the tuffs of Big Cottonwood Canyon and Campbell Creek, which probably accumulated in a paleovalley that drained eastward from a caldera source of the tuff of Big Cottonwood Creek near Tuscarora and continued to Nanny Creek (Henry, 2008). We report new $^{40}Ar/^{39}Ar$ ages to better constrain this

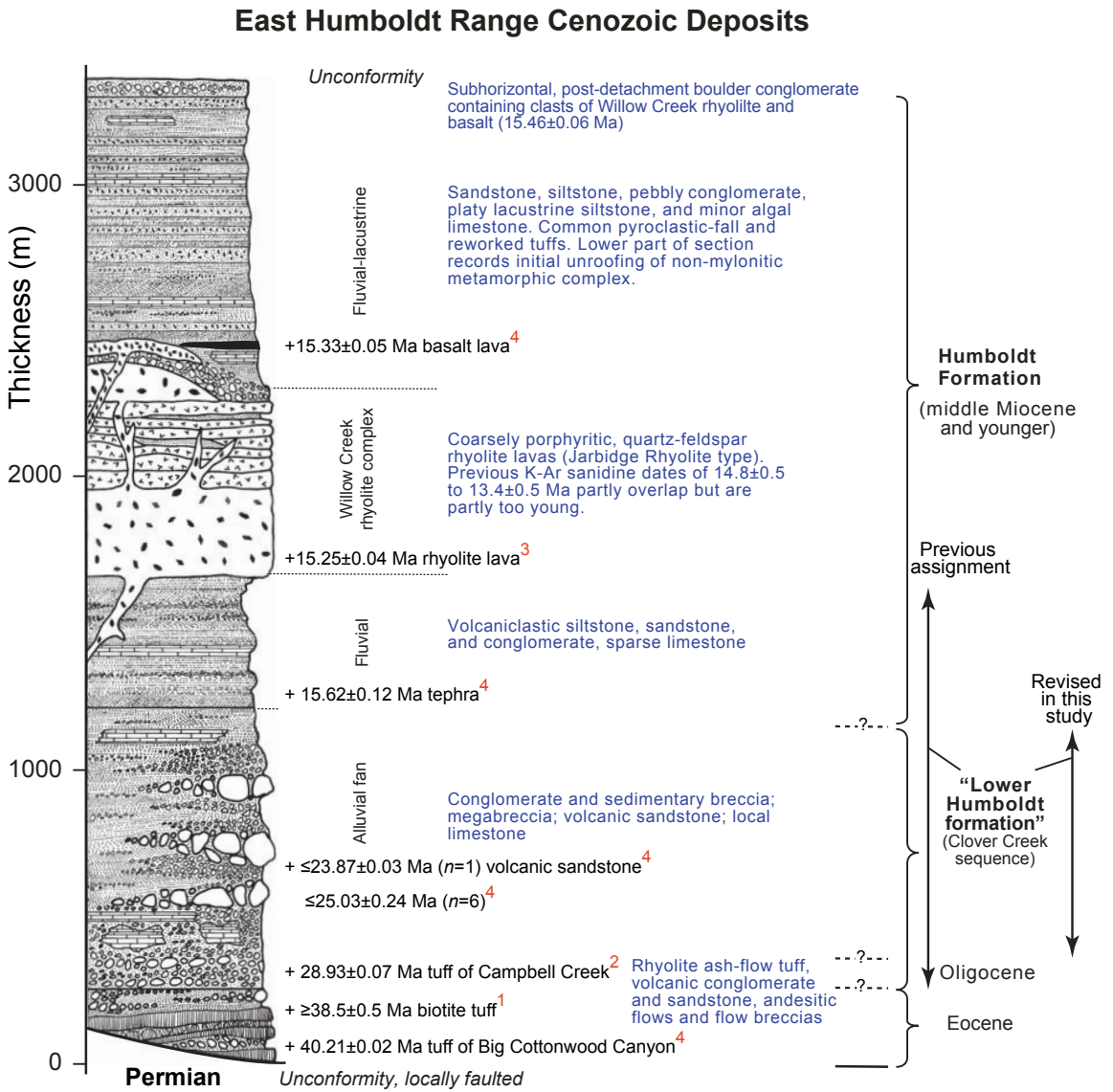

Figure 5. Generalized stratigraphic column of Cenozoic rocks in the northeastern East Humboldt Range (modified from Mueller and Snoke, 1993; Henry et al., 2011; McGrew and Snoke, 2015). $^{40}Ar/^{39}Ar$ age sources (red superscripts): (1) Brooks et al. (1995); (2) Henry et al. (2012); (3) M. Brueseke, personal commun. in McGrew and Snoke (2015); (4) this study (Table 2).

stratigraphic section, including the thickness of any Oligocene deposits.

Miocene sedimentary, volcaniclastic, and tuff deposits exposed along the western flank of the Pequop Mountains make up the Humboldt Formation (Camilleri, 2010a; Camilleri et al., 2017). New $^{40}Ar/^{39}Ar$ ages in this study bracket the age of the Humboldt Formation and are consistent with ca. 16 Ma to older than ca. 5 Ma ages from the Knoll Basin, north of the Pequop Mountains (Camilleri et al., 2017). The age of the middle-to-late Miocene Humboldt Formation indicates that major basin formation and probably extension began at ca. 16 Ma (e.g., Colgan and Henry, 2009).

3.5 Long Canyon Gold Mineralization

The northern Pequop Mountains have been the focus of recent investigations because of the discovery of the Long Canyon Carlin-type gold deposit (CTD) on the eastern flank of the range (Fig. 2) (e.g., Bedell et al., 2010; Smith et al., 2013; Milliard et al., 2015). The deposit is ~145 km east of the typical Carlin and Cortez CTD trends but shares their characteristics of probable Eocene associated intrusions, disseminated mineralization, and carbonate host rock (Muntean et al., 2011). Although not directly dated, Long Canyon mineralization is assumed to be Eocene based on the correlation with typical CTDs in Nevada (ca. 42–36 Ma; Ressel and Henry, 2006; Muntean et al., 2011). Eocene rhyolite dikes and dacite lavas in the Pequop Mountains (Bedell et al., 2010; Henry and Thorman, 2015; Milliard et al., 2015; Zuza et al., 2018) were probably sourced from a larger plutonic complex that may have been the principal heat source for mineralization (e.g., Bedell et al., 2010). Of note, CTDs in northern Nevada appear to have formed at relatively shallow depths <5 km (Kuehn and Rose, 1995; Arehart, 1996; Cline and Hofstra, 2000; Nutt and Hofstra, 2003; Ressel and Henry, 2006; John et al., 2008).

4. METHODS

We present new geologic mapping, thermochronology, and geochronology focused around the northern Pequop Mountains to constrain the geologic evolution of the REWP. Our geologic mapping of three 7.5′ quadrangles at 1:24,000-scale, published as open-file reports (e.g., Henry and Thorman, 2015; Zuza et al., 2018, 2019a), are presented in Plate 1 as a synthesized map figure. No attempt was made to improve edge matching, such as contacts, faults and polygons, across quadrangle boundaries. Field observations and structural analyses are based on this mapping.

$^{40}Ar/^{39}Ar$ multi-diffusion domain (MDD) thermochronology was conducted at the New Mexico Geochronology Research Laboratory at the New Mexico Institute of Mining and Technology on muscovite and K-feldspar following the general methods outlined by Lovera et al. (1989) and Long et al. (2018). Analytical details of the argon measurements and MDD models are provided in the Supplemental Text[1], including isotopic data in Supplemental Table S1 and MDD modeling conditions in Supplemental Table S2. Minerals were extracted from the same sample of a Cretaceous leucogranite (sample H18-40, location in Fig. 2A; N40.93581; W114.63277) in the western Pequop Mountains.

We conducted new $^{40}Ar/^{39}Ar$ dating from important Cenozoic rocks from across the study area, including sedimentary, volcaniclastic, intrusive, and tuff deposits (Fig. 2; Table 2). All $^{40}Ar/^{39}Ar$ analyses were conducted at the New Mexico Geochronology Research Laboratory using standard procedures described in Zimmerer et al. (2016) and Henry et al. (2017) (more information in the Argon Supplemental Tables 1 and 2 [footnote 1]).

Apatite fission-track (AFT) dating of three samples from the Ordovician Eureka Quartzite in the central part of the northern Pequop Mountains was conducted to track the low-temperature cooling of the range. Depending on grain size, cooling rate, grain composition and annealing kinetics, and mineral inclusions, apatite grains analyzed by AFT partially anneal at the approximate temperature range of 100–120 °C, known as the partial annealing zone (PAZ) (Gleadow and Duddy, 1981; Ketcham et al., 2007). Track-length data can be inverted in a thermal model using software such as HeFTy or QTQt (Ketcham, 2005; Ketcham et al., 2007; Gallagher, 2012). Apatite minerals were separated, mounted, etched, and analyzed for AFT ages and confined track lengths following standard methods of Donelick et al. (2005) by GeoSep Services. Grains were analyzed with a quadrupole inductively coupled plasma–mass spectrometer (ICP-MS), and ages were determined using a modified radioactive decay equation calibrated for the ICP-MS using the Durango fluorapatite standard (Donelick et al., 2005).

U-Pb geochronology on zircons from a foliated and boudinaged Jurassic sill in Meyers Canyon was conducted by laser ablation–inductively coupled plasma–mass spectrometry (LA-ICP-MS) at the Arizona LaserChron Center. Details of the LA-ICP-MS method are in the Supplemental Text (footnote 1) and analyses are in Zircon Supplemental Table 1.

5. THERMOCHRONOLOGY AND GEOCHRONOLOGY RESULTS

5.1 Argon Multi-Diffusion Domain Modeling

K-feldspar and muscovite were analyzed via MDD thermochronology methods from the same Cretaceous leucogranite (sample H18-40, location in Fig. 2A; N40.93581; W114.63277) (Fig. 6). The muscovite age spectrum reveals a steep rise in age from ca. 60–72 Ma over the initial 10% of the spectrum before generally climbing to a terminal age near 77 Ma (Fig. 6A). The K-feldspar yields significantly younger apparent ages beginning near 35 Ma and climbing to an overall flat segment at ca. 50 Ma for the final 40% of gas released (Fig. 6A). The Arrhenius parameters derived from the step-heating experiment have a form consistent with MDD behavior (Fig. 6B). The activation energy for the K-feldspar is derived from the initially linear segment of the Arrhenius plot, whereas that for muscovite is chosen to be consistent with the value of 64 ± 9 kcal/mol reported by Harrison et al. (2009). Log(r/r_o) plots are derived from the Arrhenius data and have forms mimicking their age spectra that further support an MDD model to explain the climbing age spectra that also reveal moderate inflections (Fig. 6C).

The muscovite and K-feldspar were modeled independently using a cooling-only solution (Fig. 6D). The output thermal histories that yield

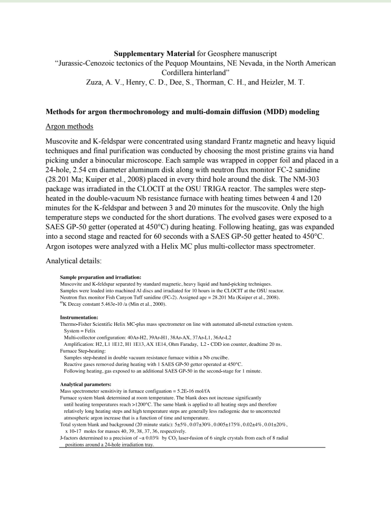
Supplementary Material for Geosphere manuscript
"Jurassic-Cenozoic tectonics of the Pequop Mountains, NE Nevada, in the North American Cordillera hinterland"
Zuza, A. V., Henry, C. D., Dee, S., Thorman, C. H., and Heizler, M. T.

Methods for argon thermochronology and multi-domain diffusion (MDD) modeling

Argon methods

Muscovite and K-feldspar were concentrated using standard Frantz magnetic and heavy liquid techniques and final purification was conducted by choosing the most pristine grains via hand picking under a binocular microscope. Each sample was wrapped in copper foil and placed in a 24-hole, 2.54 cm diameter aluminum disk along with neutron flux monitor FC-2 sanidine (28.201 Ma; Kuiper et al., 2008) placed in every third hole around the disk. The NM-303 package was irradiated in the CLOCIT at the OSU TRIGA reactor. The samples were step-heated in the double-vacuum Nb resistance furnace with heating times between 4 and 120 minutes for the K-feldspar and between 3 and 20 minutes for the muscovite. Only the high temperature steps we conducted for the short durations. The evolved gases were exposed to a SAES GP-50 getter (operated at 450°C) during heating. Following heating, gas was expanded into a second stage and reacted for 60 seconds with a SAES GP-50 getter heated to 450°C. Argon isotopes were analyzed with a Helix MC plus multi-collector mass spectrometer.

Analytical details:

Sample preparation and irradiation:
Muscovite and K-feldspar separated by standard magnetic, heavy liquid and hand-picking techniques.
Samples were loaded into machined Al discs and irradiated for 10 hours in the CLOCIT at the OSU reactor.
Neutron flux monitor Fish Canyon Tuff sanidine (FC-2). Assigned age = 28.201 Ma (Kuiper et al., 2008).
^{40}K Decay constant 5.463e-10 /a (Min et al., 2000).

Instrumentation:
Thermo-Fisher Scientific Helix MC-plus mass spectrometer on line with automated all-metal extraction system.
System = Felix
Multi-collector configuration: 40Ar-H2, 39Ar-H1, 38Ar-AX, 37Ar-L1, 36Ar-L2
Amplification: H2, L1 1E12, H1 1E13, AX 1E14, Ohm Faraday, L2 - CDD ion counter, deadtime 20 ns.
Furnace Step-heating:
Samples step-heated in double vacuum resistance furnace within a Nb crucilbe.
Reactive gases removed during heating with 1 SAES GP-50 getter operated at 450°C.
Following heating, gas exposed to an additional SAES GP-50 in the second-stage for 1 minute.

Analytical parameters:
Mass spectrometer sensitivity in furnace configuation = 5.2E-16 mol/fA
Furnace system blank determined at room temperature. The blank does not increase significantly until heating temperatures reach >1200°C. The same blank is applied to all heating steps and therefore relatively long heating steps and high temperature steps are generally less radiogenic due to uncorrected atmospheric argon increase that is a function of time and temperature.
Total system blank and background (20 minute static): 5±5%, 0.07±30%, 0.005±175%, 0.02±4%, 0.01±20%, x 10-17 moles for masses 40, 39, 38, 37, 36, respectively.
J-factors determined to a precision of ~± 0.03% by CO_2 laser-fusion of 6 single crystals from each of 8 radial positions around a 24-hole irradiation tray.

[1]Supplemental Material. Supplemental Text contains figures (i.e., structural data and topographic profile across Pleistocene fault) and argon domain diffusion (MDD) modeling methods and data table. Tables S1 and S2: Argon data. Table S3: Apatite fission-track (AFT) data. Table S4: Zircon data. Please visit https://doi.org/10.1130/GEOS.S.14607981 to access the supplemental material, and contact editing@geosociety.org with any questions.

TABLE 2. $^{40}Ar/^{39}Ar$ AGES OF CENOZOIC TEPHRA AND OTHER VOLCANIC ROCKS, PEQUOP MOUNTAINS AND EAST HUMBOLDT RANGE, NORTHEAST NEVADA

Sample[2]	Rock type	Location, Quadrangle (Q)	Latitude 83	Longitude 83	Material[3]	Ages (Ma)[1] Age (weighted mean)	±2s	K/Ca	±1s	n[4]	Comment
Single crystal											
Northern Pequop Mountains											
H14-77 [AS1]	Miocene tephra	West Pequop Summit Q	41.09474	−114.62503	s	**12.30**	0.03	21.8	5.1	9/15	25 to 85 Ma xenocrysts
H14-78 [AS1]	Miocene tephra	West Pequop Summit Q	41.09283	−114.61868	p	**15.65**	0.18	0.63	0.61	14/20	17 to 75 Ma xenocrysts
H15-39 [AS1]	Miocene tephra	Northwest Pequop Mountains	41.18124	−114.67054	s	15.18	0.04	11.3	5.1	13/16	16.8 Ma xenocrysts
Independence Valley NW											
H17-32 [AS2]	Pliocene tephra	Independence Valley NW Q	40.99053	−114.63470	s	4.46	0.24	39.3	24.3	1/24	Youngest single grain
"	"	"	"	"	"	4.84	0.79	27.1	17.3	3/24	Mean of youngest three grains
H17-66 [AS2]	Miocene tephra	Independence Valley NW Q	40.98078	−114.64449	s	**6.23**	0.02	39.4	9.3	3/23	High K/Ca group
"	Miocene tephra	Independence Valley NW Q	"	"	s	**5.87**	0.21	13.7	1.0	17/23	Low K/Ca group
"	Miocene tephra	Independence Valley NW Q	"	"	s	**6.04**	0.07	17.6	9.9	20/23	All data; 25 Ma xenocryst
H17-53 [AS2]	Miocene tephra	Independence Valley NW Q	40.95686	−114.64283	s	**8.14**	0.03	52.9	7.6	1/24	Youngest single grain, distinct from 10.3 Ma population
"	"	"	"	"	"	**10.31**	0.03	54.2	6.2	6/24	Coherent group of six grains; 14 to 39 Ma xenocrysts
WNC119-34 [AS2]	Miocene tephra	Independence Valley NW Q	40.96452	−114.64935	s	**9.84**	0.11	11.7	5.6	5/24	Best age estimate; 11 to 17 Ma xenocrysts
"	Miocene tephra	Independence Valley NW Q	"	"	p	**10.14**	0.09	0.20	0.01	11/24	Possible age
"	Miocene tephra	Independence Valley NW Q	"	"	s/p	**9.85**	0.07	3.8	6.2	16/24	Age mostly determined by sanidine data
WNC119-425 [AS1]	Miocene tephra	Independence Valley NW Q	40.96452	−114.64935	s	**10.78**	0.03	12.3	2.4	3/16	2016 analysis; dominated by 12 to 32 Ma xenocrysts
WNC119-425R [AS2]	Miocene tephra	Independence Valley NW Q	40.96452	−114.64935	s	**10.74**	0.03	14.2	2.2	3/24	2018 analysis of new mineral separate; dominated by 11 to 33 Ma xenocryts
East Humboldt Range											
H5EH-118 [AS1]	Miocene tephra	Welcome Q, Clover Creek area	41.08834	−115.08176	s	**15.62**	0.12	8.5	5.9	11/15	17 to 574 Ma xenocrysts
8713-9 [AS1]	Volcanic sandstone	Welcome Q, Clover Creek area	41.07487	−115.07893	s	23.87	0.03	289.4		1/35	Maximum age; youngest single grain distinct from 25.0 Ma population
"	"	Welcome Q, Clover Creek area	"	"	s	25.03	0.24	48.6	24.1	6/35	Maximum age from six grains; mostly 27 to 40 Ma xenocrysts.
H10-79 [AS1]	Tuff of Campbell Creek	Welcome Q, Clover Creek area	41.04325648	−115.0682496	s	28.93	0.07	54.5	5.6	16/19	Matches ages and K/Ca in Henry et al. (2012)
H13-47 [AS1]	Tuff of Big Cottonwood Canyon	Welcome Q, Clover Creek area	41.07627	−115.09308	s	**40.21**	0.02	74	18.5	8/20	Matches ages and K/Ca in Henry (2008)

Step heating						Age plateau	±2s	%^{39}Ar[5]	Isochron	±2s	MSWD	$^{40}Ar/^{36}Ari$	±2s	Integrated age	±2s
H14-107 [AS1]	Basalt clast in conglomerate	Welcome Q, Clover Creek area	41.08963	−115.01308	p	**15.46**	0.06	71.7	**15.39**	0.17	1.43	298.4	6.7	15.77	0.05
H14-92 [AS1]	Basalt lava	Welcome Q, Clover Creek area	41.08933	−115.05340	p	**15.33**	0.05	92.6	**15.28**	0.06	0.51	302.1	5	15.42	0.04
H15-34 [AS1]	Basalt dike	Welcome Q, Angel Lake	41.02343	−115.08770	p	**17.3**	0.3	87.4	NM		1.02			17.9	0.5

(1) $^{40}Ar/^{39}Ar$ analyses at the New Mexico Geochronological Research Laboratory (methodology in Zimmerer et al., 2016, and Henry et al., 2017). Neutron flux monitor Fish Canyon Tuff sanidine (FC-1) with assigned age = 28.201 Ma (Kuiper et al., 2008).
Decay constants after Min et al. (2000); $\lambda_{total} = 5.463 \times 10^{-10}$ yr^{-1}. Isotopic abundances after Steiger and Jäger (1977); $^{40}K/K = 1.167 \times 10^{-4}$.
NM = not meaningful. Ages in bold are best estimates of emplacement or eruption age.
(2) Full data tables location in brackets, either Argon Supplemental Table 1 [AS1] or Argon Supplemental Table 2 [AS2] (text footnote 1).
(3) n = number of analyses used in age calculation/total number of grains analyzed.
(4) s—sanidine; p—plagioclase.
(5) %^{39}Ar = percentage of ^{39}Ar used to define plateau age.

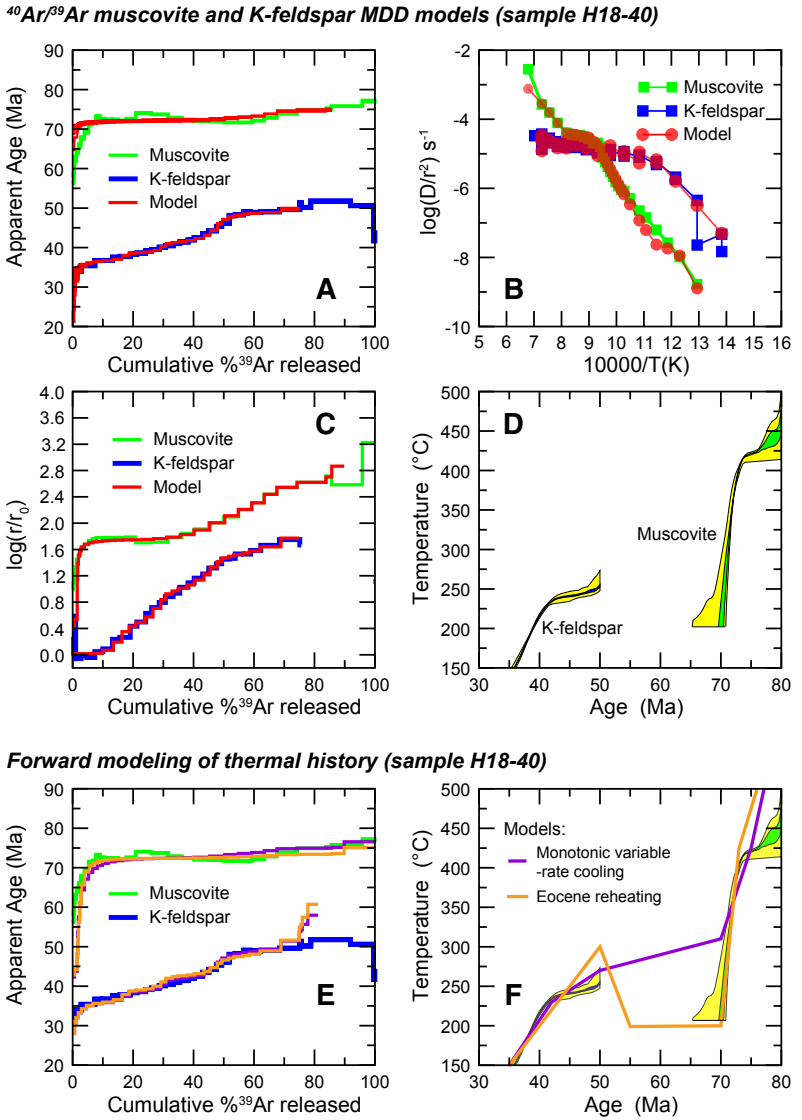

Figure 6. $^{40}Ar/^{39}Ar$ muscovite and K-feldspar multi-diffusion domain (MDD) model results from single sample H18-40 (location in Fig. 2A; N40.93581; W114.63277). (A) Measured age spectra and model spectra. (B) Arrhenius plot for measured and modeled data. In addition to the characteristic "knee" in the data, the linear slope corresponds to the activation energy, consistent with MDD behavior. (C) Log(r/r_0) plot starting at zero by convention. (D) Modeled cooling histories derived from the MDD method for these two phases that were taken from the same sample. (E–F) The predicted age spectra are shown in E, and plausible cooling paths are shown in F (i.e., monotonic variable-rate cooling versus an Eocene reheating episode).

model age spectra matching the measured age spectra show general cooling from ~400 °C at 80 Ma to ~150 °C by 35 Ma. Each mineral only constrains a part of the thermal history that is dictated by the age range revealed in their age spectra. However, we also created forward-modeled thermal histories with discrete segments with the intention of generating thermal histories compatible with both minerals (Figs. 6E and 6F). For instance, the purple line in Figure 6F that connects the muscovite and K-feldspar constrained segments demonstrates that both minerals can be well modeled with a thermal history that involves rapid cooling at ca. 70 Ma, slow cooling between 70 and 45 Ma, and rapid Eocene cooling (purple age spectra models in Fig. 6E). Similarly, a thermal history that cools to ~200 °C by 70 Ma and then reheats ~300 °C near ca. 45 Ma followed by protracted rapid cooling (orange line in Fig. 6E) yields model age spectra that closely match the measured spectra. In summary, the coupled K-feldspar and muscovite MDD analyses from the same sample suggest two main phases of cooling in the Late Cretaceous (ca. 75–70 Ma) and Eocene (ca. 40 Ma).

5.2 Apatite-Fission Track Ages

Three samples were collected (PFW 1, PFW 2, and PFW 3), and their map view configuration (within 1.5 km) and structural positions (within ~50 m stratigraphically and structurally below the Pequop fault) were close enough that we expected similar thermal histories to affect the samples (Fig. 4). Complete AFT data are presented in the AFT Supplemental Table (footnote 1) and summarized in Table 3. All samples failed a chi-squared probability test ($P(\chi^2)<5\%$; Galbraith, 1998), suggesting varying age groups with multiple kinetic populations. Dpar values are not particularly dispersive, and Dpar shows no obvious trend versus age or track length (e.g., Craddock et al., 2014; Li et al., 2019). Pooled AFT ages and mean track lengths for samples PFW1, PFW2, and PFW3 were 36.6 ± 3.8 Ma, 37.2 ± 4.8 Ma, and 23.7 ± 4.1 Ma, and 15.2 ± 1 µm, 15.1 ± 1 µm, and 15.6 ± 1.1 µm, respectively (Fig. 7; Table 3). Alone, these ages suggest that the rock

TABLE 3. APATITE FISSION-TRACK (AFT) ANALYSES

Sample	Latitude	Longitude	Ns	Pooled AFT age (Ma)	Error (1σ)	MTL (μm)	Error (1σ)	Mean Dpar (μm)	%Dpar <1.5 μm	P (χ2) (%)
PFW1	40.97812	–114.57	397	36.6	3.8	15.05	1.16	1.73	2.5	0
PFW2	40.97287	–114.575	417	37.2	4.8	15.05	0.9	1.74	5	0
PFW3	40.96679	–114.581	151	23.7	4.1	15.58	1.13	1.62	35	0

Note: MTL—mean track length; Ns—number of spontaneous tracks.

samples cooled through the AFT PAZ sometime in the late Eocene to Oligocene.

The relatively long and narrow range of track lengths implies moderately fast cooling (Fig. 7). These apparent AFT ages may not be related directly to any specific tectonic event, but rather may record residence in, or relatively slow exhumation through, the time- and space-varying PAZ (Gleadow and Brown, 2000). Therefore, we inverted the AFT ages and track-length distributions to generate a modeled thermal history for our samples (e.g., Jolivet et al., 2001; Ketcham et al., 2007). Modeling of 10,000 possible paths was conducted using the HeFTy software v1.9.1 (Ketcham, 2005), with multi-kinetic annealing and c-axis projection models of Ketcham et al. (2007). Model constraints were loosely set with initial conditions of 200–100 °C at 100–80 Ma, so that the rock samples were at or below the AFT PAZ in the Cretaceous and at 10 °C surface temperature today. All three samples show cooling below 100 °C over the 35–20 Ma range. PFW1 and PFW2 show earlier cooling (ca. 35–30 Ma) than PFW3 (ca. 25–20 Ma) (Fig. 7).

The cause of this apparent ~10 m.y. discrepancy in cooling history for samples that should have experienced similar thermal histories is unknown. Attempts to model all three samples in a single HeFTy thermal model failed to produce acceptable cooling histories. To explore this further, we investigated how variable apatite annealing kinetics may have affected the modeled thermal histories. Sample PFW3 showed the most variability in Dpar values, which ultimately reflect solubility and annealing rate (Burtner et al., 1994; Barbarand et al., 2003). Sample PFW3 had 35% of analyses with Dpar values <1.5 μm, whereas the other two samples had >96% of Dpar values >1.5 μm (Table 3; AFT Supplemental Table 1 [footnote 1]). Because

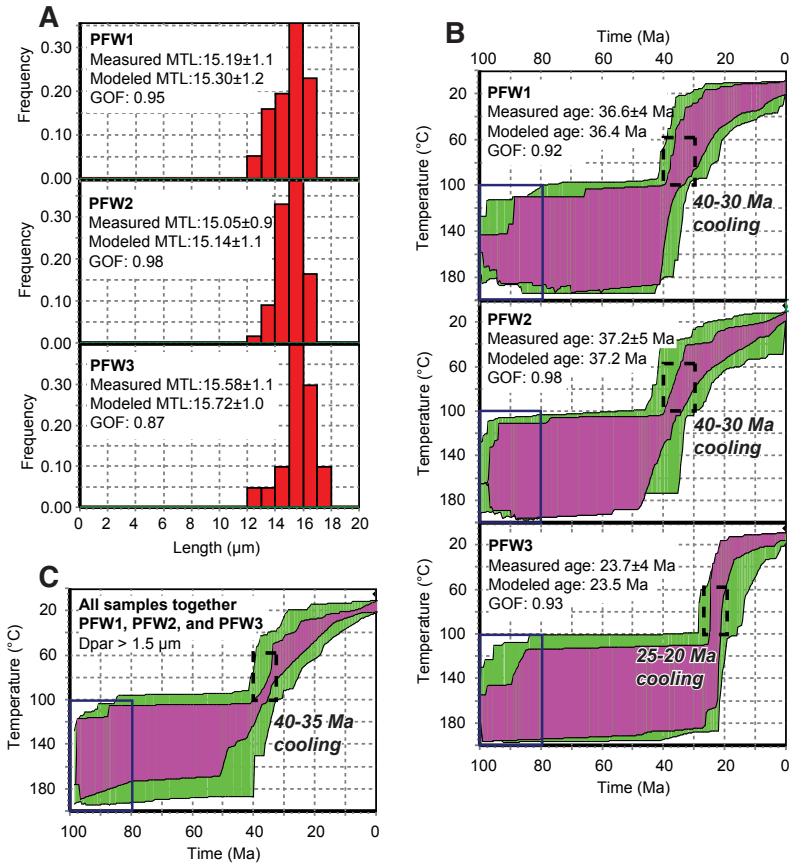

Figure 7. (A) Apatite-fission track (AFT) results from Ordovician Eureka Quartzite samples; sampling locations shown in Figure 4. (B) Individual HeFTy thermal models for the three analyzed samples: PFW1 and PFW2 show 40–30 Ma cooling, whereas PFW3 shows 25–20 Ma cooling. Green and purple envelopes represent acceptable and good model fits. (C) HeFTy thermal model of all three samples together, using only measurements with Dpar >1.5 μm. Note that no acceptable models could be generated with all of the data, but by removing measurements with Dpar <1.5 μm, acceptable and good model results were generated, showing 40–35 Ma cooling of all three samples. GOF—goodness of fit; MTL—mean track length.

lower Dpar values are indicative of lower resistance to annealing, or faster annealing rates, in apatite grains, these low Dpar measurements are best optimized in a thermal model with higher temperatures or later cooling. Modeling all three samples together using only Dpar values >1.5 μm yielded a very good model fit with 40–35 Ma cooling (Fig. 7C). We prefer this modeled thermal history because it (1) fits all three samples that were expected to share a compatible thermal history and (2) involves reasonable evaluation of the different kinetic populations in our samples. Additional confirmation comes from comparison with the K-feldspar MDD models discussed above. The structural position of the Ordovician Eureka Quartzite (Oe) AFT samples is higher than the K-feldspar MDD samples, but the two modeled Cenozoic thermal histories are compatible. The K-feldspar MDD models document cooling from ~250 °C to 150 °C at 40–35 Ma, and the AFT analyses suggest cooling to <100 °C over this timeframe (Figs. 6 and 7). Within the modeled uncertainty bounds and the different structural positions, these histories demonstrate significant post–40 Ma cooling.

5.3 $^{40}Ar/^{39}Ar$ Ages from Igneous and Sedimentary Rocks

We provide 16 new $^{40}Ar/^{39}Ar$ ages from Cenozoic rocks in the REWP region (Table 2). Single crystal analyses were conducted on sanidine or plagioclase grains, and step heating was done of three basalt samples (Table 2). Age interpretations are summarized in Table 2, including our interpreted eruption or depositional ages in bold. Below, these ages are discussed in relation to their geologic and stratigraphic context.

First, new dates bracket the age of the Clover Creek stratigraphic sequence (Fig. 5; McGrew and Snoke, 2015). The lowest several hundred meters of the overall section consist of Eocene (40.2 Ma tuff of Big Cottonwood Canyon; sample H13-47 in Table 2) and Oligocene (28.9 Ma tuff of Campbell Creek; sample H10-79 in Table 2) rhyolite ash-flow tuffs, andesitic flows, and volcanic conglomerate unconformable on non-metamorphosed Permian strata. Above the tuff of Campbell Creek, $^{40}Ar/^{39}Ar$ dating of detrital sanidine in a volcanic sandstone that underlies the rock-avalanche deposits by 3 m constrains these deposits to be younger than 25.0 Ma or 23.9 Ma (sample 8713–9 in Figs. 2 and 5; Table 2). The former age is the weighted mean of six sanidine grains that have similar K/Ca (Table 2); the latter is a single youngest grain with a distinctly higher K/Ca of 289 (not used in the mean of the six grains). We are reluctant to rely on a single grain, but the sandstone is younger than 25 Ma.

The upper >2 km of the Clover Creek section is middle Miocene and younger based on $^{40}Ar/^{39}Ar$ ages of (1) 15.62 ± 0.12 Ma (sample H5EH-118; Table 2) on tephra in a sedimentary sequence previously assigned to the "lower Humboldt formation"; (2) 15.25 ± 0.04 Ma on rhyolite lava (M. Brueseke, personal commun. in McGrew and Snoke, 2015); and (3) 15.33 ± 0.05 Ma on basalt lava that overlies the rhyolite (sample H14-92; Table 2; Fig. 5).

We dated undeformed, vertical tholeiitic basaltic dikes that cut mylonitized Prospect Mountain Quartzite in the metamorphic core complex at Angel Lake, East Humboldt Range, in the footwall of the major west-directed shear zone and detachment fault (field photographs in Fig. S1 in Supplemental Text [footnote 1]). A plagioclase megacryst from one dike yielded a plateau age of 17.3 ± 0.3 Ma representing 87.4% of released ^{39}Ar (sample H15-34 in Fig. 2; Table 2).

The last set of new $^{40}Ar/^{39}Ar$ analyses was conducted on Miocene deposits of the Humboldt Formation along the western flank of the Pequop Mountains (Camilleri, 2010a; Camilleri et al., 2017) (Table 2). The oldest dated tephra in the Pequop Mountains give ages of 15.65 ± 0.18 and 15.18 ± 0.04 Ma in two locations along the west and northwest flanks of the range (samples H14-78 and H15-39; Fig. 2; Table 2; Henry and Thorman, 2015). $^{40}Ar/^{39}Ar$ ages on tephra in the Independence Valley NW quadrangle (IVNW; Fig. 2A) range from 10.8 Ma to <4.6 Ma (Table 2). Precise ages of some tephra are uncertain because they contain multiple age populations that must include xenocrysts. For example, sample H17-53 contains a coherent group of 6 grains that yield an age of 10.31 ± 0.03 Ma and a single 8.14 ± 0.03 Ma grain (Table 2). Stratigraphic relationships permit either age. The oldest dated tephra (10.8 Ma), from drill hole WNC119 (Fig. 2; Plate 1), was collected 3 m above the base of the sequence, which rests on Paleozoic rocks (Table 2; Zuza et al., 2019a).

5.4 U-Pb Dating of Foliated Granite

Nineteen U-Pb analyses (Fig. 8) of zircon from foliated granite sample H14-82 from Meyers Canyon (location in Fig. 2 and sample photograph in Fig. 9C) yielded 17 concordant ages spanning 152 Ma to 162 Ma (Zircon Supplemental Table 1 [footnote 1]; Fig. 8). The weighted-mean age of all concordant analyses was 156.7 ± 1.3 Ma (MSWD = 4.8). Our preferred age interpretation is based on the main population of 13 analysis, which yielded a weighted-mean age of 155.6 ± 0.8 Ma (MSWD = 1.4) (Fig. 8). Either interpretation suggests a ca. 155–157 Ma age for this foliated granite, which overlaps the 154 ± 5 Ma age reported by Camilleri and Chamberlain (1997).

6. STRUCTURAL OBSERVATIONS IN THE PEQUOP MOUNTAINS

The following description of structures across the Pequop Mountains builds on published mapping by Thorman (1962) and Camilleri (1994). This summary describes the geology in our compiled geologic map in Plate 1.

6.1 Range Structure

Paleozoic bedding and tectonic foliations across the northern Pequop Mountains primarily strike north-northeast and dip east-southeast (Fig. S2 [footnote 1]; Plate 1). Two west-dipping, north-striking map-scale normal faults bound the western flank of the range (Fig. 2). The easternmost of these normal faults (named the eastern range-front fault in Fig. 2B) has late Cenozoic basin deposits dipping ~15° east in its hanging wall; one anomalous location shows an ~34°E dip (Plate 1;

Fig. 2). Borehole data indicate this eastern fault dips ~35° west, which would restore to an original dip of ~50° west when accounting for the 15° east dip of the late Cenozoic sediments in its hanging wall. The western range-front normal fault (Fig. 2B) has been more recently active, offsetting latest Pleistocene fan surfaces with fault scarps up to ~3 m. Gravity modeling (Saltus and Jachens, 1995) suggests that the Independence Valley, just west of the Pequop Mountains, contains ≥2 km of Cenozoic sediments, which is consistent with ≥3 km of slip on the western range-front normal fault. Restoration of displacement on the eastern range-front normal fault, including Paleozoic stratigraphy, the Independence thrust, and the Pequop fault observed in borehole WNC119, documents at least ~3 km of west-side down displacement (Fig. 2B). Normal faulting on the eastern flank of the northern Pequop Mountains (Plate 1), and basin sedimentation in Goshute Valley, was negligible as evidenced by drill-core data and range morphology (Zuza et al., 2019a).

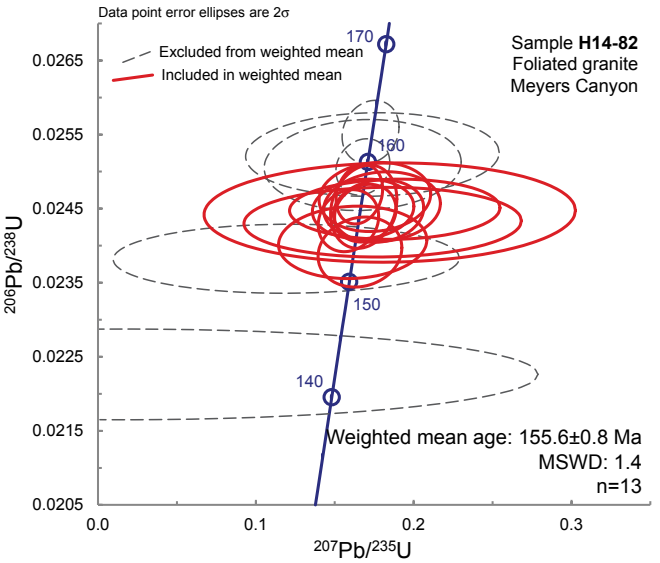

Figure 8. U-Pb concordia diagram of zircon analyses from sample H14-82 (N40.99429, W114.61276). Red ellipses included in weighted-mean calculations, and gray dashed ellipses were excluded. Plot created with Isoplot 4.1 of Ludwig (2003). MSWD—mean square of weighted deviates.

The northernmost part of the Pequop Mountains contrasts with the rest of the range in that Paleozoic and middle Miocene rocks roll over to moderate (~40°) northwest to west dips, forming a northeast-trending anticline (in the Pequop Summit quadrangle, Fig. 2A; Plate 1). West dips continue northward into Paleozoic, Eocene, and Miocene rocks in the Windermere Hills, which are bounded on the east by a major, east-dipping normal fault (Mueller, 1993; Mueller et al., 1999; Henry and Thorman, 2015) (Fig. 2A). We interpret this to be an extensional anticline formed by the propagation of oppositely dipping normal faults in an antithetic accommodation zone (Faulds and Varga, 1998). The west-dipping, range-bounding faults of the Pequop Mountains propagated northward, whereas the east-dipping, range-bounding fault of the Windermere Hills propagated southward. Opposite tilts of strata in their footwalls generated the northeast-trending anticline. Camilleri and Chamberlain (1997) and Camilleri (2010a) interpreted the anticline to be related to a Mesozoic northwest-vergent thrust fault, with an overturned anticline in the Wood Hills linking northeastward across the Independence Valley to the anticline in the northern Pequop Mountains. However, involvement of middle Miocene rocks in tilting suggests the anticline most likely formed during middle Miocene extension.

High-angle, mostly west-dipping normal faults are observed within the range and offset the Paleozoic stratigraphy and other major structures. Most of these faults have minimal stratigraphic offset, but several have offsets of hundreds of meters, such as a north-striking, down-to-the-east normal fault (labeled "north fault" in Fig. 4) mapped near Meyers Canyon (different from the "Meyers Canyon fault" of Thorman, 1970, and Henry and Thorman, 2015). Although exposures of Ordovician Eureka Quartzite across the north fault imply apparent down-to-the-west motion, the formation is at different structural levels (Fig. 4). Specifically, Eureka Quartzite has contrasting deformational styles across the fault. The Oe in the hanging wall of this fault is entirely brecciated with no coherent bedding, whereas the footwall Oe is a significant north-trending cliff-forming unit across the western flank of the range (Fig. 4) with well-developed stretching lineations. The spatial distribution of brecciated Oe is not concentrated around the north-striking "north fault," and therefore we interpret that proximity to the normal fault is not the primary cause of brecciation. Instead, the brecciated Oe may have developed at a higher and colder structural level than the intact Oe, and during either Mesozoic contraction or Cenozoic extension, the colder brittle unit brecciated, whereas the hotter unit did not. The structurally higher Oe is in the hanging wall of the Pequop fault, whereas the structurally lower Oe is in the footwall (Plate 1). Regardless of the interpretative mechanism, the quartzite units on either side of the north fault are distinctly different, and thus we infer they originated from different structural levels.

Preliminary microstructural observations from quartzite outcrops in the northwest corner of Figure 4 further corroborate different structural levels. The rock in Figure 4C was collected from a well-lineated cliff (lineation trend/plunge: 115/06) (C in Fig. 4B). Quartz grains are highly interlobate, suggestive of grain-boundary migration recrystallization (GBM), which may have operated at temperatures of 500–700 °C (e.g., Jessell, 1987; Stipp et al., 2002). This temperature range is approximate given the dependence on water content, grain size, bounding grains, and strain

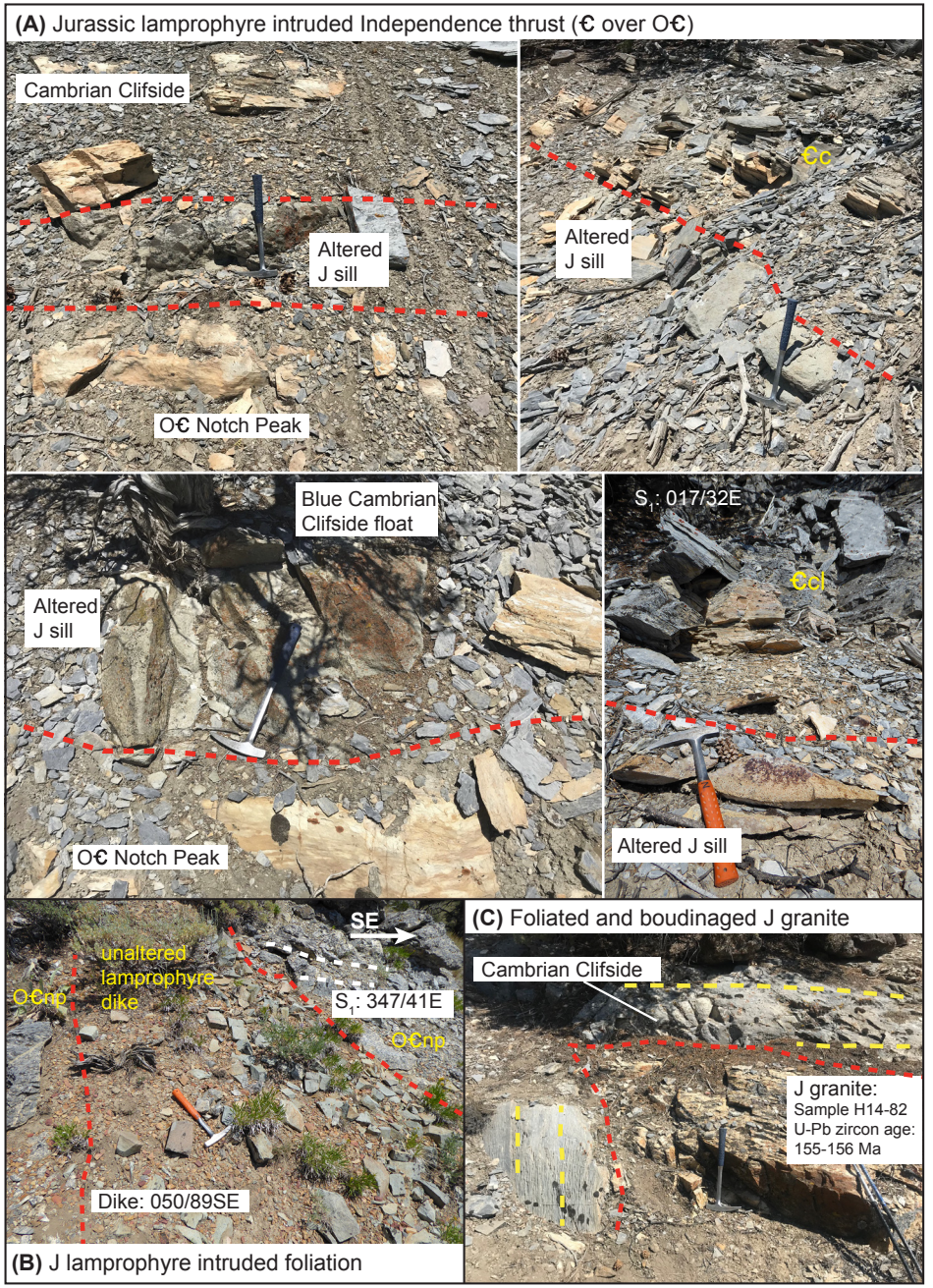

Figure 9. Field photographs of Jurassic intrusions in the Pequop Mountains, modified from Zuza et al. (2020a). (A) Jurassic lamprophyre intruded into the Independence thrust, where it places Cambrian Clifside Limestone (Єcl) over Cambrian–Ordovician Notch Peak Formation (OЄnp). All photos except bottom right from 114.6176W, 40.9390N; bottom right in this panel from 114.6161W, 40.9347N. (B) Unaltered undeformed Jurassic lamphrophyre dike crosscuts OЄnp foliation. Location: 114.59564W, 40.93222N. (C) Boudinaged Jurassic granite surrounded by Єcl marble. Note that marble flows around the granite as it pinches out. Location: 114.61275W, 40.99429N.

rate. The rock in panel Figure 4D was collected from a recessive exposure of brecciated Oe (D in Fig 4B). The quartz in the sample shows polygonal fabric with relatively straight grain boundaries and no undulose extinction, suggestive of static recrystallization (Fig. 4D). This sample is also cut by brecciation, as observed in outcrop and thin section. We refrain from further interpretation of these samples, but note their distinct difference in deformation style, from dynamic recrystallization west of the north fault to static recrystallization east of this fault (Fig. 4).

6.2 Independence Thrust

The Independence thrust is the largest mapped contractional structure in the Pequop Mountains and one of the most complete thrust structures in the REWP. The fault surface is relatively poorly exposed, but its trace traverses the range, with older rocks directly overlying younger rocks (Plate 1). On the eastern flank of the range, where the thrust is best exposed, Ordovician Pogonip Group is juxtaposed over Mississippian Chainman Shale (Plate 1). The fault involves ≥2 km stratigraphic separation, generally placing lower Paleozoic rocks over middle Paleozoic strata (Plate 1). Within ~35–50 m of the fault, rocks become highly strained, commonly exhibiting southeast-trending lineations (Fig. S2 [footnote 1]) and southeast-directed shear. Most of the mapped Independence thrust exhibits ramp relationships, with occasional flat geometries observed in the Clifside, Shafter, Dunderburg, and

Notch Peak–Pogonip units. The fault cuts upsection to the southeast, consistent with an inferred southeast transport direction. Stratigraphic offset along the fault is typically ~2 km, although below we discuss how transport-parallel stretching of the wall rock makes this estimate variable.

In two localities along the western flank of the range, the Independence thrust is intruded by weakly foliated and altered lamprophyre sills (Fig. 9A). These sills are not dated—they yielded no zircon and are too altered for other chronology methods—but they are petrographically and geochemically indistinguishable from well-dated 160–157 Ma lamprophyres in the Pequop Mountains and throughout northeastern Nevada (Ressel and Henry, 2006; Milliard et al., 2015; Zuza et al., 2018, 2019a, 2020a). Accordingly, the Independence thrust predates the probable 160–157 Ma intrusion.

6.3 Pequop Normal Fault

The Pequop normal fault appears to result in ~3 km of stratigraphic omission, juxtaposing Permian rocks over Ordovician (Figs. 3 and 4). The Pequop fault, its hanging-wall strata, and the footwall rocks are subparallel, dipping ~30° east (Zuza et al., 2018) (Fig. 4). The hanging wall of this normal fault, referred to herein as the Pequop plate, contains the older thrust relationship of Ordovician–Mississippian strata thrust over Permian rocks (red thrust fault in Fig. 4). This older thrust fault was originally named the Meyers Canyon fault (Thorman, 1970; Henry and Thorman, 2015) because it was mapped westward to Independence Valley through Meyers Canyon (Fig. 4). However, new mapping (Zuza et al., 2019a) reinterprets that this structure is truncated to the west by the Pequop normal fault (Fig. 4; Plate 1), and thus does not project westward into Meyers Canyon. Therefore, we abandon the name "Meyers Canyon fault." The thrust relationships of this aforementioned fault involve approximately 2 km stratigraphic separation (Fig. 4), which is similar to the Independence thrust, discussed above, and therefore we interpret that the Pequop plate contains a structurally higher part of the Independence thrust (Fig. 4). This relationship implies that Pequop normal faulting displaced an earlier structural geometry of the Independence thrust.

The Jurassic Independence thrust-hanging wall within the Pequop plate is incised by the Nanny Creek paleovalley infilled by Eocene (41.0–39.5 Ma) volcanic rocks (Brooks et al., 1995; Henry, 2008; Henry et al., 2011) (Fig. 2A; Plate 1). The Eocene rocks are roughly subparallel to Mississippian, Pennsylvanian, and Permian strata on the sides of the paleovalley. This relationship suggests that these Paleozoic rocks were subhorizontal in the Eocene during or prior to Nanny Creek paleovalley incision and Eocene deposition, but after major thrust faulting.

6.4 Intra-Formational Deformation

Stratigraphic contacts on the geologic maps are generally parallel (Plate 1) (e.g., Thorman, 1962, 1970; Camilleri, 2010a; Henry and Thorman, 2015; Zuza et al., 2018, 2019a), misleadingly portraying undeformed stratigraphy. However, the Paleozoic units are variably internally deformed by bedding-parallel faulting, local boudinage development, shearing, outcrop-scale thrust faulting, and folding (Fig. 10). Deformation is strongly partitioned to the mechanically weaker horizons, such as the shales (and metamorphic phyllite and schist equivalents) and calcite marbles, with the more competent beds not noticeably deformed. Granitoid, quartzite, chert, and dolomite rocks are boudinaged with weaker calcite marble flowing around them (Figs. 10A and 10B). Map-scale boudinage is observed across the range: Ordovician Kanosh Quartzite disappears for tens to hundreds of meters along strike, with limestone layers flowing around the quartzite outcrops (Zuza et al., 2018) (Plate 1). Dolomite within the Ordovician–Cambrian Notch Peak Formation exhibits similar outcrop- to map-scale boudinage encased in limestone (Plate 1) (Camilleri, 2010a; Zuza et al., 2018). Well-developed stretching lineations, asymmetric shear fabrics, and boudinage across the range are consistent with northwest-southeast stretching and/or top-southeast shear (Figs. 10 and S2 [footnote 1]). In particular, top-southeast shear is observed in most of the lower Paleozoic rocks across the range (Fig. 10D).

The lower Paleozoic section shows variable strain partitioning, with some competent layers showing little to no evidence of deformation, preserving, for example, chaotic soft sediment deformation restricted to meter-scale beds and completely undeformed algal mats (e.g., Hellbusch, 2012). Other nearby layers show strongly sheared fabrics and isoclinal folds (Fig. 10). Most observed fold hinges trend northeast, consistent with top-southeast shear, but local fold hinges of recumbent isoclinal folds in Ordovician–Cambrian units trend east to south (Fig. 10E), with no discernable pattern to their inclination or vergence. These anomalous fold hinges are subparallel to the predominant southeast-trending lineation observed across the range (Fig. S2 [footnote 1]), and we interpret them as local *a*-type folds (Malavieille, 1987) that are consistent with the dominant observations of top-southeast shearing.

Brittle structures, such as outcrop-scale thrust faults, in the Paleozoic stratigraphy show similar kinematics of top-southeast shear. For example, a fault-bend fold within Ordovician Pogonip Group has 059°-trending fold hinge and southeast vergence (Fig. 10C). In another locality, a cliff face of Devonian Guilmette Formation exhibits numerous thrust faults in a complex duplex fault system (Fig. 11). Observed striations from these faults trend southeast, faults display horizontal to northwest dips, and faults are southeast-directed. A simple line-length restoration of this outcrop suggests minimum shortening strain of 25%–30% (Fig. 11). A west-directed thrust fault is observed along Interstate 80 in the Devonian Guilmette Formation (Fig. 10F). The stratigraphically highest units show open folds (Plate 1). Bedding plane slip is present at many stratigraphic levels and commonly difficult to recognize except in ideal exposures (Fig. 10G in the Pequop Formation). Some beds are sharply truncated, and omitted, at the outcrop scale, suggesting extensional bedding-parallel attenuation affected the rocks in the Pequop Mountains. Because the structural thickness of the Neoproterozoic–Triassic rocks is similar to the regional stratigraphic

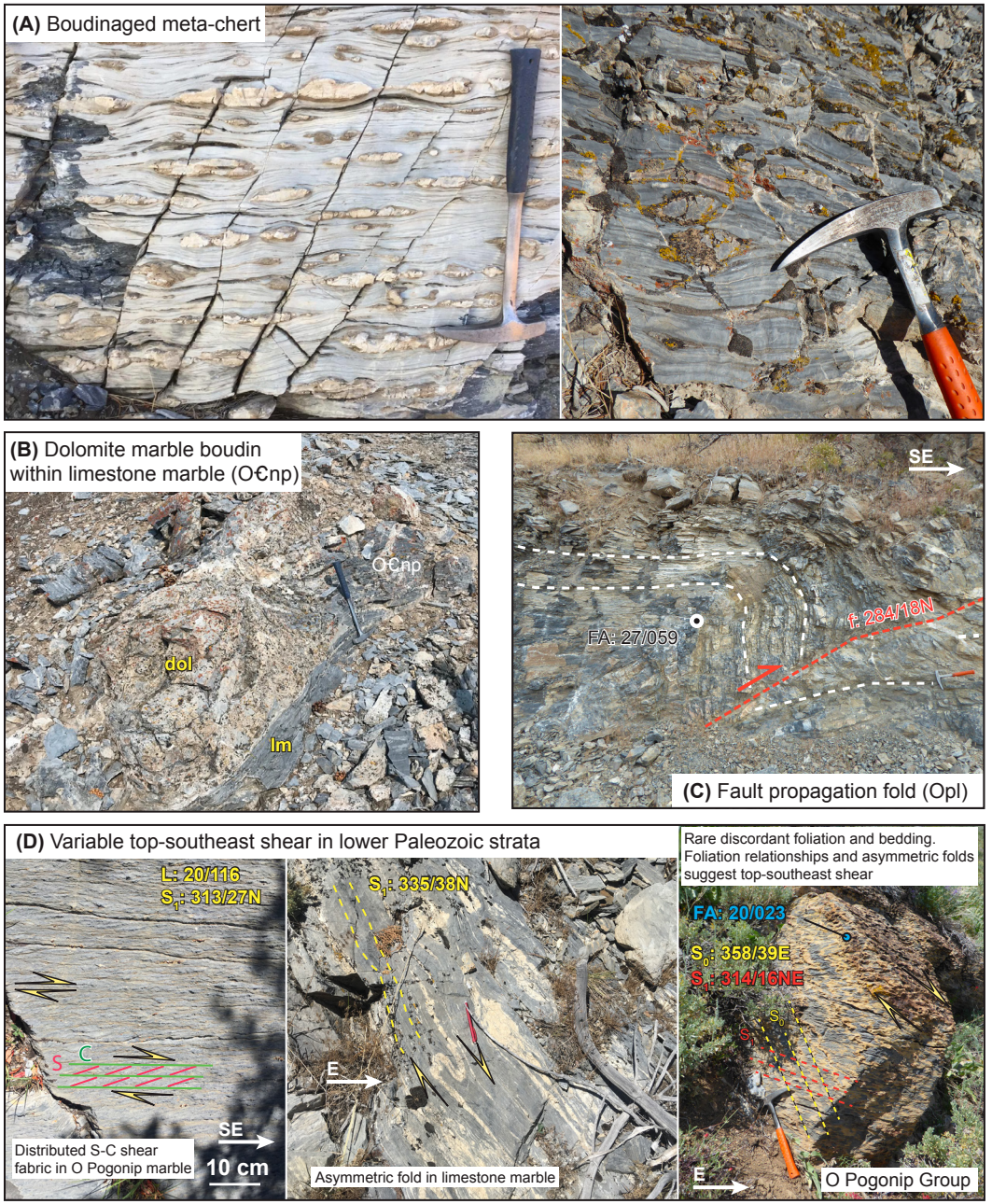

Figure 10. Field photographs of variable deformation in the Pequop Mountains. (A) Boudinaged meta-chert in O€np showing SE stretching, with the right photo showing top-SE shear; (B) dark calcite marble (lm) flowing around more rigid dolomite (dol) marble boudin; (C) southeast-directed thrust faulting (f) within the Cambrian–Ordovician rocks; (D) variable expressions of pervasive top-southeast shear observed across the range; and (E) isoclinal folds with variable shallowly plunging fold axes (FA). Locations: (A) –114.636513W, 40.914893N; (B) 114.61808W, 40.938775N; (C) 114.600652W, 40.975283N; (D) (left to right) 114.59328W, 40.97021N; 114.61262W, 40.994288N; 114.576177W, 40.94675N. (E) (left to right) 114.640088W, 40.932855N; 114.615102W, 40.967954N; 114.602142W, 40.932022N; (F) 114.59252W, 41.07429N; (G) 114.58844W, 41.13150N; (H) ~114.560056W, 41.074889N. (*Continued on following page.*)

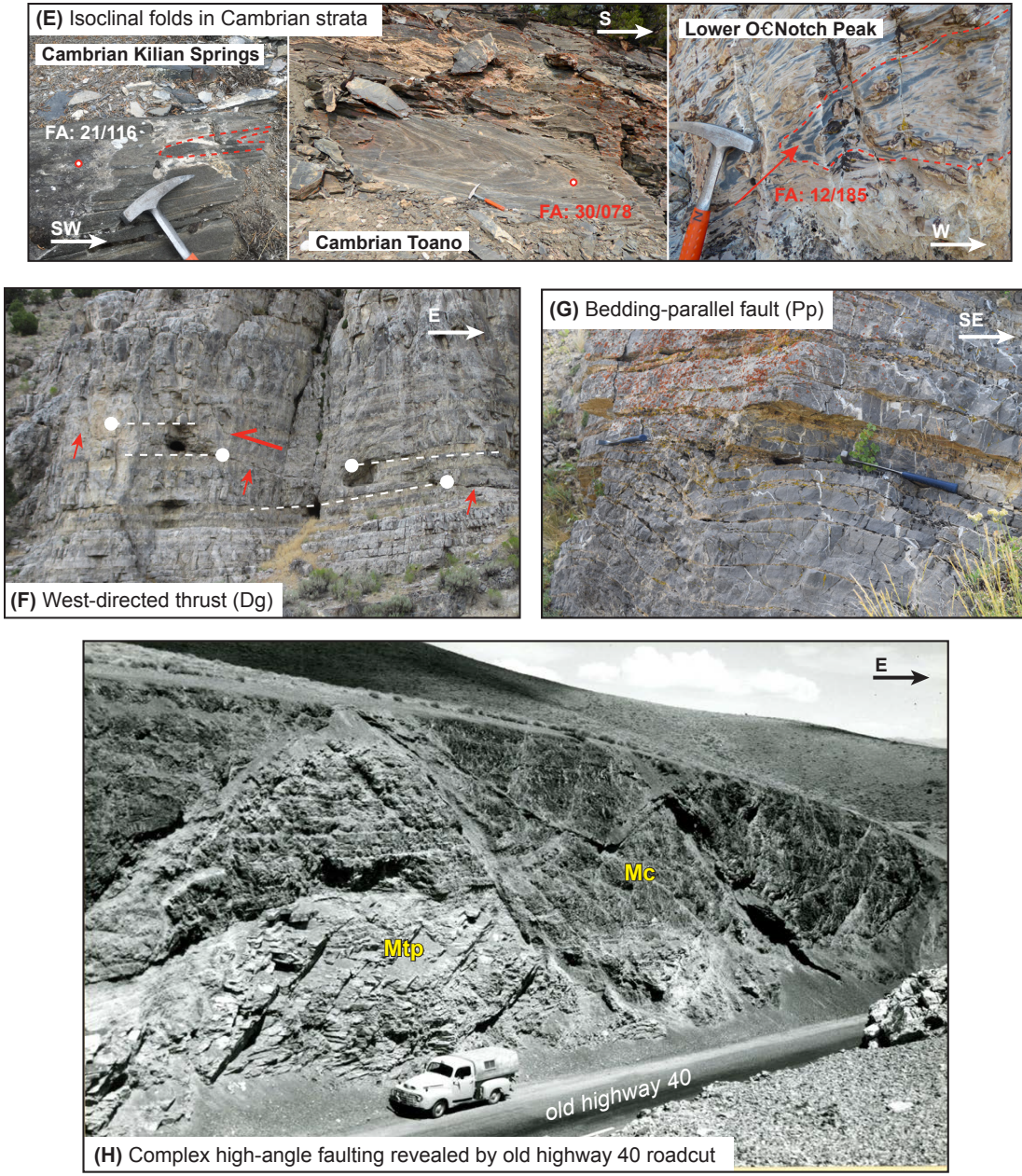

Figure 10 (*continued*). (F–H) Other structural complexities within the range include (F) west-directed reverse faulting in the Devonian Guilmette Formation north of Interstate 80 (red arrows point to fault; white dashed lines are offset marker beds; 0.5–1.0 m tall sagebrush for scale); (G) bedding-parallel fault in the Permian Pequop Formation that omitted section (note bed pinchout marked by two rock hammers); and (H) complex high-angle normal faulting that is missed without fortuitous road cuts (photo from 1961; view no longer exists due to modern highway construction). Mtp—Mississippian Tripon Pass; Mc—Mississippian Chainman Shale.

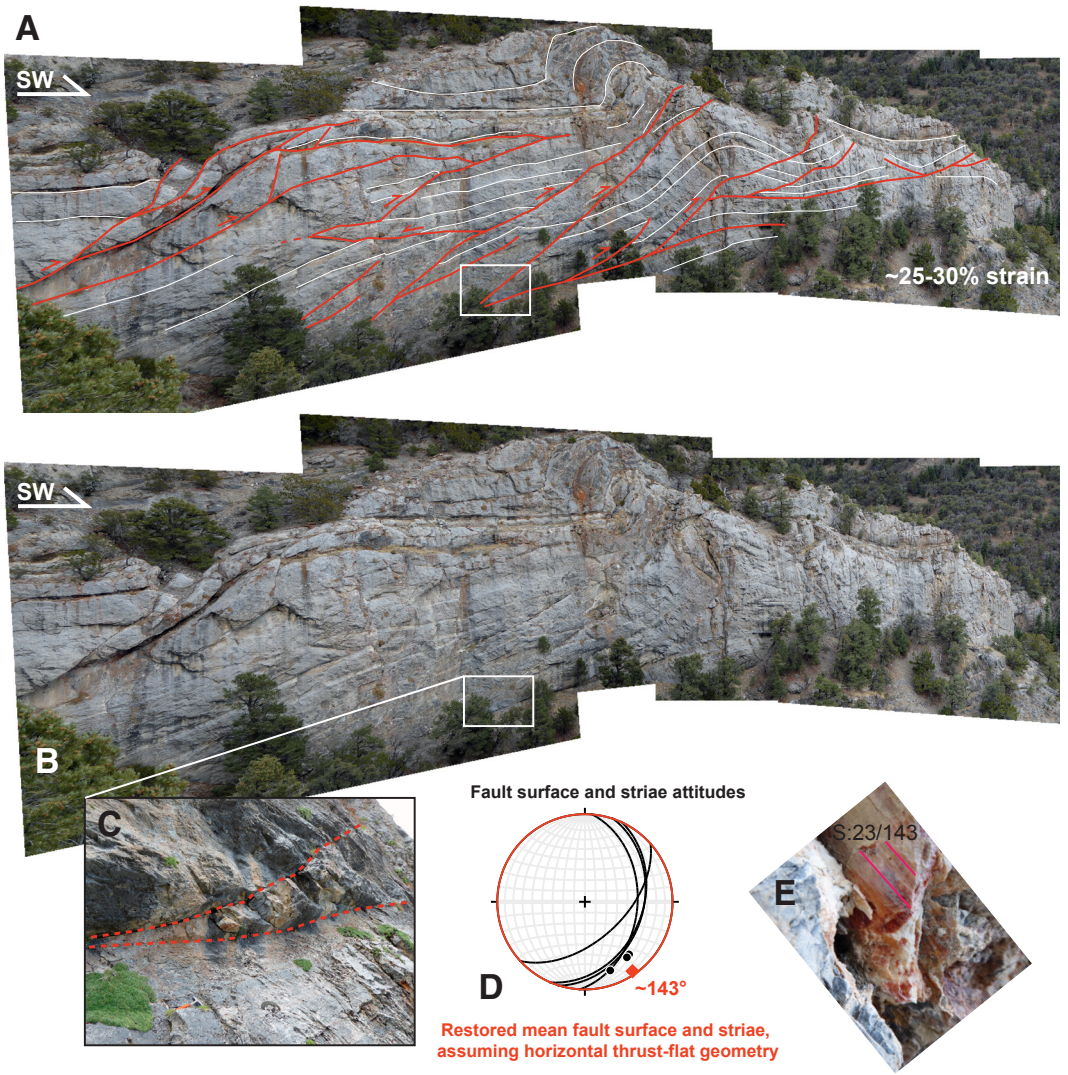

Figure 11. Thrust faulting and duplex development in the Devonian Guilmette Formation. (A) Interpreted and (B) uninterpreted collage of field photographs showing southeast propagating thrust faults and duplexes that correspond to ~25%–30% shortening strain based on line-length balancing. (C) Close-up view of some of the thrust faults. Note orange hammer for scale, which provides relative scale for cliff exposure. (D) Stereonet showing fault attitudes (planes) and fault striations (lines) from basal subhorizontal faults. Restoration of Cenozoic tilting (see text for discussion) brings the fault planes to subhorizontal during faulting; restoring the average thrust plane to horizontal yields a restored mean striae orientation (red). (E) Fault striations on a thrust fault surface.

thickness (Fig. 3), Mesozoic contractional deformation of the bedrock units (e.g., folding and faulting) appears to have been of similar magnitude to later extension, thinning, and unit attenuation (e.g., boudinage, attenuation faulting). Figure 10H shows high-angle faults that drop stratigraphically higher Mississippian Chainman Shale over Mississippian Tripon Pass Limestone.

7. TEMPERATURE-DEPTH CONSTRAINTS TO TEST DEEP BURIAL MODELS

Peak temperature estimates from rocks across the range are used to reconstruct the paleo-geothermal gradient, which can test hypotheses of deep burial. Thorman et al. (2019) and Zuza et al. (2020a) presented a compilation of new and published conodont alteration index (CAI), calcite-dolomite thermometry, and Raman spectroscopy on carbonaceous material (RSCM) plotted against structural depth (Fig. 12). Here we add semiquantitative temperature estimates from thermochronology and field-based petrologic observations.

In the Long Canyon deposit, disturbed biotite $^{40}Ar/^{39}Ar$ spectra and well-defined hornblende plateaus for intrusive samples that cut Ordovician Pogonip Group, as discussed in section 4.2 (Zuza et al., 2020a), suggest that this region experienced temperatures close to 300 °C. These temperature estimates are imprecise but consistent with the other available estimates (Fig. 12). The abundance of tremolite and lack of diopside observed within the Cambrian Kilian Springs siliceous carbonate rocks (e.g., Thorman, 1962; Camilleri and Chamberlain, 1997; Zuza et al., 2019a) suggests temperatures between 500 and 600 °C, depending on X_{CO2} (Spear, 1993) (Fig. 12), in agreement with the presence of titanite and absence of rutile (e.g., Frost et al., 2001).

The lack of appropriate rock types in the northern Pequop Mountains precludes reliable pressure estimates (e.g., Camilleri and Chamberlain, 1997). The equilibrium conditions of observed metamorphic minerals are more strongly controlled by temperature than pressure, and garnet-bearing rocks do not have the right assemblages for traditional net-transfer barometry. Camilleri and Chamberlain (1997) inferred pressures of ~5 kbar for the Z€pm based on the assertion that the Pequop fault "duplicates much of the Paleozoic section" (p. 82) to bury the metamorphic strata. Thorman et al. (2019) demonstrated that CAI data showed the stratigraphic section was never buried more than its normal stratigraphic depth. The Independence thrust relationships suggest ~2 km of structural overburden (Fig. 2B). An indirect check of these estimates is their implied geothermal gradient. If Z€pm experienced temperatures of 500 °C, and ~5 kbar equates to ~19 km depth (ρ: 2.7 g/cm³), this implies a geothermal gradient of ~26 °C/km during metamorphism. Although this value is possible, the peak-temperature versus depth data set (Zuza et al., 2020a; updated in this study) suggests higher gradients of 40+°C/km (Fig. 12), which correlates with other geothermal gradient estimates across the eastern Great Basin (e.g., Miller and Gans, 1989; Hurlow et al., 1991; Hudec, 1992; Howland, 2016; Long and Soignard, 2016). For context, surface heat-flow estimates for the modern REWP region and broader Great Basin region are 100–150 mW/m² (e.g., Lachenbruch, 1979; Blackwell et al., 2011), which equates to geothermal gradients of 30–50 °C/km assuming convective heat transfer, reasonable thermal diffusivity, and heat production values. As modern analogs, heat flow in the

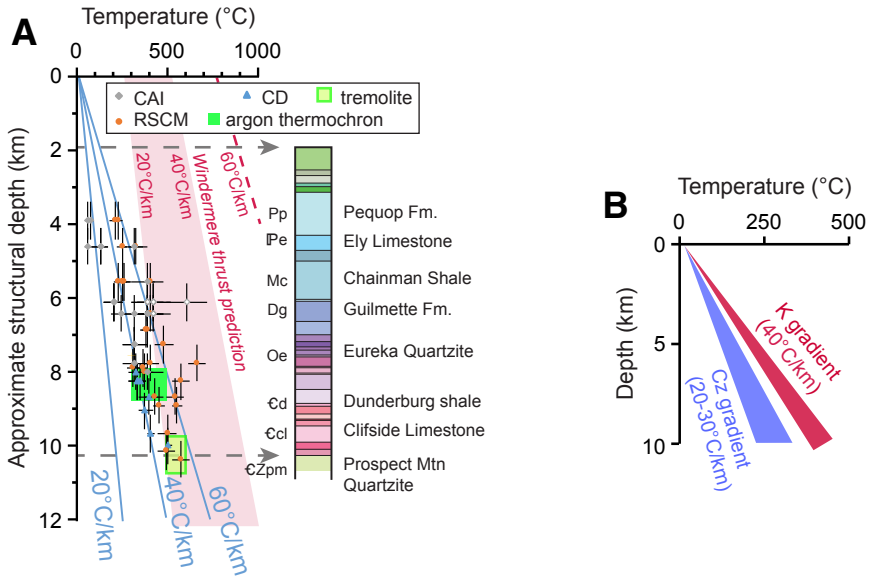

Figure 12. (A) Stratigraphic depth (0.5 km uncertainty) versus peak temperature (T_p) across the Pequop Mountains. Note that ~2 km thickening is invoked based on mapped Independence thrust relationships; see text. Accompanying stratigraphic column (same vertical scale) shows observed thicknesses (Zuza et al., 2018, 2019a). Data: Conodont color alteration index (CAI) (Zuza et al., 2020a); Raman spectroscopy on carbonaceous material (RSCM) (Zuza et al., 2020a; Howland, 2016); calcite-dolomite thermometry (CD) (Howland, 2016); quartz recrystallization microstructures (Latham, 2016; this study); argon thermochronology (Zuza et al., 2019a); the presence of metamorphic tremolite (this study). CAI data with white symbol and gray outline are interpreted to have been affected by hydrothermal fluids. Predicted thermal structure assuming Windermere thrust hypothesis is shown in red for three reasonable thermal gradients. (B) Estimates for geothermal-gradient evolution through time based on available thermochronology data (Zuza et al., 2019a). K—Late Cretaceous; Cz—Cenozoic.

Himalaya and its hinterland (i.e., near Lhasa) are >100 mW/m², often >150 mW/m² (Francheteau et al., 1984; Derry et al., 2009), and most of the thickened Andes has >100 mW/m² (Cardoso et al., 2010). In our view, models that require low Cretaceous geothermal gradients (≤25 °C/km) are unreasonable given the voluminous intrusions in eastern Nevada and drawing from other orogenic plateau analogs, but without more direct pressure constraint, peak depth estimate remains speculative.

8. DISCUSSION

To interpret the complex geology of the Pequop Mountains and the broader REWP, we first provide our constraints on Cenozoic extension that affected the region, which allows for a reconstructed framework for us to base interpretations for Mesozoic deformation. We then present a simple kinematic model (Figs. 13 and 14) that adheres to known field observations and places this work in a broader tectonic context.

8.1 Constraints on Cenozoic Extension in the Broader REWP

The timing of initial Cenozoic extension and exhumation in the REWP is debated. West-directed shearing and mylonitization of ca. 29 Ma granite in the East Humboldt Range suggests that normal-sense motion initiated after this time (Wright and Snoke, 1993; McGrew and Snoke, 2015; McGrew, 2018; Zuza et al., 2020b). Low- to medium-temperature thermochronology (i.e., zircon and apatite helium and mica $^{40}Ar/^{39}Ar$) data sets from the REWP suggest Oligocene–Miocene cooling may have been associated with exhumation (e.g., Gifford, 2008; McGrew and Snoke, 2015; Wolfe, 2016; Gonzalez et al., 2019; Metcalf et al., 2019; Mueller, 2019). The long-standing issue with Oligocene extension in this region is the lack of significant coeval basin deposits (e.g., Henry et al., 2011). The Clover Creek stratigraphy in the East Humboldt Range contains rock-avalanche megabreccia deposits with a previously ambiguous Oligocene–Miocene age that has been used as evidence for possible Oligocene extension (e.g., McGrew and Snoke, 2015; Camilleri et al., 2017). We provided updated ages for the Clover Creek stratigraphy (Fig. 5) that better constrain any potential for Oligocene extension-related deposits.

The lowest part of the Clover Creek section consists of concordant ca. 40.2 Ma tuff of Big Cottonwood Canyon and ca. 28.9 Ma tuff of Campbell Creek (Fig. 5). Above this, rock-avalanche deposits are constrained to younger than 25.0 Ma (or 23.9 Ma) (Table 2). Molluscan fauna (*Biomphalaria pseudoammonius*) from limestones in an unspecified part of the section were tentatively interpreted to be Eocene to Oligocene (Good et al., 1995). However, only limestone below the megabreccia-bearing zone could be that old (Fig. 5). These new dates leave an ~700-m-thick megabreccia-bearing section constrained only as younger than 25.0 Ma (or 23.9 Ma), which may be evidence for Oligocene extension, or alternatively, available age constraints allow the megabreccia to be ca. 16 Ma and simply the oldest part of middle Miocene extensional basin fill (Fig. 5). The entire Clover Creek section dips equally steeply to the east-northeast (McGrew and Snoke, 2015; our observations). The lack of fanning of dips or angular unconformities suggests little, if any, deformation during deposition of the Clover Creek sequence. The presence of megabreccia is not age diagnostic. Megabreccia blocks up to 230 m long are abundant in ca. 10 Ma deposits along the west side of the Pequop Mountains (Zuza et al., 2019a). Megabreccia along the west side of the Wood Hills (Thorman, 1970) is only constrained as older than ca. 12 Ma (Camilleri, 2010b). Further investigation, especially additional dating of the megabreccia-bearing part of the Clover Creek sequence and analysis and dating of the interpreted Oligocene "Holborn" clastic rocks in the northernmost Pequop Mountains, could help resolve this issue.

Basalt dikes that cut the mylonitic shear zone in the East Humboldt Range (Fig. S1 [footnote 1]) are ca. 17.3 Ma (Table 2). The basalt dikes are compositionally and temporally part of the middle Miocene assemblage that includes the northern Nevada rift and similar mafic rocks throughout northern Nevada (John et al., 2000; Brueseke et al., 2014). The emplacement ages implied by the plagioclase dating suggest that the wall rocks were below plagioclase closure temperatures of ~225–300 °C (e.g., Cassata et al., 2009) at ca. 17 Ma. These results confirm that mylonitic shearing in the metamorphic core complex was complete by ca. 17 Ma.

Widespread Miocene basins in the REWP region are associated with a main pulse of extension, range tilting, and exhumation (e.g., Henry et al., 2011; Camilleri et al., 2017) The oldest $^{40}Ar/^{39}Ar$ ages from the Miocene Humboldt Formation along the western flank of the Pequop Mountains of ca. 15.7–15.2 Ma (samples H14-78 and H15-39; Fig. 2; Table 2; Henry and Thorman, 2015) are similar to the Knoll Basin, north of the Pequop Mountains (Camilleri et al., 2017). These observations are consistent with studies that demonstrate major basin formation and extension beginning ca. 16 Ma (e.g., Colgan and Henry, 2009). However, younger ages from tephra in the Independence Valley NW quadrangle (IVNW; Fig. 2A) (10.8 Ma to <4.6 Ma; Table 2), compared to 16–15 Ma discussed above, suggest the area was a paleotopographic high in the middle Miocene or faulting started later in this area. Megabreccia blocks of Eureka Quartzite, Pogonip Group, and Notch Peak Formation up to 230 m long are common in the lower part of the Independence Valley NW sequence (e.g., Zuza et al., 2019a). These blocks are identical to the bedrock in the range to the east, suggesting that a significant part of range tilting and bedrock exposure had occurred by ca. 10 Ma.

8.2 Cenozoic Extension in the Pequop Mountains

The low-angle Pequop normal fault is cut by high-angle normal faults, and thus Pequop fault motion was probably part of the oldest phase of extension in the northern Pequop Mountains. All observations of the Pequop fault, which includes the crest of the northern range and drill-core data along the western range flank (Zuza et al., 2018, 2019a) (Figs. 2B and 4; Plate 1), display hanging-wall, flat-footwall flat relationships. The large extent of this flat-flat geometry would imply significant transport distance, but we interpret that this geometric relationship may partly result from the west-directed

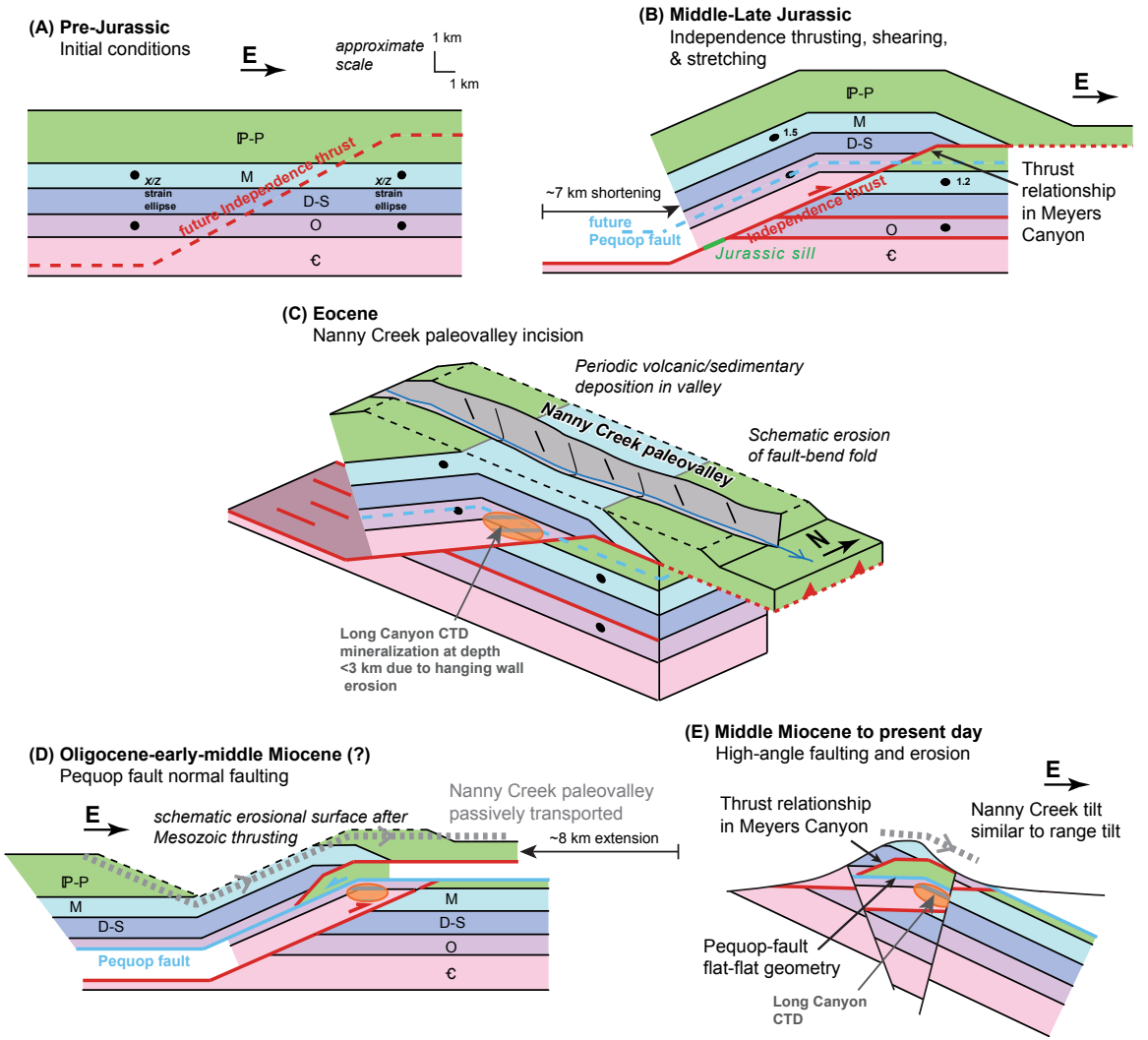

Figure 13. Model demonstrating envisioned kinematic history of the northern Pequop Mountains from the Jurassic to present. (A) Pre-Jurassic initial conditions showing Neoproterozoic–Paleozoic stratigraphy. (B) In the Middle Jurassic, ~7 km of horizontal shortening along the Independence thrust as a fault bend fold generally places lower Paleozoic units over middle Paleozoic units. Transport-parallel stretching and fault-normal thinning are shown schematically as black *XZ* strain ellipses. Jurassic sill intrudes the Independence thrust fault. (C) Eocene incision of the Nanny Creek paleovalley, deposition of contemporaneous volcanic rocks, and Long Canyon gold mineralization. (D) Post-Eocene, probable Oligocene(?)–Miocene Pequop normal fault motion transports a part of the Independence thrust and Nanny Creek paleovalley westward in its hanging wall. This model assumes ~8 km horizontal extension. (E) Eastward tilting of the range and erosion leads to the geometries observed across the Pequop Mountains today. CTD—Carlin-type gold deposit.

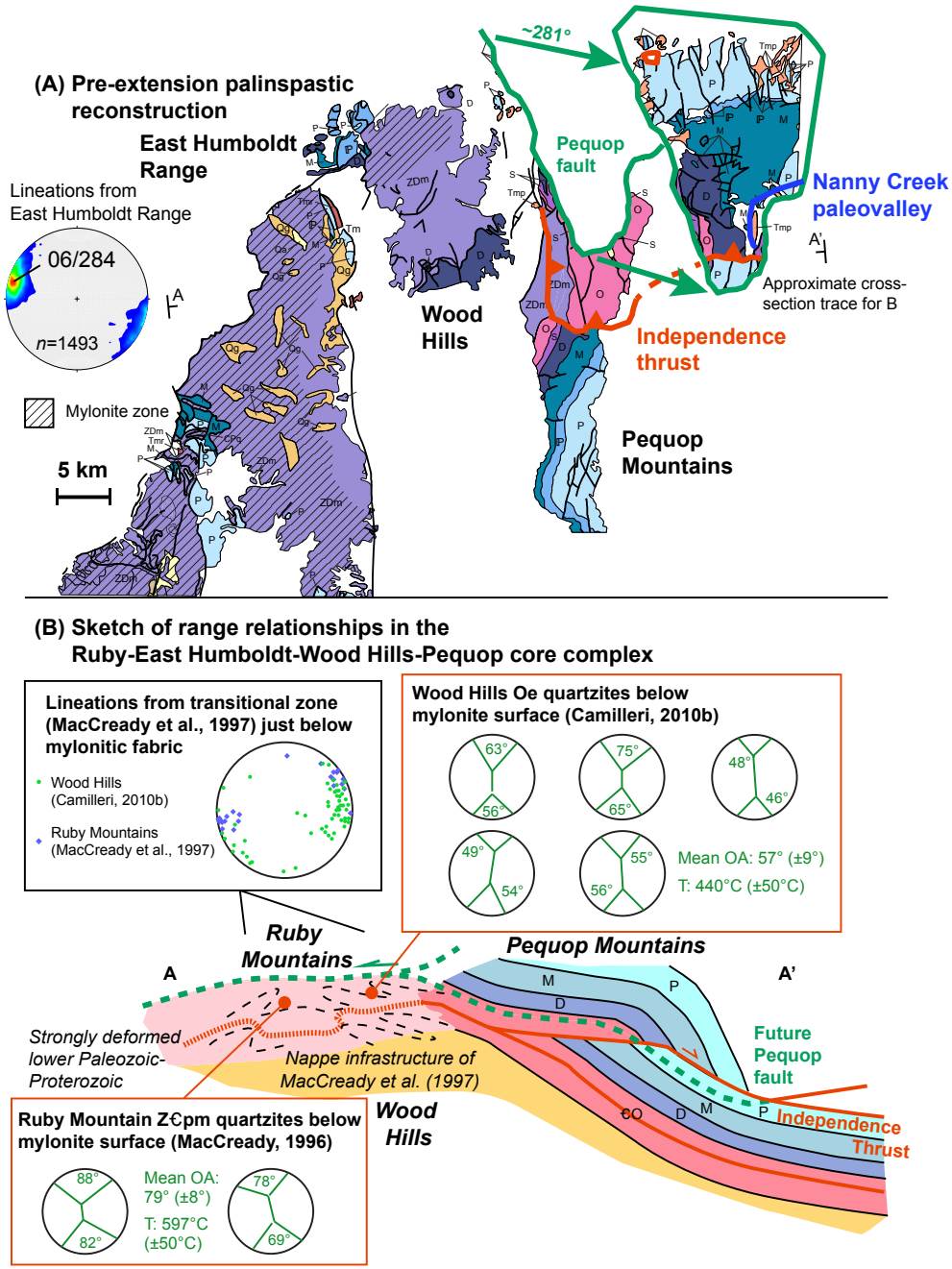

Figure 14. Schematic restoration of the Ruby Mountain–East Humboldt Range–Wood Hills–Pequop Mountains (REWP) core complex. (A) Palinspastic restoration of map view geometries of the pre-extension geology of the REWP, consistent with the McQuarrie and Wernicke (2005) restoration in Figure 1B. This restoration uses the geologic base map in Figure 2A. Restoration juxtaposes (1) lower Paleozoic rocks across the East Humboldt Range (EHR), Wood Hills (WH), and Pequop Mountains; (2) mylonitized shear zone of the EHR (e.g., McGrew et al., 2000) and the WH (Camilleri, 2010b); and (3) nappe structures in the Ruby Mountains, EHR, and WH. Restoration of the Pequop normal fault (dark green) aligns the pre-extensional geometry of the Independence thrust (red). Inset stereonet shows lineation measurements from the East Humboldt Range (compiled from McGrew and Snoke, 2015; Dee and Ressel, 2016; McGrew, 2018; Zuza et al., 2020b; our unpublished mapping); these measurements parallel the inferred Pequop-fault motion vector. Also shown is profile A–A′ in Figure 14B. (B) Cross-section model based on the geology in Figure 14A, demonstrating how the geology of the EHR fits with the Pequop Mountains. Using quartz c-axis opening angles from the Wood Hills (Camilleri, 2010b) and Ruby Mountains (MacCready, 1996), temperatures were calculated using the empirical relationships of Faleiros et al. (2016). The rocks below the mylonitic shear zone in the Ruby Mountains (Z€pm) are hotter than in the Wood Hills Ordovician Eureka Quartzite (Oe), consistent with the model presented here and the significant intrusions in the Ruby Mountains and EHR. OA—opening angle; T—temperature.

Pequop normal fault overprinting the preexisting west-dipping back-limb geometry of the Jurassic Independence thrust. Geologic mapping and observed structural relationships show that the Pequop plate consists of hanging wall (i.e., Ordovician–Mississippian strata) and footwall rocks of the Independence thrust (Pennsylvanian–Permian rocks) (Fig. 4). The Pequop plate was transported over Ordovician strata in the hanging wall of the Independence thrust (Plate 1). Therefore, the thrust relationships are a piercing line for Pequop-fault displacement estimates. We suggest that the thrust relationships in the Pequop fault hanging wall restore to the east-southeast, where similar thrust relationships (i.e., Ordovician–Mississippian strata over Pennsylvanian–Permian rocks) project from the mapped Independence thrust (Fig. 14A). This implies ~8 km of west-northwest–directed, normal-sense transport along the Pequop fault. Although the Pequop fault appears to remove ~3 km of stratigraphy—i.e., Pennsylvanian strata placed directly on Oe-Ordovician Fish Haven Dolomite (Fig. 3)—this geometric relationship is complicated because Independence thrust-footwall rocks are placed over Independence thrust hanging-wall rocks (Fig. 14A). We expand discussion of these geometric details in section 8.4.

Previous estimates suggest Late Cretaceous timing of Pequop-fault activity based on incision of the fault's hanging wall (i.e., the Pequop plate) by the Nanny Creek paleovalley (Brooks et al., 1995; Camilleri and Chamberlain, 1997) (Fig. 2A; Plate 1). However, here we argue that field relationships do not provide unequivocal evidence of the relative timing of paleovalley incision and Pequop-fault activity (Plate 1). Instead, based on regional and local geologic relationships, we interpret post-Eocene Pequop faulting for the following reasons. (1) The Eocene Nanny Creek volcanic sequence was deposited on middle Mississippian Chainman Shale at the bottom of the paleovalley in the northern Pequop Mountains and on rocks as young as Permian on the edge of paleovalley to the north. To the west, in the Windermere Hills and southern Snake Mountains, the volcanic sequence rests on middle Mississippian to Lower Triassic strata. Late Cretaceous–earliest Cenozoic extension and footwall exhumation should have exposed deeper stratigraphy by the Eocene. A more recent analogy is that Miocene strata as old as 10.8 Ma related to unequivocal Miocene-to-present extension in the Pequop Mountains were deposited on units as deep as Cambrian–Ordovician strata (Plate 1). (2) The ~1.5-km-deep Nanny Creek paleovalley was probably incised during the most significant phase of crustal thickening and uplift in the Mesozoic, similar to paleovalleys across California and Nevada (Henry, 2008; Henry et al., 2011), not at the same time as the Eocene volcanism that infilled the valley (e.g., Camilleri and Chamberlain, 1997). A preferred reasonable model for Eocene deposition within this paleovalley is for significant relief between the valley bottom and intervalley paleohighs. This scenario requires that the region was still a relatively coherent highland dissected by paleovalleys before significant normal faulting but is incompatible with the Pequop plate having already moved as the hanging wall of the Pequop normal fault prior to the Eocene. (3) Our preferred kinematic restoration involves an ~281° displacement vector that parallels stretching lineations and proposed extension vectors in the Ruby Mountains–East Humboldt Range mylonites (e.g., Snoke et al., 1997), as well as the direction of middle Miocene and younger extension throughout the northern Basin and Range (Colgan and Henry, 2009; Colgan et al., 2010) (Fig. 14A). Therefore, the Pequop fault may have been active contemporaneously with, and kinematically related to, the late Oligocene–early Miocene shearing in the East Humboldt Range (e.g., Snoke, 1980; Wright and Snoke, 1993) or with the middle Miocene episode of major extension.

We interpret that the Pequop fault passively transported the incised Nanny Creek paleovalley during normal-sense motion. This model implies that the Nanny Creek paleovalley incised the rocks that would become the Pequop plate, including parts of the Independence thrust hanging wall, in the Mesozoic, prior to Cenozoic normal faulting. The entire Pequop plate, including thrust-hanging wall and Nanny Creek volcanics, were offset by the Pequop fault and juxtaposed against Ordovician strata after the youngest Nanny Creek volcanics (i.e., ca. 39 Ma; Henry et al., 2011). In this interpretation, Pequop plate normal faulting was an early phase of extension either immediately preceding or during the high-magnitude, middle Miocene (ca. 16–17 Ma to ca. 12–10 Ma) phase of extension (Colgan and Henry, 2009).

The ~8 km of extension along the Pequop normal fault may have fed slip into the Ruby Mountain–East Humboldt Range detachment system, and the breakaway for the REWP metamorphic core complex should be east of the Pequop Mountains, potentially near the Toano Range (Fig. 1) (e.g., Ketner et al., 1998). Based on pressure-temperature (*P-T*) estimates from the East Humboldt Range (EHR), Hurlow et al. (1991) suggested 15–17 km of normal-sense slip on this detachment fault system based on the geometry required to exhume rocks from ~12 km depth. However, the Hurlow et al. (1991) interpretation is a maximum estimate because it assumes that mylonitic shear zone and brittle detachment faulting entirely exhumed rocks from ~12 km, which ignores probable Miocene-to-present eastward range tilting. As discussed below, Miocene-to-present eastward tilting of the Pequop Mountains exhumed at least 6 km of the western range flank. Given the Miocene basin west of the EHR is thicker than that west of the Pequop Mountains (e.g., Fig. 2) (e.g., Dee and Ressel, 2016; Zuza et al., 2020a), the EHR was probably tilted and exhumed a similar or greater magnitude than the Pequop Mountains, which suggests that only roughly half of the estimate of normal-sense shearing by Hurlow et al. (1991) may have been accommodated by late Oligocene–early Miocene motion. For the following calculation, we conservatively assume low-angle faulting accommodated 8–15 km of extension.

Wright and Snoke (1993) suggest that mylonitic shearing and major detachment faulting in the REWP were active for ~6 m.y., or less, from 29 Ma to 23 Ma. Based on piezometric stress estimates and stress-strain rate calculations, Hacker et al. (1990) postulated that the EHR mylonites could have exhumed the footwall rocks in <3 m.y. Extension magnitudes of 8–15 km yield extension rates of ~2.5–1.3 mm/yr (6 m.y. activity) or 5.0–2.7 mm/yr (3 m.y. activity) for the coupled REWP normal-sense fault system. These magnitudes equate to only ~20% extensional strain for the entire REWP system over these timescales, or extensional strain rates of $1–2 \times 10^{-15}$ s^{-1}.

If early low-angle extension in the REWP occurred in the late Oligocene, the lack of significant contemporaneous basins, as discussed previously, may be explained by one of several non-unique mechanisms. Local orogenic collapse following Eocene volcanism and crustal heating may have generated ductile shear zones at depth and isolated basins without accommodating significant west-east stretching of the Basin and Range (Colgan and Henry, 2009). Oligocene pure-shear stretching of the middle crust may have accommodated and been balanced by influx of mantle melts (e.g., Gans, 1987), evidenced by Oligocene intrusions (Wright and Snoke, 1993; McGrew et al., 2000), or low-viscosity lower crust (mode 1c extension of Rey et al., 2001), which buoyantly elevated the surface at this time to resist basin sedimentation. Alternatively, this earlier phase of extension immediately preceded ca. 17 Ma crosscutting dikes and was the earliest phase of progressive Miocene-to-present extension.

Subsequent middle Miocene-to-present extension in the Pequop Mountains is evidenced by the two high-angle normal faults that bound the western flank of the range. The combined normal-sense offset on these two faults is ~6 km, based on (1) basin thickness and (2) offset of the Pequop fault and Independence thrust faults (Fig. 2B). The range was probably tilted ~40° eastward since the Eocene, as evidenced by tilted sedimentary strata interbedded with Eocene volcanic rocks within the Nanny Creek paleovalley in the Pequop Summit quadrangle (Brooks et al., 1995; Henry and Thorman, 2015). Assuming that this tilting occurred in the Miocene-to-present and was entirely rigid-body rotation implies ~7–8 km displacement on the western range-bounding normal faults. Six to 8 km of normal-sense fault offset corresponds to ~3–4 km horizontal extension, assuming ~60° fault dip. The timing of this phase of extension and range tilting is constrained by the ca. 16 Ma deposition age of the Miocene Humboldt Formation (Henry and Thorman, 2015; Camilleri et al., 2017). The oldest dated Humboldt sample along the western flank of the Pequop Mountains is the 15.8 Ma tephra in the northwest (Table 2; Henry and Thorman, 2015), which is consistent with a 17–16 Ma extension initiation that is observed across much of the Basin and Range (Colgan and Henry, 2009). The presence of megabreccia blocks of Eureka Quartzite, Pogonip Group, and Notch Peak Formation in ca. 10 Ma deposits indicates that significant uplift and probable tilting of the Pequop Mountains had been accomplished by then. Assuming extension along initially high-angle faults began locally at either ca. 16 Ma or 10 Ma yields late Cenozoic fault-slip rates of 0.4–0.8 mm/yr or horizontal extension rates of 0.2–0.4 mm/yr. The extensional strain rate over this time period would have been 1.5×10^{-15} s^{-1} to 6.9×10^{-16} s^{-1}.

The westernmost range-bounding normal fault in the study area displaces late Pleistocene fan deposits (Qfi), with vertical separations up to ~3 m (Fig. S3 [footnote 1]; Plate 1). Although the fan surface is not directly dated, it is older than the highstand of pluvial Lake Clover (Reheis, 1999), which has been dated to 17.3–19.5 ka (Munroe and Laabs, 2013). This yields a maximum vertical separation rate of ~0.16 mm/yr, which, assuming a 60° fault dip, equates to a late Pleistocene extension rate of ~0.1 mm/yr (Fig. 2). Trenching of the western boundary fault of the East Humboldt Range indicated a vertical separation rate of 0.06–0.2 mm/yr (Wesnousky and Willoughby, 2003), or an extension rate of 0.03–0.12 mm/yr, assuming 60° fault dip (Fig. 2).

These late Pleistocene extension rates (i.e., ~0.1 mm/yr) are slightly less than our derived late Cenozoic rates discussed above (i.e., 0.2–0.4 mm/yr). The late Cenozoic geologic extension rates and extensional strain rates are also higher than average Pleistocene extension rates derived from fault scarp analyses across the central Great Basin (e.g., <0.1 mm/yr for most individual ranges; Koehler and Wesnousky, 2011) and geodetic strain rates (e.g., average over REWP region of $\sim 1.5 \times 10^{-16}$ s^{-1}; Hammond et al., 2011), respectively. The late Cenozoic rates are broad average calculations, and thus these discrepancies may be the result of the imprecise geologic record. Alternatively, extension rates may have varied spatially and/or temporally (e.g., Pérouse and Wernicke, 2017), including possible deceleration of extension from 0.2 to 0.4 mm/yr to late Pleistocene–present rates of ~0.1 mm/yr resulting from progressive crustal thinning, rotation of faults to less favorable orientations, or as part of a more regional slowdown of Basin and Range extension due to changes in relative plate motion at 10–8 Ma (Atwater and Stock, 1998; DeMets and Merkouriev, 2016).

If ~2–3 km of stratigraphy were vertically exhumed during low-angle Pequop-normal faulting, as suggested in our model, and ~6–8 km were exhumed along the western flank of the range during high-angle faulting, these estimates require at least ~9 km of vertical Cenozoic exhumation. These values are compatible with exposure of the lower Paleozoic–upper Neoproterozoic stratigraphy in the western Pequop Mountains (Figs. 2 and 3), suggesting that these aforementioned structures can account for all required Cenozoic exhumation. These simple calculations also demonstrate that Eocene or earlier extension is not required to exhume the Pequop Mountains, which agrees with the lack of field or thermochronologic evidence for pre–39 Ma extension in the Pequop Mountains. The constraints from observed extensional structures confirm no large missing or eroded package of rocks could have buried the Pequop Mountains to great depth as suggested in the Windermere thrust hypothesis (Camilleri and Chamberlain, 1997).

Restriction of extension in the Pequop Mountains to late Oligocene–Miocene provides another constraint for the debate about driving mechanisms for Basin and Range extension (e.g., Colgan and Henry, 2009). If gravitational collapse of thickened crust drives extension (e.g., Jones et al., 1998; Sonder and Jones 1999), extension is predicted to proceed shortly after peak thickening in the Late Cretaceous (e.g., Chapman et al., 2015). The small Elko and White Sage Basins indicate Eocene extension in the region was minor (Dubiel et al., 1996; Henry, 2018). Post-Eocene extension highlights the importance of changes in plate boundary conditions in controlling intracontinental extension (e.g., Atwater 1970; Stock and Molnar 1988; Colgan and Henry, 2009; Yin, 2010), as well as a possible contribution from thermal weakening following Eocene–Oligocene magmatic sweeps southwestward across the Great Basin (Henry and Boden, 1998; Best et al., 2016). Schellart et al. (2010) argued that the north-south width of the subducting Farallon slab may have controlled the transition

from Sevier-Laramide contraction to subsequent extension. A narrower subducting plate geometry would allow toroidal return flow around slab edges to enhance westward trench retreat and upper plate extension. In their compilation, drastic narrowing of the subducting slab width just prior to ca. 30 Ma (i.e., from ~>10,000 km to <4000 km) may lead to a soft onset of extension in the Oligocene as recorded in the REWP. However, an Oligocene extension initiation age is puzzling because of the paucity of Oligocene basins, other than the poorly resolved Clover Creek basin (Fig. 5; e.g., McGrew and Snoke, 2015).

8.3 Mesozoic Contractional Deformation and Metamorphism in the Pequop Mountains

Field relations and geo- and thermochronology indicate that most, possibly all, deformation and initial metamorphism occurred in the Middle-Late Jurassic. Late Jurassic intrusions are variably deformed, including the 155–157 Ma boudinaged granitic sill in Meyers Canyon (Camilleri, 2010a; this study), ca. 160 Ma foliated granitic sill (Bedell et al., 2010), and undeformed ca. 160–157 Ma lamprophyre dikes and sills that cut metamorphic foliation (this study; Bedell et al., 2010; Milliard et al., 2015; Zuza et al., 2018, 2019a, 2020a). The lamprophyre sill that intruded the Independence thrust (Fig. 9) indicates that the fault was active prior to ca. 157 Ma (Zuza et al., 2020a). Accordingly, this deformation can be attributed to early Elko orogeny-aged contraction (Thorman et al., 1990, 1992). We further infer that structures parallel to, and showing the same kinematics as, Independence thrusting formed during this time, including foliation and lineation development in the Paleozoic rocks, boudinage, most folds, and outcrop-scale reverse faults (Fig. 10). Bedding-parallel faults and stretching lineations, asymmetric folds, and thrust faults throughout the range show dominantly southeast-directed transport (Figs. 10C and 10D). Minor northwest-directed faulting (e.g., Fig. 10F) is interpreted as local backthrusts. Metamorphic foliations in Cambrian rocks in the Toano Range to the east are cut by the Late Jurassic Silver Zone Pass pluton (Ketner et al., 1998), which supports that shearing and foliation occurred prior to ca. 157 Ma (Mortensen et al., 2000). Cretaceous deformation could overprint Jurassic deformation in the Pequop Mountains, but the parallelism between demonstrably Jurassic structures and structures of unknown age suggests that the simplest interpretation is that most of the strain occurred in the Jurassic.

We argue that initial Jurassic metamorphism was overprinted and obscured by Cretaceous metamorphism. The 75–85 Ma titanite and Lu-Hf garnet ages and 70–90 Ma $^{40}Ar/^{39}Ar$ mica spectra indicate high Late Cretaceous temperatures (>500 °C) in the lower Paleozoic rocks of the western part of the Pequop Mountains and Wood Hills and up to ~300 °C in the eastern Peqoup Mountains (Fig. 12; Thorman and Snee, 1988; Camilleri and Chamberlain, 1997; Wills, 2014; Zuza et al., 2018, 2019a). Monazite and zircon ages are similar in the East Humboldt Range (Hallett and Spear, 2015), and a Late Cretaceous thermal-metamorphic pulse occurred throughout eastern Nevada (Miller and Gans, 1989). This thermal pulse was coeval with numerous leucocratic intrusions in the Ruby Mountains–East Humboldt Range, Wood Hills, and Pequop Mountains (e.g., Bedell et al., 2010; Howard et al., 2011; McGrew et al., 2000; Zuza et al., 2019a). However, two lines of evidence support an earlier Jurassic phase of metamorphism. Ductile deformation of lower Paleozoic rocks, which required temperatures of >300 °C, record the same southeast-directed contraction as all other Pequop contractional deformation, which we interpret to have occurred in the Jurassic. Late Cretaceous contraction was more east-directed across the eastern Great Basin (e.g., DeCelles and Coogan, 2006; Yonkee and Weil, 2015), although distinguishing Jurassic and Cretaceous structures could still be ambiguous. The metamorphic gradient across the Jurassic Independence thrust in the upper plate of the Pequop fault indicates metamorphism predates the thrust. We suggest the foliation-parallel syn-kinematic micas formed in the Jurassic but were completely reset during Cretaceous reheating. The crosscutting, postkinematic micas may have formed during static Cretaceous metamorphism. Late Cretaceous reheating overprinted and mostly obliterated any dateable record of Jurassic metamorphism. Episodes of heating in both the Jurassic and Late Cretaceous are consistent with significant intrusion at both times and with evidence of Jurassic metamorphism in the Ruby Mountains (Hudec, 1992).

Biotite and muscovite argon spectra are not disturbed after the Late Cretaceous (Zuza et al., 2019a), indicating rocks in the western Pequop Mountains cooled at that time and were not heated above ~300 °C in the Cenozoic. The smallest domains in K-feldspar MDD analyses track temperatures down to 200–150 °C (e.g., Lovera et al., 1989) and indicate that this region was heated to between 200 °C and 300 °C in the Eocene (Fig. 6). A ZHe age from Z€pm is ca. 43 Ma (Wolfe, 2016), which similarly records cooling through ~200 °C. Taken together, these data suggest that following high thermal gradients in the Late Cretaceous, the Eocene thermal gradient was lower at 20–30 °C/km (Fig. 12B).

8.4 Kinematic Model for the Pequop Mountains

Figure 13 presents a simplified kinematic model for the structural evolution of the Pequop Mountains. The model is schematic but offers a step-by-step inferred history that results in present-day map patterns (Plate 1). Prior to the Jurassic, Neoproterozoic–Paleozoic strata were ~8–9 km thick, with the Prospect Mountain Quartzite at the base of the section (Fig. 13A). Before ca. 157 Ma, in the Middle-Late Jurassic, Elko orogeny southeast-directed deformation and/or shortening strain and accompanying intrusions resulted in regional syn-kinematic metamorphism in Neoproterozoic to Devonian rocks that is recorded by strong shearing and motion along the Independence thrust. Common boudinage, stretching lineations, and layer-parallel shear fabrics occurred contemporaneously with southeast-directed tectonic transport and transport-parallel stretching of the Independence thrust wall rock (Fig. 13B) (e.g., Fischer and Coward, 1982). Camilleri (1998) interpreted 15%–30% fault-parallel stretching of the wall rock. During non-coaxial deformation, two quadrants of a 2D strain ellipse experience shortening, and the other two undergo extension. This type of deformation

is commonly observed in Himalayan shear zones (Long et al., 2016, 2019) and Sevier thrust structures (Yonkee, 2005). Similarly, extensional shear zones can involve local contractional folding (e.g., Miller et al., 1983; Snoke et al., 1997). Because the fault wall rock was nonrigid, with marked stretching, the Independence thrust may be classified as a stretching fault (Means, 1989). We schematically show stretched stratigraphy, with a southeast-elongation direction parallel to thrust transport (Fig. 13B). Given the observed stratigraphic duplication and an arbitrary 30° west dip to the Independence thrust, Figure 13B demonstrates ~7 km shortening (33% shortening strain).

In the Late Cretaceous, significant thermal pulses are recorded by thermochronometers and garnet growth in the deeper structural parts of the range. No evidence for Cretaceous deformation in the Pequop Mountains was observed, although reactivation of Middle-Late Jurassic structures is possible. The Nanny Creek paleovalley formed prior to 41 Ma (Eocene) and possibly much earlier (Fig. 13C). Nanny Creek conglomerate, tuff, lava, and volcanic breccia were deposited subparallel to the underlying Paleozoic strata that define a broad hanging-wall anticline of the Independence thrust (Fig. 13C), which matches field observations (Plate 1).

The Long Canyon deposit was mineralized contemporaneously with Eocene intrusion and volcanism, with heat provided by the Eocene magma source. CTDs to the west formed at relatively shallow depths of <5 km (Kuehn and Rose, 1995; Arehart, 1996; Cline and Hofstra, 2000; Nutt and Hofstra, 2003; Ressel and Henry, 2006). If Long Canyon formed similarly, the Cambrian–Ordovician contact should have been shallower than 5 km in the Eocene. The stratigraphic position of the Long Canyon deposit suggests it formed at a depth of ~5–7 km (Fig. 3), but because the deposit is in the hanging wall of the Independence thrust (Fig. 2B)—with ≥2 km stratigraphic vertical separation—mineralization at structural depths ≤5 km following Jurassic thrusting and coupled erosion is likely. Restoration of the Pequop fault indicates Long Canyon lay below the Nanny Creek paleovalley in the Eocene, possibly at ≤3 km depth (Fig. 13C). Long Canyon host rocks would have been buried to >15 km depth by the hypothesized Cretaceous overthrust, which would require major pre-Eocene exhumation for Long Canyon to form at shallow depth.

Extension began along the Pequop normal fault post-Eocene, between latest Oligocene and earliest-to-middle Miocene(?), and transported the upper part of the Independence thrust panel and the Nanny Creek paleovalley westward. Displacement was largely bedding and thrust parallel but cut across the thrust from footwall to hanging wall in a westward transport direction. Geologic relationships permit a breakaway to the east of the Pequop Mountains, possibly above or east of the Toano Range. Normal faulting resulted in the present geometry of the Pequop plate, including hanging wall–footwall flat relationships (Fig. 13D; Plate 1) and juxtaposed Pennsylvanian–Permian rocks and the Independence thrust over Oe rocks in the Pequop footwall. Our schematic evolution requires ~8 km extension to result in these observed geometries (Fig. 13D). This model suggests that the Ordovician–Permian rocks of the Pequop normal-fault hanging wall, into which the Nanny Creek paleovalley was cut, were subhorizontal because the attitude of the paleovalley sequence mimics that of the Paleozoic rocks. Thus, the Pequop fault flat was subhorizontal at this time, and this structural relationship bears on the subsequent magnitude of Miocene-to-present rotation of these rocks (Fig. 13D).

Lastly, in the middle Miocene to present, high-angle normal faulting, eastward tilting of the Pequop Mountains by ~40°, and subsequent erosion resulted in the geometries observed today (Fig. 13E). Although this kinematic evolution is non-unique, it provides a geologic history that results in our observed map relationships (Fig. 2; Plate 1).

8.5 Relationship of Pequop Mountains within the Ruby Mountains–East Humboldt Range Core Complex

The relationship between the Pequop Mountains and the more strongly deformed rocks of the Ruby–East Humboldt Range can be inferred by restoring disaggregation of the ranges in map view. First, we restore ~40% extension by moving the ranges closer together (Fig. 14). Next, slip along the Pequop fault is restored, moving the Pequop plate to the east-southeast. For this restoration, Pennsylvanian–Permian rocks in the Pequop plate are positioned along strike of similar strata in the central Pequop Mountains (Fig. 14). Note that the thrust relationships observed in the Pequop plate restore along the pseudo-trace of the Independence thrust. A test of this restoration comes from the mylonitic lineations in the Ruby Mountains–East Humboldt Range (~284° vector from 1493 lineation measurements in the East Humboldt Range; contoured stereonet in Fig. 14) (e.g., McGrew and Snoke, 2015; Dee and Ressel, 2016; McGrew, 2018; Zuza et al., 2020b; our unpublished mapping), which suggest top-to-NW transport, the same as Cenozoic extension more broadly (Colgan and Henry, 2009). Our restoration of the Pequop plate follows a roughly parallel vector (Fig. 14). This implies that the Pequop normal fault is either a fault splay of the main normal-sense shear zone in the Ruby Mountains–East Humboldt Range or a related but not connected fault with the same transport direction.

We suggest that the Pequop Mountains and Wood Hills expose roughly similar structural levels, although the Wood Hills were deformed at hotter temperatures. The stratigraphy in the eastern Wood Hills (Thorman, 1962, 1970) mirrors that of the western Pequop Mountains (Zuza et al., 2018, 2019a). The Z€ rocks exposed along the western flank of the Pequop Mountains are similar to those in the Wood Hills, and the garnet-/tremolite-in metamorphic isograds in the westernmost Pequop Mountains are thought to correspond to those identified in the Wood Hills (Camilleri and Chamberlain, 1997; Wills, 2014). No major structural break separates these ranges, and the simplest case is that they represent similar structural levels. Thermometry results of ~600 °C suggest that the Wood Hills may have been slightly hotter than the Pequop Mountains (Fig. 11) (Hodges et al., 1992; Wills, 2014), potentially due to the proximity to the pervasively intruded Ruby Mountains–East Humboldt Range.

The restoration in Figure 14 illustrates several important features of the REWP geology. First, mylonitic fabrics with northwest-trending

lineations in the northwestern Wood Hills align with similar fabrics in the Ruby Mountains–East Humboldt Range (Camilleri, 2010b) (Fig. 14A). Mylonites in both locations overlie a transitional zone with west-southwest–trending lineations, which compose the transition to the core complex infrastructure (MacCready et al., 1997; Camilleri, 2010b) (Fig. 14A). The relationship between nearly recumbent folds in the East Humboldt Range and Wood Hills remains unclear, but they are located at similar structural positions beneath the mylonitic fabrics and may be genetically related. MacCready et al. (1997) suggested that the inward-verging folds beneath the principal mylonite zone in the Ruby Mountains–East Humboldt Range are related to syn-extensional flow, with associated fold nappes, which were related to infilling the middle crust following high-magnitude extension (e.g., Rey et al., 2009; Whitney et al., 2013; Brun et al., 2018). An alternative model is that the northwest-vergent folds in the Wood Hills are backthrusts to the SE-directed Independence thrust (Thorman, 1970; Camilleri and Chamberlain, 1997; Camilleri, 2010b). Although plausible, significant differences in structural style exist between the northwest-vergent nearly recumbent isoclinal folds of the Wood Hills and the fault-bend folds of the Independence thrust.

To further test this restoration, quartz c-axis orientations from quartzites below the main detachment were analyzed from existing published data sets (MacCready, 1996; Camilleri, 2010b) to use their opening angle as a proxy for temperature (e.g., Law, 2014; Faleiros et al., 2016). In the Wood Hills, a mean opening angle from Oe samples of ~57° (our interpretation of data from Camilleri, 2010b) corresponds to temperatures of 440 °C (Fig. 14B), which is similar to the temperature range for Pequop Mountains Oe (Fig. 12), indicating that these rocks are from similar structural positions. These temperatures are lower than the corresponding temperature from Z€pm rocks in the Ruby Mountains based on a greater opening angle: 597 °C and ~79° (our interpretation of data from MacCready, 1996) opening angle, respectively (Fig. 14B). Hotter temperatures for the Ruby Mountains Z€pm sample are consistent with them being from greater structural depths from within the pervasively intruded Ruby Mountains.

8.6 Jurassic Orogeny and Crustal Thickening in Northeast Nevada

Jurassic contractional deformation has been documented in northeastern Nevada and northwestern Utah in the Ruby Mountains, Pequop Mountains, Toano Range, Pilot Range, Crater and Silver Island Range, and Newfoundland Mountains (Fig. 15). In the southern Ruby Mountains, Colgan et al. (2010) show an east-vergent thrust cutting lower Cambrian stratigraphy. The thrust appears similar to the Independence thrust, although no definitive crosscutting relationships are known. Hudec (1992) interpreted that metamorphic pressures recorded in Neoproterozoic McCoy Creek Group intruded by ca. 153 Ma Dawley Canyon granite represent Middle-Late Jurassic shortening. Other older-over-younger relationships in the Ruby Mountains–East Humboldt Range may represent similar deformation (Snoke et al., 1997), but they are extensively intruded and migmatically deformed, rendering the original configuration unclear. Consideration of these faults in a restored pre-Cenozoic framework (e.g., Fig. 1B; McQuarrie and Wernicke, 2005) suggests an ~20 km wavelength ~80-km-wide thrust belt from the Ruby Mountains in the west to the Newfoundland Mountains, Utah, in the east, with a décollement near the base of the Neoproterozoic–Paleozoic section (Fig. 15A). The thrust-décollement horizons and relative propagation direction can be inferred from the lowermost strata involved in thrusting (Figs. 3 and 15B). A thrust fault in the southern Ruby Mountains cuts lower Cambrian stratigraphy (Colgan et al., 2010), and the Independence thrust cuts lower-middle Cambrian Toano Formation (Fig. 3) (Camilleri, 2010a; this study). To the east, Jurassic thrusting cuts Cambrian Clifside in the Toano Range (Ketner et al., 1998) and farther east, a subhorizontal fault is at the base of middle Ordovician rocks in the Newfoundland Mountains, crosscut by a Jurassic pluton (Figs. 3 and 15B) (Allmendinger and Jordan, 1984). These observations are consistent with a kinematically linked thrust system cutting upsection to the east toward the Newfoundland Mountains (Figs. 3 and 15).

A simple cross-section model based on these stratigraphic cut-off relationships and no internal wall-rock deformation suggests a minimum of ~19 km shortening over an ~105 km restored section length (~18% strain) (Fig. 15B). However, given that intra-unit strain observed in the Pequop Mountains is approximately 30%, and the Independence thrust results in a similar ~30% strain (this study), it is probable that Jurassic deformation in northeast Nevada may have accommodated comparable ~30% strain.

Late Jurassic deformation and magmatism have been reported from across Nevada and western Utah, from the Luning-Fencemaker thrust (Thorman et al., 1990, 1991; Wyld et al., 2001, 2003; Wyld, 2002; Thorman and Peterson, 2003; Thorman, 2011a, 2011b; Anderson, 2020) in the west to the study area in the Pequop Mountains to the Newfoundland Mountains in Utah (Allmendinger and Jordan, 1984) (Fig. 15C). This deformation includes contractional structures that developed prior to and coeval with Jurassic magmatism, and local extensional structures that are generally syn- and post-intrusions (Allmendinger and Jordan, 1984; Miller and Hoisch, 1995). Late Jurassic extensional structures have not been observed in the Pequop Mountains, but Miller and Hoisch (1992, 1995) discuss normal faults that are spatially associated with Late Jurassic plutons in the Newfoundland and Silver Island Mountains (Fig. 15C). This region would have spanned ~230 km in the west-east direction (Fig. 15) assuming restored Cenozoic extension (McQuarrie and Wernicke, 2005). The simplest explanation of these coeval structures is that they were part of a single composite east-directed retroarc thrust system that operated at ca. 165–157 Ma. The youngest rocks in the region that predate the deformation are Early Jurassic crossbedded sandstones correlative to the Nugget and Navajo Formations (Thorman et al., 1991).

Wyld et al. (2001) suggested >50% Jurassic shortening strain across the Luning-Fencemaker fold-thrust belt, and Miller and Hoisch (1995) estimated 35–65 km of Jurassic shortening in eastern Nevada (Fig. 15C). In this study, we estimated ~30% shortening across the Pequop Mountains and suggest ~25% strain on a regional scale from the Ruby Mountains to Silver Island, equating to ~37 km shortening (Fig. 15C). We speculatively consider observations from Rhys et al. (2015) to suggest ~30% shortening strain between the Luning-Fencemaker

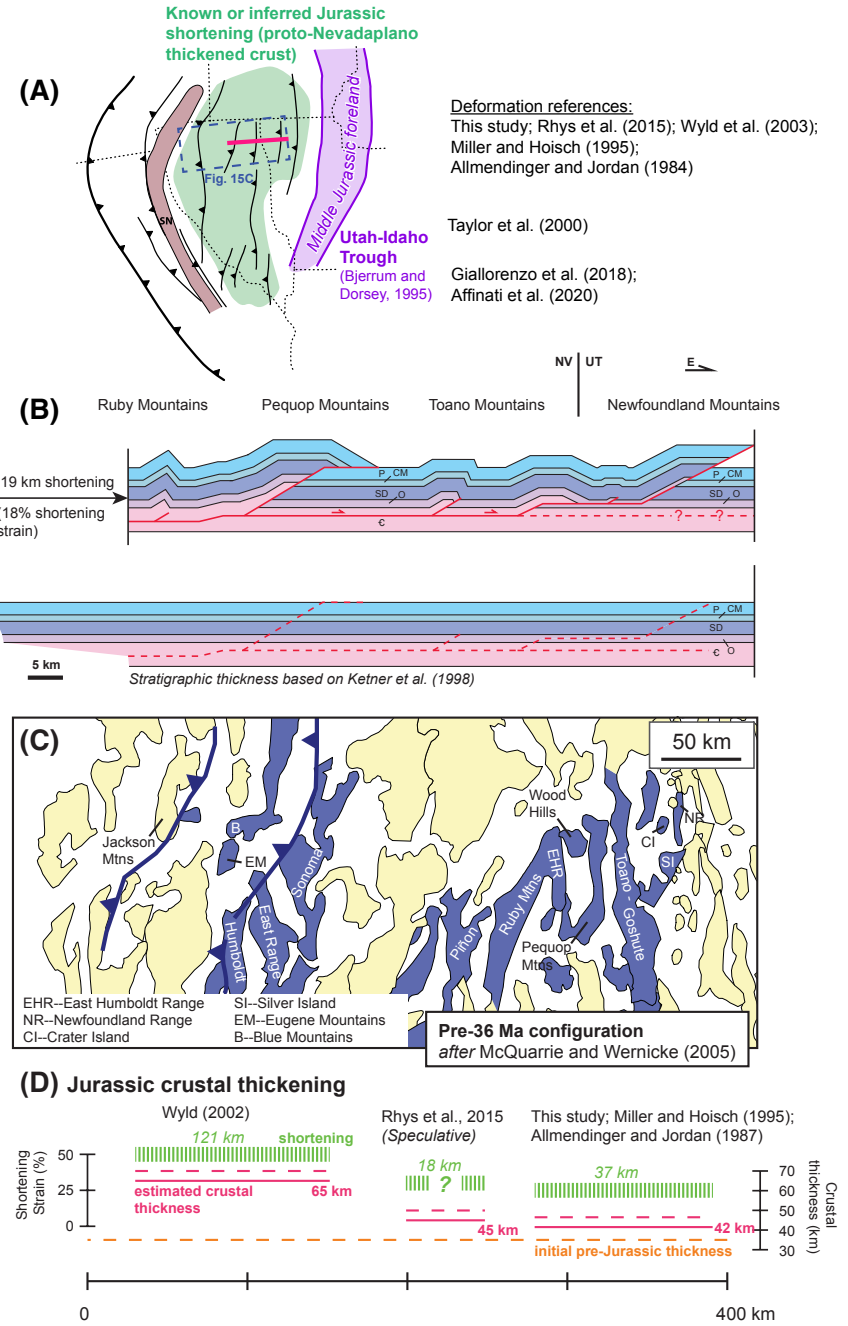

Figure 15. (A) Palinspastic map of Nevada showing approximate positions of contractional belts in the retroarc of the Sierra Nevada (SN), with their respective references listed in the appropriate latitude of the study area. A possible foreland to this phase of contractional deformation is shown in purple (Bjerrum and Dorsey, 1995). Base map from Yonkee and Weil (2015). Red line shows approximate profile trace for Figure 15B, and blue box is Figure 15C. (B) Deformed state and retrodeformed cross-section models show idealized fold-thrust belt geometry from the Ruby Mountains in the west to the Newfoundland Mountains in the east. This cross section was constructed by linking known or probable Jurassic thrust fault décollement levels, as depicted in Figure 3, using a stratigraphic framework and thickness of Ketner et al. (1998). Sources for fault relationships, from west to east respectively, include Colgan et al. (2010), this study, Ketner et al. (1998), and Allmendinger and Jordan (1984). Cross section is constructed assuming minimum fault slip for eroded hanging-wall cutoffs, and the retrodeformed cross-section model involves a line-length restoration. (C) Pre-extension restoration of McQuarrie and Wernicke (2005) showing approximate distribution of ranges in northern Nevada, with slight modifications because complete closure of the basins is incompatible with local geology. The ranges in northeast Nevada were probably overlapping prior to Cenozoic extension, and thus exposures across each range may correlate vertically or laterally. (D) On the same horizontal scale as Figure 15C, estimated minimum shortening (green dashed line) across Nevada with relevant references, approximate pre-Jurassic crustal thickness (orange) assuming it was an extended passive margin (e.g., Christensen and Mooney, 1995), and predicted thickness after pure-shear thickening of initial crust by the magnitude of estimated shortening (dashed red line) plus 5 km of erosion (red line).

and eastern Nevada structures. Taken together, these estimates suggest a minimum of ~176 km Jurassic shortening across northern Nevada, or net 30% strain over a region with a pre-extensional ~400 km width (Fig. 15C). Assuming 20 m.y. of shortening, this equates to contractional strain rates of ~5×10^{-16} s^{-1}.

These shortening magnitudes would have led to some degree of crustal thickening either via in situ pure-shear thickening (Zuza et al., 2016, 2019b), by feeding slip eastward to allow westward underthrusting of thick North American basement (Long, 2018), or a combination of these mechanisms. Based on analogs from the construction of the Tibetan Plateau (Wang et al., 2011; Gao et al., 2013; Zuza et al., 2016, 2019b), we assume that most thickening progressed in situ and calculate the minimum crustal thickening that would have resulted from the observed crustal shortening. We assume that the pre-Jurassic crustal thickness was ~35 km, given that it was an extended passive margin (e.g., Christensen and Mooney, 1995). Paleozoic orogeny (e.g., Cashman et al., 2008; Lawton et al., 2017) may have thickened this crust, which makes these calculations minimum initial thickness values. We use shortening magnitudes discussed above (thick dashed green line in Fig. 15D) to calculate pure-shear thickening (dashed red line in Fig. 15D) and allow for 5 km of erosion (solid red line in Fig. 15D). This exercise suggests that the Jurassic proto-Nevadaplano may have been thickened to ~40–45 km in central-eastern Nevada, and even thicker in the west. The resulting crustal thickening could have developed a moderate-scale foreland basin to the east (Fig. 15A), as postulated by Thorman et al. (1990) and Bjerrum and Dorsey (1995). Assuming isostatic compensation, and erosion varying from 0 to 5 km, the thickened crust estimates suggest paleo-elevations of 4.4–5 km, 1.8–2.5 km, and 1.4–2.0 km, for the west-to-east segments in Figure 15D. These estimates for Late Jurassic crustal thickness and elevation are close to estimates for the Late Cretaceous (DeCelles, 2004; Snell et al., 2014; Chapman et al., 2015), which significantly lessens the required magnitude of Late Cretaceous shortening strain to result in the thickened Nevadaplano. In this sense, we argue that Middle-Late Jurassic deformation played an appreciable role in initial building of the Nevadaplano. This implies that erosion, and possibly paleovalley incision, would have started during this time, and the observed paleovalley network of Henry (2008) may have been a relatively long-lived system (e.g., Janecke et al., 2000). Late Cretaceous Sevier fold-thrust shortening observed in central Utah (e.g., DeCelles and Coogan, 2006; Yonkee and Weil, 2015) may have focused shortening and crustal thickening east of present-day Nevada, which was already somewhat thickened, and this may explain why Late Cretaceous structures are relatively rare across west-central Nevada (cf. Long et al., 2014).

The observed magnitude of Jurassic crustal shortening would have resulted in a similar magnitude of westward crustal and/or mantle lithosphere underthrusting beneath the Jurassic Sierran arc, which may have contributed to the magmatic flux at this time following models of Cordillera cyclicity (e.g., DeCelles and Graham, 2015; Cao et al., 2016) (Fig. 16). Specifically, Middle-Late Jurassic shortening strongly correlates with contemporaneous terrane accretion in the Sierran forearc (Schweickert et al., 1988; Schweickert, 2015), increased North American–Farallon convergence rates (e.g., Smith et al., 1993; Yonkee and Weil, 2015), enhanced Jurassic arc magmatism, and a marked increase in crustal thickness in the Sierran arc (Profeta et al., 2015; Cao and Paterson, 2016; Kirsch et al., 2016) (Fig. 16A). A similar correlation of events occurred in the Late Cretaceous (Fig. 16A), and therefore we suggest that retroarc shortening involved a dynamic pulsed evolution with Late Jurassic and Late Cretaceous growth phases separated by relative quiescence (Zuza et al., 2020a). Alternatively, Early Cretaceous ca. 139–132 Ma Lu-Hf garnet ages in the Raft River–Albion–Grouse Creek (Kelly et al., 2015; Cruz-Uribe et al., 2015) region may represent evidence for a more protracted history of Late Jurassic to Late Cretaceous deformation (e.g., DeCelles and Graham, 2015).

8.7 Tectonic Model Limitations

The Jurassic to Cenozoic model presented above involves several non-unique interpretations. Here we present alternative models or other limitations to consider alongside our interpretations. The Mesozoic-Cenozoic tectonic history of the REWP involved overprinting deformation with subparallel kinematics. Specifically, Middle-Late Jurassic and Late Cretaceous deformation involved east-to-southeast vergent deformation and shearing (e.g., Thorman et al., 1991; Miller and Hoisch, 1995; DeCelles and Coogan, 2006; Yonkee and Weil, 2015; Zuza et al., 2020a; this study; lineations in Fig. S2 [footnote 1]). Cenozoic extension was subparallel to this vector, with both the consistent stretching lineations observed in the Ruby Mountains–East Humboldt Range (e.g., Snoke, 1980; Hurlow, 1987; Wright and Snoke, 1993; McGrew and Snoke, 2015) (Fig. 14) and observations of Miocene-to-present extension following a 280–290° vector (Colgan and Henry, 2009). Lineations observed in the lower Paleozoic stratigraphy were interpreted to have formed in the Jurassic based on parallelism with the interpreted transport direction of the Jurassic Independence thrust (Zuza et al., 2020a) and observations of metamorphic fabrics intruded by Late Jurassic dikes and plutons (Ketner et al., 1998; this study). It remains possible that some of these lineations and sheared fabrics formed during Late Cretaceous contraction or during Cenozoic extension. However, we observed no crosscutting relationships to directly support post-Jurassic ages. Almost all observed kinematics suggest top-southeast shearing, opposite the Cenozoic top-west normal-sense shearing observed in the East Humboldt Range, which argues against an extensional origin for these fabrics in the Pequop Mountains.

Our interpretation of Jurassic shortening across the Great Basin (Fig. 15) assumes a simplistic 2D cross-section geometry, where eastward subduction generally drives east-directed shortening (Fig. 16B). This scenario was likely more complicated. The Jurassic subduction system along the western margin of North America probably embayed eastward at Oregon-Washington latitudes (i.e., near the Blue Mountains, Oregon) (e.g., Anderson, 2015; Yonkee and Weil, 2015). This geometry may have resulted in a complex restraining-bend geometry that could have resulted in transpressional deformation in northeast Nevada.

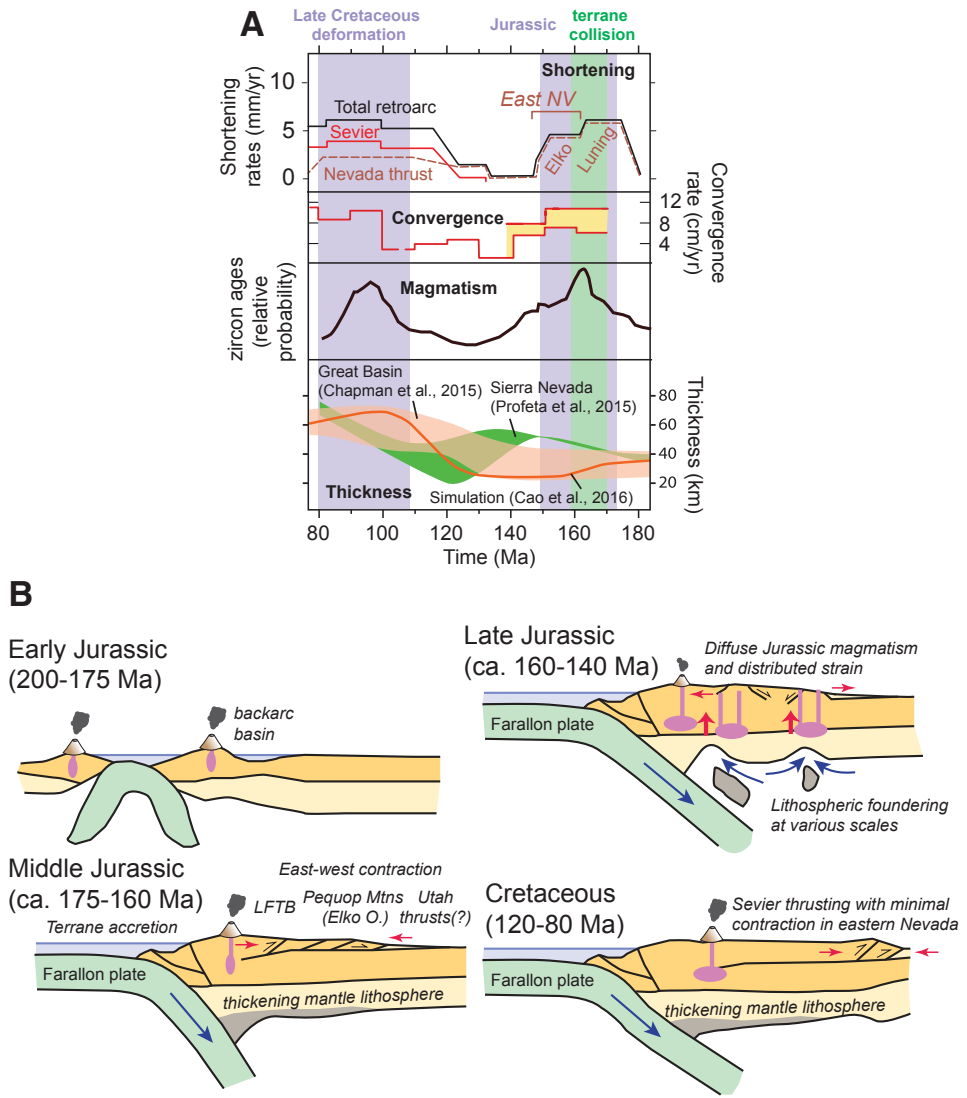

Figure 16. (A) Correlation chart showing Cordilleran retroarc shortening rates (Yonkee and Weil, 2015) modified to include Elko orogeny deformation (Thorman et al., 1991; Miller and Hoisch, 1995; Zuza et al., 2020a); North America–Farallon convergence rates from Yonkee and Weil (2015) based on Seton et al. (2012) and Engebretson et al. (1984); detrital zircon ages from the Sierra Nevada (Kirsch et al., 2016) as a proxy for magmatic flux; and crustal thickness estimates from various sources for the Great Basin and Sierra Nevada. Purple background shading represents Jurassic and Late Cretaceous phases of deformation, and green bar represents the timing of terrane accretion (Schweickert et al., 1988). NV—Nevada. (B) Schematic model of Mesozoic tectonics of the North American Cordillera, across the approximate latitude of 41°N. LFTB—Luning-Fencemaker thrust belt. Modified from Zuza et al. (2020a). Elko O.—Elko orogeny.

We only observed east-southeast–directed kinematics (Fig. S2 [footnote 1]; Plate 1), but others have documented south-southeast deformation of potentially similar age in northeast Nevada (e.g., Riva, 1970; Oversby, 1972; Smith et al., 1983; Coats, 1987; Anderson, 2020). Therefore, a range of east- to south-directed deformation may be related to regional transpression. An implication of this interpretation is that Jurassic deformation may not have progressed across Nevada and a proto-orogenic plateau as interpreted in this study (Figs. 15 and 16) but could have been restricted to transpressional features along the arc-subduction system (Anderson, 2015). We acknowledge this alternative interpretation but favor our model because (1) the correlation between magmatism, plate convergence, and shortening is remarkably similar to a comparable Late Cretaceous correlation with Sevier deformation (Fig. 16), (2) contemporaneous Middle-Late Jurassic deformation has been documented across much of Nevada (Fig. 1B), despite the high potential for poor preservation, which indicates it was not spatially restricted as one might predict for transpressional structures, and (3) our interpreted model is compatible with observations of the Utah-Idaho trough foreland basin (Bjerrum and Dorsey, 1995) (Fig. 15A).

In our view, the paleovalley drainage network across the Great Basin formed in the Mesozoic (e.g., Henry, 2008), persisted into the Cenozoic, and Eocene volcanic rocks were subsequently deposited in these established channels. Alternatively, the observed paleovalley network could have formed in the Paleogene during uplift and erosion as the Farallon slab flattened under western North America or the Pacific plate underwent cryptic coupling with the North American plate (e.g., Anderson, 2014; Lund Snee and Miller, 2020). Subsequent westward slab rollback led to Eocene volcanism and deposition of Eocene volcanic rocks in these paleovalleys (Henry, 2008; Henry and John, 2013). However, we contend that earlier Mesozoic crustal thickening and surface uplift would have generated a topographic gradient capable of generating large paleovalley networks, and river systems would have exploited these preexisting valleys during any dynamic surface uplift in the Paleogene.

Observations of tuff deposits in the paleovalleys as old as 45 Ma require their formation by this time (Henry, 2008).

8.8 Setting for Long Canyon Gold Mineralization

The sedimentary rock-hosted gold deposit at Long Canyon is concentrated in Ordovician Pogonip House Formation limestone, near the contact with the underlying O€ Notch Peak Formation dolomite (Figs. 2 and 3). Gold at Long Canyon expands the occurrence of CTDs geographically east—~150 km east of typical CTDs (e.g., Muntean et al., 2011)—and into a new geologic setting: shelf carbonates rather than silty slope carbonates of the Carlin trend (e.g., Bedell et al., 2010; Smith et al., 2013). Two structural features appear to have concentrated mineralization: (1) a broad anticline that is part of the hanging-wall fault-bend-fold of the Independence thrust, and (2) unit- and outcrop-scale boudins of less reactive dolomite within reactive silty limestones (Smith et al., 2013). Exploration of the same Ordovician limestone on the western flank of the range has been less successful, so far, which suggests that this combination of structures focused and trapped fluid flow.

We suggest that the Long Canyon deposit was influenced by the location of the hanging-wall anticline hinge line of the Independence thrust (Figs. 2 and 17), where the extension in the fold hinge enhanced boudinage of the Notch Peak Formation dolomite. The deposit is located at this fold hinge position, or just behind it to the northwest (i.e., hinterland-ward relative to thrust transport direction), along the hanging-wall flat part of the thrust. This position was most favorable because it could accommodate the most fault-transport- and bedding-parallel stretching via (1) tensile stress state in the hanging-wall anticline fold crest (e.g., Watkins et al., 2015) and/or (2) thrust sheet stretching during bedding-parallel transport (e.g., Fischer and Coward, 1982) (Fig. 17). Fluids may have migrated along the Independence thrust and subparallel planes and foliations. Fluid flow was trapped by the hanging-wall anticline (Leonardson, 2011) and focused in the boudin necks. Similar to other CTDs, this model for Long Canyon requires a structural culmination and reactive silty limestones (e.g., Leonardson, 2011; Muntean et al., 2011). CTDs to the west appear to focus around Jurassic structures (e.g., Rhys et al., 2015).

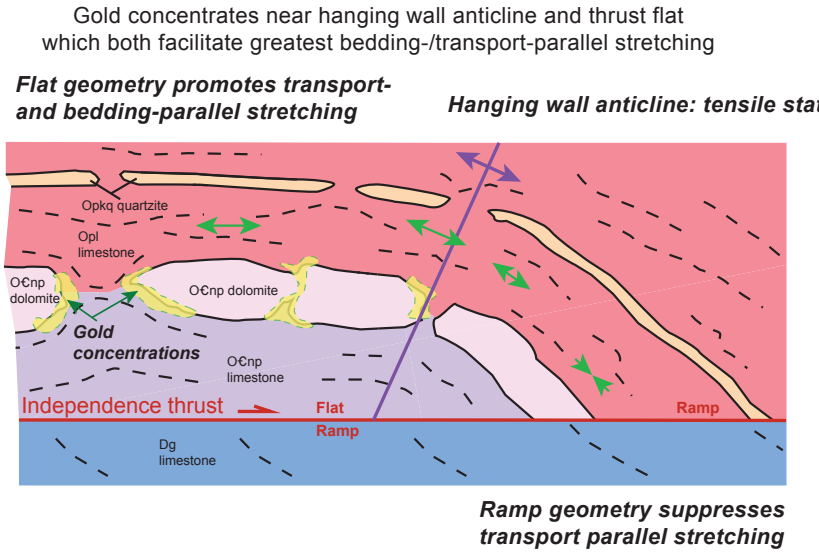

Figure 17. Sketch showing favorable conditions for concentrated gold deposition in the northern Pequop Mountains. Long Canyon gold deposits concentrate in boudin necks (e.g., Smith et al., 2013), in a hanging-wall anticline of the Independence thrust and/or along the hanging-wall flat portion of this thrust. We interpret that thrust-transport-parallel stretching of the hanging wall is greatest along a thrust flat, whereas the thrust ramp suppresses some stretching (shown with green arrows).

Three phases of intrusions (i.e., Jurassic, Cretaceous, and Eocene) are thought to be important for typical CTDs, with the Eocene pulse providing the final heat and fluid source for mineralization (Henry and Boden, 1998; Ressel and Henry, 2006). Small Eocene highly differentiated rhyolite dikes in the western Pequop Mountains and dacite lavas in the northern part (Plate 1) (e.g., Bedell et al., 2010; Milliard et al., 2015; Zuza et al., 2019a) require an underlying granitic magma chamber that may have driven mineralization. A large magnetic anomaly in Goshute Valley to the southeast of the Pequop Mountains has been interpreted as a large pluton at depth that may have fed the dikes observed in the Pequop Mountains (e.g., Raines et al., 1996; Kucks et al., 2006; Bedell et al., 2010) (Fig. 18). Our K-feldspar argon ages, MDD modeling, and AFT data are consistent with a pulse of Eocene heat and subsequent cooling (Figs. 6 and 7).

Our restoration of ~8 km, west-directed extension (281°) along the Pequop fault places the Nanny Creek paleovalley above the Long Canyon deposit (Figs. 13 and 14). The paleovalley eroded as deeply as the Mississippian Chainman Shale, and as a result of this erosion, the Long Canyon deposit would have formed at depths of ≤3 km. Other CTDs may have been located under paleovalley river systems, including the Cortez Hills deposit located ~1 km beneath a paleovalley (John et al., 2008). These observations highlight that CTD mineralization may be enhanced beneath advantageous hydrological configurations, such as large paleovalley systems, that influence shallow fluid-flow and host-rock interactions (e.g., Person et al., 2008). The

contact between massive limestones of the Guilmette Formation and overlying silty Tripon Pass Limestone, which is a favorable host zone for CTDs in the southern Carlin trend (Koehler et al., 2015), may also be favorable in the Pequop Mountains. The presence of hydrothermally altered conodonts in the lower Tripon Pass Limestone ~1 km south of the Independence Valley NE quadrangle is consistent with significant hydrothermal fluid circulation (Thorman et al., 2019; Zuza et al., 2020a).

9. CONCLUSIONS

Field and structural observations from the northern Pequop Mountains, NE Nevada, provide insight into the complex history of Mesozoic contraction and Cenozoic extension in the hinterland of the North American Cordillera. Key findings from this work include the following:

(1) Significant southeast-directed contractional deformation in the Pequop Mountains, including Independence thrust motion and intra-unit deformation, occurred in the Middle-Late Jurassic as constrained by crosscutting igneous rocks. This was part of the Middle-Late Jurassic Elko orogeny (ca. 170–157 Ma). No evidence for Cretaceous shortening was observed, but a Late Cretaceous thermal overprint was strong. Integrated with other observations across Nevada and Utah, Cordillera hinterland shortening in the Great Basin region was probably pulsed, with Late Jurassic and Late Cretaceous phases. Shortening led to crustal thickening, with Middle-Late Jurassic thickening of the proto-Nevadaplano orogenic plateau. Therefore, this plateau probably had a long-lived, two-phase, 100 m.y. history until its dismemberment in the Cenozoic.

(2) Field relationships and peak temperature-depth estimates suggesting a high Cretaceous geothermal gradient of 40 °C/km preclude deep burial of the Neoproterozoic–Paleozoic stratigraphy. This interpretation is at odds with models for regional burial by the cryptic Windermere thrust sheet.

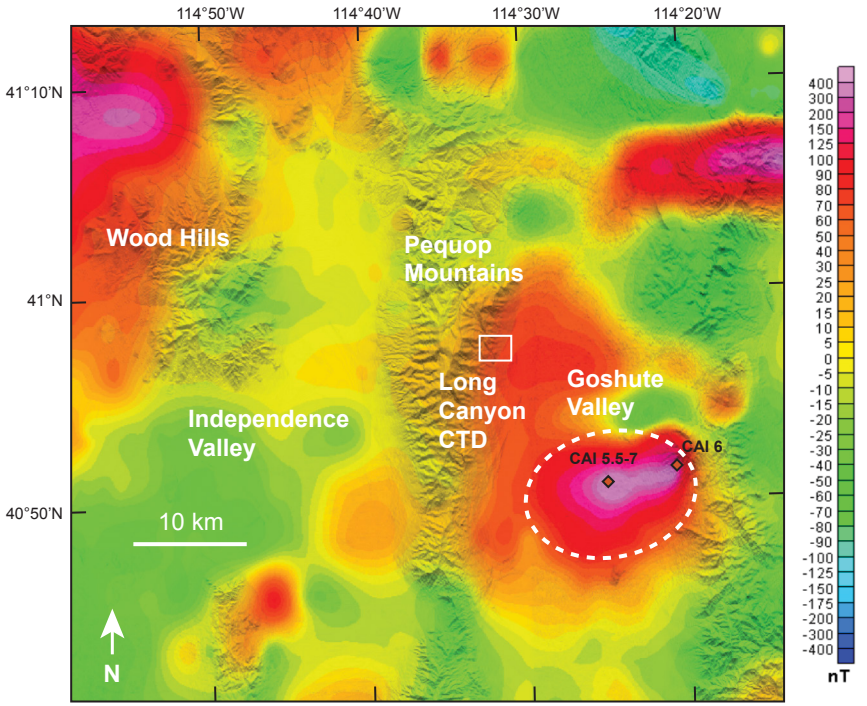

Figure 18. Magnetic anomaly map of the northern Pequop Mountains and surrounding valleys (Kucks et al., 2006) overlain on hillshaded relief map. The large magnetic anomaly in Goshute Valley (dashed white oval) may represent a large pluton that sourced Jurassic or Eocene felsic dikes in the Pequop Mountains (e.g., Bedell et al., 2010). Conodont color alteration index (CAI) data reported in Crafford (2007) are very high around this anomaly (CAI 5.5–7) for Ely Limestone samples, which supports this region being a very significant heat source. CTD—Carlin-type gold deposits.

(3) Middle-Late Jurassic, Late Cretaceous, and Eocene intrusions are dispersed across the Pequop Mountains. These intrusions were associated with thermal pulses that would have led to the observed elevated thermal gradient across the range, and $^{40}Ar/^{39}Ar$ and AFT thermochronology tracks the conductive cooling following these pulses.

(4) The Pequop fault was a major normal fault that is interpreted to have passively transported part of the Independence thrust and the Eocene Nanny Creek paleovalley westward. The normal fault may have been kinematically linked with the main normal-sense mylonitic shear zone in the Ruby Mountain–East Humboldt Range, possibly suggesting that the main breakaway was located east of the Pequop Mountains. We interpret that the fault was active in the late Oligocene(?)–middle Miocene, just prior to the more recent phase of high-angle, middle Miocene extensional range-front faulting.

(5) Gold mineralization at Long Canyon focused in the hanging-wall anticline of the Jurassic Independence thrust, within the necks of Jurassic boudins. The Jurassic structural framework was critical for Long Canyon mineralization, with Eocene magmatism

providing heat, and possibly the metals and fluids, for mineralization. A pronounced magmatic anomaly to the southeast of the Pequop Mountains in Goshute Valley probably marks a large plutonic source for one or more episode of igneous intrusion across the Pequop Mountains.

ACKNOWLEDGMENTS

This research was supported by the U.S. Geological Survey National Cooperative Geologic Mapping Program via State Map awards (G14AC00237, G16AC00186, G17AC00212, G18AC00198, and G19AC00383) and the National Science Foundation Tectonics program (EAR 1830139). Any use of trade, firm, or product names is for descriptive purposes only and does not imply endorsement by the U.S. Government. We thank Newmont Mining Corporation, especially Jeff Blackmon, for discussions and information about Pequop area geology. Agnico Eagle Mines Limited and geologists Gregg Loptien, Christina Ricks, and Jim Leavitt are acknowledged for geologic data and discussions of Pequop geology. We thank Steve Ruppel, Jerry Walker, and Fred Zoerner for discussions about Pequop area stratigraphy and structure. Margo Odlum provided valuable insight into the thermochronology data, and Connie Nutt provided useful comments on our manuscript. We thank Bill McIntosh, Lisa Peters, Jake Ross, and Nels Iverson for their help with $^{40}Ar/^{39}Ar$ dating in the New Mexico Geochronology Research Laboratory. Irene Edgerton provided cartographic assistance. We appreciate editorial handling and comments by Andrea Hampel. Detailed constructive reviews by Samuele Papeschi, Tom Anderson, and Eric James Ryan and Associate Editor Francesco Mazzarini greatly improved this paper.

REFERENCES CITED

Affinati, S.C., Hoisch, T.D., Wells, M.L., and Vervoort, J.D., 2020, Pressure-temperature-time paths from the Funeral Mountains, California, reveal Jurassic retroarc underthrusting during early Sevier orogenesis: Geological Society of America Bulletin, v. 132, p. 1047–1065, https://doi.org/10.1130/B35095.1.

Allmendinger, R.W., 1992, Fold and thrust tectonics of the western United States exclusive of the accreted terranes, *in* Burchfiel, B.C., et al., eds., The Cordilleran Orogen: Conterminous U.S.: Boulder, Colorado, Geological Society of America, Geology of North America, v. G-3, p. 583–608, https://doi.org/10.1130/DNAG-GNA-G3.583.

Allmendinger, R.W., and Jordan, T.E., 1984, Mesozoic structure of the Newfoundland Mountains, Utah: Horizontal shortening and subsequent extension in the hinterland of the Sevier belt: Geological Society of America Bulletin, v. 95, no. 11, p. 1280–1292, https://doi.org/10.1130/0016-7606(1984)95<1280:MSOTNM>2.0.CO;2.

Allmendinger, R.W., Sharp, J.W., Von Tish, D., Serpa, L., Brown, L., Kaufman, S., Oliver, J., and Smith, R.B., 1983, Cenozoic and Mesozoic structure of the eastern Basin and Range province, Utah, from COCORP seismic-reflection data: Geology, v. 11, no. 9, p. 532–536, https://doi.org/10.1130/0091-7613(1983)11<532:CAMSOT>2.0.CO;2.

Allmendinger, R.W., Miller, D.M., and Jordan, T.E., 1984, Known and inferred Mesozoic deformation in the hinterland of the Sevier belt, northwest Utah, *in* Kerns, G.J., and Kerns, R.L., eds., Geology of Northwest Utah, Southern Idaho, and Northeast Nevada: Utah Geological Association Publication, p. 21–34.

Allmendinger, R.W., Nelson, K.D., Potter, C.J., Barazangi, M., Brown, L.D., and Oliver, J.T., 1987, Deep seismic reflection characteristics of the continental crust: Geology, v. 15, no. 4, p. 304–310, https://doi.org/10.1130/0091-7613(1987)15<304:DSRCOT>2.0.CO;2.

Anderson, T.H., 2014, Dynamic processes in the lithosphere leading to extension, rifting and basin formation: European Geosciences Union, General Assembly, v. 16.

Anderson, T.H., 2015, Jurassic (170–150 Ma) basins: The tracks of a continental-scale fault, the Mexico-Alaska megashear, from the Gulf of Mexico to Alaska, *in* Anderson, T.H., Didenko, A.N., Johnson, C.L., Khanchuk, A.I., and MacDonald, J.H., Jr., eds., Late Jurassic Margin of Laurasia—A Record of Faulting Accommodating Plate Rotation: Geological Society of America Special Paper 513, p. 107–188, https://doi.org/10.1130/2015.2513(03).

Anderson, T.H., 2020, Middle (174–164 Ma) through Late (164–154 Ma) Jurassic deformational, magmatic, and stratigraphic events in Nevada: Inferred relations to far-field plate movements and mantle flow: Geological Society of Nevada Symposium Proceedings, p. 1–17.

Arehart, G.B., 1996, Characteristics and origin of sediment-hosted disseminated gold deposits: A review: Ore Geology Reviews, v. 11, no. 6, p. 383–403, https://doi.org/10.1016/S0169-1368(96)00010-8.

Armstrong, R.L., 1968, Sevier orogenic belt in Nevada and Utah: Geological Society of America Bulletin, v. 79, p. 429–458, https://doi.org/10.1130/0016-7606(1968)79[429:SOBINA]2.0.CO;2.

Atwater, T., 1970, Implications of plate tectonics for the Cenozoic tectonic evolution of western North America: Geological Society of America Bulletin, v. 81, no. 12, p. 3513–3536, https://doi.org/10.1130/0016-7606(1970)81[3513:IOPTFT]2.0.CO;2.

Atwater, T., and Stock, J., 1998, Pacific-North America plate tectonics of the Neogene southwestern United States: an update: International Geology Review, v. 40, no. 5, p. 375–402, https://doi.org/10.1080/00206819809465216.

Axen, G.J., van Wijk, J.W., and Currie, C.A., 2018, Basal continental mantle lithosphere displaced by flat-slab subduction: Nature Geoscience, v. 11, no. 12, p. 961–964, https://doi.org/10.1038/s41561-018-0263-9.

Bahadori, A., Holt, W.E., and Rasbury, E.T., 2018, Reconstruction modeling of crustal thickness and paleotopography of western North America since 36 Ma: Geosphere, v. 14, no. 3, p. 1207–1231, https://doi.org/10.1130/GES01604.1.

Barbarand, J., Carter, A., Wood, I., and Hurford, T., 2003, Compositional and structural control of fission-track annealing in apatite: Chemical Geology, v. 198, no. 1–2, p. 107–137, https://doi.org/10.1016/S0009-2541(02)00424-2.

Bedell, R., Struhsacker, E., Craig, L., Miller, M., Coolbaugh, M., Smith, J., Parratt, R.L., and Goldfarb, R.J., 2010, The Pequop mining district, Elko County, Nevada: An evolving new gold district, *in* Goldfarb, R.J., Marsh, E.E., and Monecke, T., eds., The Challenge of Finding New Mineral Resources: Global Metallogeny, Innovative Exploration, and New Discoveries: Special Publications of the Society of Economic Geologists, v. 15, p. 29–56.

Beranek, L.P., Link, P.K., and Fanning, C.M., 2016, Detrital zircon record of mid-Paleozoic convergent margin activity in the northern US Rocky Mountains: Implications for the Antler orogeny and early evolution of the North American Cordillera: Lithosphere, v. 8, no. 5, p. 533–550, https://doi.org/10.1130/L557.1.

Best, M.G., Armstrong, R.L., Graustein, W.C., Embree, G.F., and Ahlborn, R.C., 1974, Mica granites of the Kern Mountains pluton, eastern White Pine County, Nevada: Remobilized basement of the Cordilleran miogeosyncline?: Geological Society of America Bulletin, v. 85, p. 1277–1286, https://doi.org/10.1130/0016-7606(1974)85<1277:MGOTKM>2.0.CO;2.

Best, M.G., Barr, D.L., Christiansen, E.H., Gromme, S., Deino, A.L., and Tingey, D.G., 2009, The Great Basin Altiplano during the middle Cenozoic ignimbrite flareup: Insights from volcanic rocks: International Geology Review, v. 51, no. 7–8, p. 589–633, https://doi.org/10.1080/00206810902867690.

Best, M.G., Christiansen, E.H., de Silva, S., and Lipman, P.W., 2016, Slab-rollback ignimbrite flareups in the southern Great Basin and other Cenozoic American arcs: A distinct style of arc volcanism: Geosphere, v. 12, no. 4, p. 1097–1135, https://doi.org/10.1130/GES01285.1.

Bird, P., 1998, Kinematic history of the Laramide orogeny in latitudes 35°–49°N, western United States: Tectonics, v. 17, no. 5, p. 780–801, https://doi.org/10.1029/98TC02698.

Bjerrum, C.J., and Dorsey, R.J., 1995, Tectonic controls on deposition of Middle Jurassic strata in a retroarc foreland basin, Utah-Idaho trough, western interior, United States: Tectonics, v. 14, no. 4, p. 962–978, https://doi.org/10.1029/95TC01448.

Blackwell, D., Richards, M., Frone, Z., Batir, J., Ruzo, A., Dingwall, R., and Williams, M., 2011, Temperature at depth maps for the conterminous US and geothermal resource estimates: Geothermal Resource Council Transactions, v. 35.

Bond, G.C., Kominz, M.A., Steckler, M.S., and Grotzinger, J.P., 1989, Role of thermal subsidence, flexure, and eustasy in the evolution of early Paleozoic passive-margin carbonate plat forms, *in* Crevello, P., et al., eds., Controls on Carbonate Platform and Basin Development: SEPM (Society for Sedimentary Geology) Special Publication, v. 44, p. 39–61, https://doi.org/10.2110/pec.89.44.0039.

Brooks, W.E., Thorman, C.H., and Snee, L.W., 1995, The $^{40}Ar/^{39}Ar$ ages and tectonic setting of middle Eocene northeast Nevada volcanic field: Journal of Geophysical Research, v. 100, p. 10,403–10,416, https://doi.org/10.1029/94JB03389.

Brueseke, M.E., Callicoat, J.S., Hames, W., and Larson, P.B., 2014, Mid-Miocene rhyolite volcanism in northeastern Nevada: The Jarbidge Rhyolite and its relationship to the Cenozoic evolution of the northern Great Basin (USA): Geological Society of America Bulletin, v. 126, p. 1047–1067, https://doi.org/10.1130/B30736.1.

Brun, J.P., Sokoutis, D., Tirel, C., Gueydan, F., Van den Driessche, J., and Beslier, M.O., 2018, Crustal versus mantle core complexes: Tectonophysics, v. 746, p. 22–45, https://doi.org/10.1016/j.tecto.2017.09.017.

Burchfiel, B.C., and Davis, G.A., 1975, Nature and controls of Cordilleran orogenesis, western United States: Extension of an earlier synthesis: American Journal of Science, v. 275A, p. 363–396.

Burchfiel, B.C., Cowan, D.S., and Davis, G.A., 1992, Tectonic overview of the Cordilleran orogen in the western United States, *in* Burchfiel, B.C., Lipman, P.W., and Zoback, M.L., eds., Geology of North America, The Cordilleran Orogen: Conterminous U.S.: Boulder, Colorado, Geological Society of America, v. G-3, https://doi.org/10.1130/DNAG-GNA-G3.407.

Burtner, R.L., Nigrini, A., and Donelick, R.A., 1994, Thermochronology of Lower Cretaceous source rocks in the Idaho-Wyoming thrust belt: American Association of Petroleum Geologists Bulletin, v. 78, no. 10, p. 1613–1636.

Camilleri, P.A., 1994, Mesozoic and Cenozoic tectonic and metamorphic evolution of the Wood Hills and Pequop Mountains. Elko County, Nevada [Ph.D. dissertation]: Laramie, University of Wyoming, 196 p.

Camilleri, P.A., 1998, Prograde metamorphism, strain evolution, and collapse of footwalls of thick thrust sheets: A case study from the Mesozoic Sevier hinterland USA: Journal of Structural Geology, v. 20, no. 8, p. 1023–1042, https://doi.org/10.1016/S0191-8141(98)00032-7.

Camilleri, P., 2010a, Geologic map of the northern Pequop Mountains, Elko County, Nevada: Nevada Bureau of Mines and Geology Map 171, scale 1:48,000, 15 p.

Camilleri, P., 2010b, Geologic map of the Wood Hills, Elko County, Nevada: Nevada Bureau of Mines and Geology Map 172, scale 1:48,000, 16 p.

Camilleri, P.A., and Chamberlain, K.R., 1997, Mesozoic tectonics and metamorphism in the Pequop Mountains and Wood Hills region, northeast Nevada: Implications for the architecture and evolution of the Sevier orogen: Geological Society of America Bulletin, v. 109, no. 1, p. 74–94, https://doi.org/10.1130/0016-7606(1997)109<0074:MTAMIT>2.3.CO;2.

Camilleri, P., Yonkee, A., Coogan, J., DeCelles, P., McGrew, A., and Wells, M., 1997, Hinterland to foreland transect through the Sevier orogen, northeast Nevada to north central Utah: Structural style, metamorphism, and kinematic history of a large contractional orogenic wedge: Geology Studies, v. 42, p. 297–309.

Camilleri, P., Deibert, J., and Perkins, M., 2017, Middle Miocene to Holocene tectonics, basin evolution, and paleogeography along the southern margin of the Snake River Plain in the Knoll Mountain–Ruby–East Humboldt Range region, northeastern Nevada and south-central Idaho: Geosphere, v. 13, no. 6, p. 1901–1948, https://doi.org/10.1130/GES01318.1.

Canada, A.S., Cassel, E.J., McGrew, A.J., Smith, M.E., Stockli, D.F., Foland, K.A., Jicha, B.R., and Singer, B.S., 2019, Eocene exhumation and extensional basin formation in the Copper Mountains, Nevada, USA: Geosphere, v. 15, no. 5, p. 1577–1597, https://doi.org/10.1130/GES02101.1.

Cao, W., and Paterson, S., 2016, A mass balance and isostasy model: Exploring the interplay between magmatism, deformation and surface erosion in continental arcs using central Sierra Nevada as a case study: Geochemistry, Geophysics, Geosystems, v. 17, no. 6, p. 2194–2212, https://doi.org/10.1002/2015GC006229.

Cao, W., Paterson, S., Saleeby, J., and Zalunardo, S., 2016, Bulk arc strain, crustal thickening, magma emplacement, and mass balances in the Mesozoic Sierra Nevada arc: Journal of Structural Geology, v. 84, p. 14–30, https://doi.org/10.1016/j.jsg.2015.11.002.

Cardoso, R.R., Hamza, V.M., and Alfaro, C., 2010, Geothermal Resource Base for South America: A Continental Perspective. Proceedings World Geothermal Congress 2010, Bali, Indonesia, 25–29 April 2010.

Cashman, P., Trexler, J., Snyder, W., Davydov, V., and Taylor, W., 2008, Late Paleozoic deformation in central and southern Nevada, *in* Duebendorfer, E.M., and Smith, E.I., eds., Field Guide to Plutons, Volcanoes, Faults, Reefs, Dinosaurs and Possible Glaciation of Selected Areas of Arizona, California and Nevada: Geological Society of America Field Guide 11, p. 21–42.

Cassata, W.S., Renne, P.R., and Shuster, D.L., 2009, Argon diffusion in plagioclase and implications for thermochronometry: A case study from the Bushveld Complex, South Africa: Geochimica et Cosmochimica Acta, v. 73, p. 6600–6612, https://doi.org/10.1016/j.gca.2009.07.017.

Chapman, J.B., Ducea, M.N., DeCelles, P.G., and Profeta, L., 2015, Tracking changes in crustal thickness during orogenic evolution with Sr/Y: An example from the North American Cordillera: Geology, v. 43, no. 10, p. 919–922, https://doi.org/10.1130/G36996.1.

Christensen, N.I., and Mooney, W.D., 1995, Seismic velocity structure and composition of the continental crust: A global view: Journal of Geophysical Research. Solid Earth, v. 100, no. B6, p. 9761–9788, https://doi.org/10.1029/95JB00259.

Cline, J.S., and Hofstra, A.H., 2000, Ore-fluid evolution at the Getchell Carlin-type gold deposit, Nevada, USA: European Journal of Mineralogy, v. 12, no. 1, p. 195–212, https://doi.org/10.1127/ejm/12/1/0195.

Coats, R.R., 1987, Geology of Elko County, Nevada: Nevada Bureau of Mines and Geology Bulletin 101, 112 p.

Colgan, J.P., and Henry, C.D., 2009, Rapid middle Miocene collapse of the Mesozoic orogenic plateau in northcentral Nevada: International Geology Review, v. 51, p. 920–961, https://doi.org/10.1080/00206810903056731.

Colgan, J.P., Howard, K.A., Fleck, R.J., and Wooden, J.L., 2010, Rapid middle Miocene extension and unroofing of the southern Ruby Mountains, Nevada: Tectonics, v. 29, no. 6, https://doi.org/10.1029/2009TC002655.

Coney, P.J., and Harms, T.A., 1984, Cordilleran metamorphic core complexes: Cenozoic extensional relics of Mesozoic compression: Geology, v. 12, no. 9, p. 550–554, https://doi.org/10.1130/0091-7613(1984)12<550:CMCCCE>2.0.CO;2.

Cooper, F.J., Platt, J.P., Anczkiewicz, R., and Whitehouse, M.J., 2010, Footwall dip of a core complex detachment fault: Thermobarometric constraints from the northern Snake Range (Basin and Range, USA): Journal of Metamorphic Geology, v. 28, no. 9, p. 997–1020, https://doi.org/10.1111/j.1525-1314.2010.00907.x.

Copeland, P., Currie, C.A., Lawton, T.F., and Murphy, M.A., 2017, Location, location, location: The variable lifespan of the Laramide orogeny: Geology, v. 45, no. 3, p. 223–226, https://doi.org/10.1130/G38810.1.

Craddock, W.H., Kirby, E., Zhang, H., Clark, M.K., Champagnac, J.D., and Yuan, D., 2014, Rates and style of Cenozoic deformation around the Gonghe Basin, northeastern Tibetan Plateau: Geosphere, v. 10, no. 6, p. 1255–1282, https://doi.org/10.1130/GES01024.1.

Crafford, A.E.J., 2007, Geologic map of Nevada: U.S. Geological Survey Data Series 249, 1 CD-ROM, 46 p.

Cruz-Uribe, A.M., Hoisch, T.D., Wells, M.L., Vervoort, J.D., and Mazdab, F.K., 2015, Linking thermodynamic modelling, Lu–Hf geochronology and trace elements in garnet: New P–T–t paths from the Sevier hinterland: Journal of Metamorphic Geology, v. 33, no. 7, p. 763–781, https://doi.org/10.1111/jmg.12151.

DeCelles, P.G., 2004, Late Jurassic to Eocene evolution of the Cordilleran thrust belt and foreland basin system, western USA: American Journal of Science, v. 304, no. 2, p. 105–168, https://doi.org/10.2475/ajs.304.2.105.

DeCelles, P.G., and Coogan, J.C., 2006, Regional structure and kinematic history of the Sevier fold-and-thrust belt, central Utah: Geological Society of America Bulletin, v. 118, no. 7–8, p. 841–864, https://doi.org/10.1130/B25759.1.

DeCelles, P.G., and Graham, S.A., 2015, Cyclical processes in the North American Cordilleran orogenic system: Geology, v. 43, no. 6, p. 499–502, https://doi.org/10.1130/G36482.1.

DeCelles, P.G., Lawton, T.F., and Mitra, G., 1995, Thrust timing, growth of structural culminations, and synorogenic sedimentation in the type Sevier orogenic belt, western United States: Geology, v. 23, no. 8, p. 699–702, https://doi.org/10.1130/0091-7613(1995)023<0699:TTGOSC>2.3.CO;2.

DeCelles, P.G., Ducea, M.N., Kapp, P., and Zandt, G., 2009, Cyclicity in Cordilleran orogenic systems: Nature Geoscience, v. 2, no. 4, p. 251–257, https://doi.org/10.1038/ngeo469.

Dee, S., and Ressel, M.W., 2016, Preliminary geologic map of the Herder Creek quadrangle, Elko County, Nevada: Nevada Bureau of Mines and Geology Open-File Report 2016-5, 1:24,000 scale, 5 p.

Dee, S., Henry, C.D., Ressel, M.W., and Zuza, A.V., 2017, Preliminary geologic map of the north half of the Independence Valley NW quadrangle and the adjacent part of the Independence Valley NE quadrangle, Elko County, Nevada: Nevada Bureau of Mines and Geology Open-File Report 17-6, scale 1:24,000, 4 p.

DeMets, C., and Merkouriev, S., 2016, High-resolution reconstructions of Pacific-North American plate motion: 20 Ma to present: Geophysical Journal International, v. 207, p. 741–773, https://doi.org/10.1093/gji/ggw305.

Derry, L.A., Evans, M.J., Darling, R., and France-Lanord, C., 2009, Hydrothermal heat flow near the Main Central thrust, central Nepal Himalaya: Earth and Planetary Science Letters, v. 286, no. 1–2, p. 101–109, https://doi.org/10.1016/j.epsl.2009.06.036.

Dickinson, W.R., 2004, Evolution of the North American cordillera: Annual Review of Earth and Planetary Sciences, v. 32, p. 13–45, https://doi.org/10.1146/annurev.earth.32.101802.120257.

Dickinson, W.R., and Snyder, W.S., 1978, Plate tectonics of the Laramide orogeny, *in* Matthews, V., ed., Laramide Folding Associated with Basement Block Faulting in the Western United States: Geological Society of America Memoir 151, p. 335–366, https://doi.org/10.1130/MEM151-p355.

Donelick, R.A., O'Sullivan, P.B., and Ketcham, R.A., 2005, Apatite fission-track analysis: Reviews in Mineralogy and Geochemistry, v. 58, no. 1, p. 49–94, https://doi.org/10.2138/rmg.2005.58.3.

Drescher, A., Patel, P., Middleton, G., Camilleri, P.A., Deibert, J.E., and Schwartz, J.J., 2019, Late Oligocene extension in the East Humboldt-Wood Hills-Pequop metamorphic core complex: New constraints from ages of detrital zircons in the Humboldt Formation along the northern margin of the Pequop Mountains, northern Nevada: Geological

Society of America Abstracts with Programs, v. 51, no. 5, https://doi.org/10.1130/abs/2019AM-330465.
Dubiel, R.F., Potter, C.J., Good, S.C., and Snee, L.W., 1996. Reconstructing an Eocene extensional basin: The White Sage Formation, eastern Great Basin, *in* Bertan, K.K., ed., Reconstructing the History of Basin and Range Extension Using Sedimentology and Stratigraphy: Geological Society of America Special Paper 303, p. 1–14, https://doi.org/10.1130/0-8137-2303-5.1.
Ducea, M., 2001, The California arc: Thick granitic batholiths, eclogitic residues, lithospheric- scale thrusting, and magmatic flare-ups: GSA Today, v. 11, no. 11, p. 4–10, https://doi.org/10.1130/1052-5173(2001)011<0004:TCATGB>2.0.CO;2.
Elison, M.W., 1995, Causes and consequences of Jurassic magmatism in the northern Great Basin: implications for tectonic development, *in* Miller, D.M., and Busby, C., eds., Jurassic Magmatism and Tectonics of the North American Cordillera: Geological Society of America Special Paper 299, p. 249–266, https://doi.org/10.1130/SPE299-p249.
Engebretson, D.C., Cox, A., and Gordon, R.G., 1984, Relative motions between oceanic plates of the Pacific basin: Journal of Geophysical Research. Solid Earth, v. 89, p. 10,291–10,310, https://doi.org/10.1029/JB089iB12p10291.
Faleiros, F.M., Moraes, R.D., Pavan, M., and Campanha, G.A.D.C., 2016, A new empirical calibration of the quartz c-axis fabric opening-angle deformation thermometer: Tectonophysics, v. 671, p. 173–182, https://doi.org/10.1016/j.tecto.2016.01.014.
Faulds, J.E., and Varga, R.J., 1998, The role of accommodation zones and transfer zones in the regional segmentation of extended terranes, *in* Faulds, J.E., and Stewart, J.H., eds., Accommodation Zones and Transfer Zones: The Regional Segmentation of the Basin and Range Province: Geological Society of America Special Paper 323, p. 44, https://doi.org/10.1130/0-8137-2323-X.1.
Fischer, M.W., and Coward, M.P., 1982, Strains and folds within thrust sheets: An analysis of the Heilam sheet, northwest Scotland: Tectonophysics, v. 88, no. 3–4, p. 291–312, https://doi.org/10.1016/0040-1951(82)90241-4.
Fletcher, R.C., and Hallet, B., 1983, Unstable extension of the lithosphere: A mechanical model for basin-and-range structure: Journal of Geophysical Research. Solid Earth, v. 88, no. B9, p. 7457–7466, https://doi.org/10.1029/JB088iB09p07457.
Francheteau, J., Jaupart, C., Shen, X.J., Kang, W., Lee, D., Bai, J., Wei, H., and Deng, H., 1984, High heat flow in southern Tibet: Nature, v. 307, no. 5946, p. 32–36, https://doi.org/10.1038/307032a0.
Fraser, G.S., Ketner, K.B., and Smith, M.C., 1986, Geologic map of the Spruce Mountain 4 quadrangle, Elko County, Nevada: U.S. Geological Survey Map MF-1846, scale 1:24000.
Frerichs, W.E., and Pekarek, A.H., 1994, Lower Miocene petroleum potential of northeast Elko County, Nevada, *in* Schalla, R.A., and Johnson, E.H., eds., Oil Fields of the Great Basin: Reno, Nevada Petroleum Society, p. 151–158.
Frost, B.R., Chamberlain, K.R., and Schumacher, J.C., 2001, Sphene (titanite): Phase relations and role as a geochronometer: Chemical Geology, v. 172, no. 1–2, p. 131–148, https://doi.org/10.1016/S0009-2541(00)00240-0.
Galbraith, R.F., 1998, The trouble with "probability density" plots of fission track ages: Radiation Measurements, v. 29, no. 2, p. 125–131, https://doi.org/10.1016/S1350-4487(97)00247-3.
Gallagher, K., 2012, Transdimensional inverse thermal history modeling for quantitative thermochronology: Journal of Geophysical Research. Solid Earth, v. 117, https://doi.org/10.1029/2011JB008825.
Gans, P.B., 1987, An open-system, two-layer crustal stretching model for the eastern Great Basin: Tectonics, v. 6, no. 1, p. 1–12, https://doi.org/10.1029/TC006i001p00001.
Gans, P.B., and Miller, E.L., 1983, Style of mid-Tertiary extension in east-central Nevada, *in* Nash, W.P., and Gurgel, K.D., eds., Geological Excursions in the Overthrust Belt and Metamorphic Complexes of the Intermontane Region: Utah Geological and Mineral Survey Special Study 59, p. 107–160.
Gao, R., Wang, H., Yin, A., Dong, S., Kuang, Z., Zuza, A.V., Li, W., and Xiong, X., 2013, Tectonic development of the northeastern Tibetan Plateau as constrained by high-resolution deep seismic-reflection data: Lithosphere, v. 5, no. 6, p. 555–574, https://doi.org/10.1130/L293.1.
Gébelin, A., Teyssier, C., Heizler, M.T., and Mulch, A., 2015, Meteoric water circulation in a rolling-hinge detachment system (northern Snake Range core complex, Nevada): Geological Society of America Bulletin, v. 127, no. 1–2, p. 149–161, https://doi.org/10.1130/B31063.1.
Gehrels, G.E., and Dickinson, W.R., 1995, Detrital zircon provenance of Cambrian to Triassic miogeoclinal and eugeoclinal strata in Nevada: American Journal of Science, v. 295, no. 1, p. 18–48, https://doi.org/10.2475/ajs.295.1.18.
Gehrels, G.E., Dickinson, W.R., Riley, B.C.D., Finney, S.C., and Smith, M.T., 2000, Detrital zircon geochronology of the Roberts Mountains allochthon, Nevada, *in* Gehrels, G.E., and Soreghan, M.J., eds., Paleozoic and Triassic Paleogeography and Tectonics of Western Nevada and Northern California: Geological Society of America Special Paper 347, p. 19–42, https://doi.org/10.1130/0-8137-2347-7.19.
Giallorenzo, M.A., Wells, M.L., Yonkee, W.A., Stockli, D.F., and Wernicke, B.P., 2018, Timing of exhumation, Wheeler Pass thrust sheet, southern Nevada and California: Late Jurassic to middle Cretaceous evolution of the southern Sevier fold-and-thrust belt: Geological Society of America Bulletin, v. 130, no. 3–4, p. 558–579, https://doi.org/10.1130/B31777.1.
Gifford, J.N., 2008, Quantifying Eocene and Miocene extension in the Sevier hinterland in Northeastern Nevada [Ph.D. dissertation]: Gainesville, University of Florida, 48 p.
Gleadow, A.J., and Brown, R.W., 2000, Fission-track thermochronology and the long-term denudational response to tectonics, *in* Summerfield, M.A., ed., Geomorphology and Global Tectonics: Chichester, Wiley, p. 57–76.
Gleadow, A.J.W., and Duddy, I.R., 1981, A natural long-term track annealing experiment for apatite: Nuclear Tracks, v. 5, no. 1–2, p. 169–174, https://doi.org/10.1016/0191-278X(81)90039-1.
Gonzalez, N., Metcalf, J.R., and McGrew, A.J., 2019, Thermochronology of upper crustal rocks in the Wood Hills, Nevada: Documenting the transition from contraction to extension in the U.S. Cordillera: Geological Society of America Abstracts with Programs, v. 51, no. 5, https://doi.org/10.1130/abs/2019AM-337822.
Good, S.C., Nester, P.L., and Snoke, A.W., 1995, Lacustrine mollusks from the Lower Humboldt Formation, northeastern Nevada, and possible late Eocene to Oligocene age: Geological Society of America Abstracts with Programs, v. 27, no. 1, p. 49.
Gottlieb, E.S., 2017, Geologic insights from zircon inheritance [Ph.D. dissertation]: Palo Alto, California, Stanford University, 354 p.
Greene, D.C., 2014, The Confusion Range, west-central Utah: Fold-thrust deformation and a western Utah thrust belt in the Sevier hinterland: Geosphere, v. 10, p. 148–169, https://doi.org/10.1130/GES00972.1.
Hacker, B.R., Yin, A., Christie, J.M., and Snoke, A.W., 1990, Differential stress, strain rate, and temperatures of mylonitization in the Ruby Mountains, Nevada: Implications for the rate and duration of uplift: Journal of Geophysical Research. Solid Earth, v. 95, p. 8569–8580, https://doi.org/10.1029/JB095iB06p08569.
Hadlari, T., Davis, W.J., Dewing, K., Heaman, L.M., Lemieux, Y., Ootes, L., Pratt, B.R., and Pyle, L.J., 2012, Two detrital zircon signatures for the Cambrian passive margin of northern Laurentia highlighted by new U-Pb results from northern Canada: Geological Society of America Bulletin, v. 124, no. 7–8, p. 1155–1168, https://doi.org/10.1130/B30530.1.
Hallett, B.W., and Spear, F.S., 2013, The P-T history of anatectic pelites of the Northern East Humboldt Range, Nevada: Evidence for tectonic loading, decompression, and anataxis: Journal of Petrology, v. 55, no. 1, p. 3–36, https://doi.org/10.1093/petrology/egt057.
Hallett, B.W., and Spear, F.S., 2015, Monazite, zircon, and garnet growth in migmatitic pelites as a record of metamorphism and partial melting in the East Humboldt Range, Nevada: The American Mineralogist, v. 100, no. 4, p. 951–972, https://doi.org/10.2138/am-2015-4839.
Hamilton, W., and Myers, W.B., 1966, Cenozoic tectonics of the western United States: Reviews of Geophysics, v. 4, no. 4, p. 509–549, https://doi.org/10.1029/RG004i004p00509.
Hammond, W.C., Blewitt, G., Kreemer, C., Murray-Moraleda, J.R., and Svarc, J.L., 2011, Global Positioning System Constraints on Crustal Deformation Before and During the 21 February 2008 Wells, Nevada M 6.0 Earthquake, *in* DePolo, C.M., and LaPointe, D.D., eds., The 21 February 2008 MW 6.0 Wells, Nevada Earthquake: A Compendium of Earthquake-Related investigations prepared by the University of Nevada, Reno: Nevada Bureau of Mines and Geology Special Publication, v. 36, p. 181–196.
Harrison, T.M., 1982, Diffusion of ^{40}Ar in hornblende: Contributions to Mineralogy and Petrology, v. 78, no. 3, p. 324–331, https://doi.org/10.1007/BF00398927.
Harrison, T.M., Duncan, I., and Mcdougall, I., 1985, Diffusion of ^{40}Ar in biotite: Temperature, pressure and compositional effects: Geochimica et Cosmochimica Acta, v. 49, p. 2461–2468, https://doi.org/10.1016/0016-7037(85)90246-7.
Harrison, T.M., Célérier, J., Aikman, A.B., Hermann, J., and Heizler, M.T., 2009, Diffusion of ^{40}Ar in muscovite: Geochimica et Cosmochimica Acta, v. 73, no. 4, p. 1039–1051, https://doi.org/10.1016/j.gca.2008.09.038.
Haschke, M., and Gunther, A., 2003, Balancing crustal thickening in arcs by tectonic vs. magmatic means: Geology, v. 31, no. 11, p. 933–936, https://doi.org/10.1130/G19945.1.
Haynes, S.R., 2003, Development of the Eocene Elko Basin, Northeastern Nevada: Implications for Paleogeography and Regional Tectonism [M.S. thesis]: Vancouver, BC, The University of British Columbia, 159 p.
Hellbusch, C.A., 2012, Implications for stratigraphic omission and structural thinning in the Pequop Mountains: geologic map of the Devonian Guilmette Formation, Elko County, Nevada [M.S. thesis]: Pocatello, Idaho State University, 115 p.

Henry, C.D., 2008, Ash-flow tuffs and paleovalleys in northeastern Nevada: Implications for Eocene paleogeography and extension in the Sevier hinterland, northern Great Basin: Geosphere, v. 4, p. 1–35, https://doi.org/10.1130/GES00122.1.

Henry, C.D., 2018, The Eocene Elko Basin and Elko Formation, NE Nevada: Paleotopographic controls on area, thickness, facies distribution, and petroleum potential: Salt Lake City, Utah, American Association of Petroleum Geologists Annual Convention and Exhibition, Poster 170, May 20–23.

Henry, C.D., and Boden, D.R., 1998, Eocene magmatism: The heat source for Carlin-type gold deposits of northern Nevada: Geology, v. 26, no. 12, p. 1067–1070, https://doi.org/10.1130/0091-7613(1998)026<1067:EMTHSF>2.3.CO;2.

Henry, C.D., and John, D.A., 2013, Magmatism, ash-flow tuffs, and calderas of the ignimbrite flareup in the western Nevada volcanic field, Great Basin, USA: Geosphere, v. 9, p. 951–1008, https://doi.org/10.1130/GES00867.1.

Henry, C.D., and Thorman, C.H., 2011, Geologic Map of the Wells Area, Elko County, Nevada *in* DePolo, C.M., and LaPointe, D.D., eds., The 21 February 2008 MW 6.0 Wells, Nevada Earthquake: A Compendium of Earthquake-Related Investigations Prepared by the University of Nevada, Reno: Nevada Bureau of Mines and Geology Special Publication, v. 36.

Henry, C.D., and Thorman, C.H., 2015, Preliminary geologic map of the Pequop Summit quadrangle, Elko County, Nevada: Nevada Bureau of Mines and Geology Open-File Report 15-8, scale 1:24,000, 12 p.

Henry, C.D., McGrew, A.J., Colgan, J.P., Snoke, A.W., and Brueseke, M.E., 2011, Timing, distribution, amount, and style of Cenozoic extension in the northern Great Basin, *in* Lee, J., and Evans, J.P., eds., Geologic Field Trips to the Basin and Range, Rocky Mountains Snake River Plain, and Terranes of the U.S. Cordillera: Geological Society of America Field Guide 21, p. 27–66, https://doi.org/10.1130/2011.0021(02).

Henry, C.D., Hinz, N.H., Faulds, J.E., Colgan, J.P., John, D.A., Brooks, E.R., Cassel, E.J., Garside, L.J., Davis, D.A., and Castor, S.B., 2012, Eocene-Early Miocene paleotopography of the Sierra Nevada-Great Basin-Nevadaplano based on widespread ash-flow tuffs and paleovalleys: Geosphere, v. 8, p. 1–27, https://doi.org/10.1130/GES00727.1.

Henry, C.D., Castor, S.B., Starkel, W.A., Ellis, B.S., Wolff, J.A., Laravie, J.A., McIntosh, W.C., and Heizler, M.T., 2017, Geology and evolution of the McDermitt caldera, northern Nevada and southeastern Oregon, western USA: Geosphere, v. 13, p. 1066–1112, https://doi.org/10.1130/GES01454.1.

Hickey, K., Tosdal, R., Haynes, S., and Moore, S., 2005, Tectonics, Paleogeography, Volcanic Succession, and the Depth of Formation of Eocene Sediment-Hosted Gold Deposits of the Northern Carlin Trend, Nevada: Geological Society of Nevada Field Trip Guidebook, v. 3, p. 97–105.

Hodges, K.V., Snoke, A.W., and Hurlow, H.A., 1992, Thermal evolution of a portion of the Sevier hinterland: the northern Ruby Mountains-East Humboldt Range and Wood Hills, northeastern Nevada: Tectonics, v. 11, no. 1, p. 154–164, https://doi.org/10.1029/91TC01879.

Hoisch, T.D., Wells, M.L., Beyene, M.A., Styger, S., and Vervoort, J.D., 2014, Jurassic Barrovian metamorphism in a western U.S. Cordilleran metamorphic core complex, Funeral Mountains, California: Geology, v. 42, no. 5, p. 399–402, https://doi.org/10.1130/G35352.1.

Howard, K.A., 2003, Crustal structure in the Elko-Carlin region, Nevada, during Eocene gold mineralization: Ruby-East Humboldt metamorphic core complex as a guide to the deep crust: Economic Geology and the Bulletin of the Society of Economic Geologists, v. 98, no. 2, p. 249–268, https://doi.org/10.2113/gsecongeo.98.2.249.

Howard, K.A., Wooden, J.L., Barnes, C.G., Premo, W.R., Snoke, A.W., and Lee, S.Y., 2011, Episodic growth of a Late Cretaceous and Paleogene intrusive complex of pegmatitic leucogranite, Ruby Mountains core complex, Nevada, USA: Geosphere, v. 7, no. 5, p. 1220–1248, https://doi.org/10.1130/GES00668.1.

Howland, C., 2016, High thermal gradient in the upper plate of a core complex, determined by calcite-dolomite and RSCM thermometry, Pequop Mountains, NV [B.S. Honors Thesis]: Schenectady, New York, Union College, 135 p.

Hudec, M.R., 1992, Mesozoic structural and metamorphic history of the central Ruby Mountains metamorphic core complex, Nevada: Geological Society of America Bulletin, v. 104, no. 9, p. 1086–1100, https://doi.org/10.1130/0016-7606(1992)104<1086:MSAMHO>2.3.CO;2.

Hudec, M.R., and Wright, J.E., 1990, Mesozoic history of the central part of the Ruby Mountains–East Humboldt Range metamorphic core complex, Nevada: Geological Society of America Abstracts with Programs, v. 22, no. 3, p. 30.

Hurlow, H.A., 1987, Structural geometry, fabric, and chronology of a Tertiary extensional shear zone - detachment system, southwestern East Humboldt Range, Elko County, NV [M.S. thesis]: University of Wyoming, Laramie, Wyoming, 141 p.

Hurlow, H.A., Snoke, A.W., and Hodges, K.V., 1991, Temperature and pressure of mylonitization in a Tertiary extensional shear zone, Ruby Mountains–East Humboldt Range, Nevada: Tectonic implications: Geology, v. 19, no. 1, p. 82–86, https://doi.org/10.1130/0091-7613(1991)019<0082:TAPOMI>2.3.CO;2.

Janecke, S.U., VanDenburg, C.J., Blankenau, J.J., and M'gonigle, J.W., 2000, Long-distance longitudinal transport of gravel across the Cordilleran thrust belt of Montana and Idaho: Geology, v. 28, no. 5, p. 439–442, https://doi.org/10.1130/0091-7613(2000)28<439:LLTOGA>2.0.CO;2.

Jessell, M.W., 1987, Grain-boundary migration microstructures in a naturally deformed quartzite: Journal of Structural Geology, v. 9, no. 8, p. 1007–1014, https://doi.org/10.1016/0191-8141(87)90008-3.

John, D.A., Wallace, A.R., Ponce, D.A., Fleck, R.B., and Conrad, J.E., 2000, New perspectives on the geology and origin of the northern Nevada rift, *in* Cluer, J.K., Price, J.G., Struhsacker, E.M., Hardyman, R.F., and Morris, C.L., eds., Geology and Ore Deposits 2000: The Great Basin and Beyond: Geological Society of Nevada Symposium Proceedings, 15–18 May 2000, p. 127–154.

John, D.A., Henry, C.D., and Colgan, J.P., 2008, Magmatic and tectonic evolution of the Caetano caldera, north-central Nevada: A tilted, mid-Tertiary eruptive center and source of the Caetano Tuff: Geosphere, v. 4, no. 1, p. 75–106, https://doi.org/10.1130/GES00116.1.

Jolivet, M., Brunel, M., Seward, D., Xu, Z., Yang, J., Roger, F., Tapponnier, P., Malavieille, J., Arnaud, N., and Wu, C., 2001, Mesozoic and Cenozoic tectonics of the northern edge of the Tibetan plateau: Fission-track constraints: Tectonophysics, v. 343, p. 111–134, https://doi.org/10.1016/S0040-1951(01)00196-2.

Jones, C.H., Sonder, L.J., and Unruh, J.R., 1998, Lithospheric gravitational potential energy and past orogenesis: Implications for conditions of initial Basin and Range and Laramide deformation: Geology, v. 26, no. 7, p. 639–642, https://doi.org/10.1130/0091-7613(1998)026<0639:LGPEAP>2.3.CO;2.

Jones, J.V., III, 1999, Deformational, magmatic, and metamorphic history of the central Ruby Mountains, Elko County, Nevada [M.S. thesis]: Laramie, University of Wyoming, 272 p.

Jordan, T.E., 1981, Thrust loads and foreland basin evolution, Cretaceous, western United States: American Association of Petroleum Geologists Bulletin, v. 65, no. 12, p. 2506–2520.

Kelly, E.D., Hoisch, T.D., Wells, M.L., Vervoort, J.D., and Beyene, M.A., 2015, An Early Cretaceous garnet pressure–temperature path recording synconvergent burial and exhumation from the hinterland of the Sevier orogenic belt, Albion Mountains, Idaho: Contributions to Mineralogy and Petrology, v. 170, no. 2, p. 1–22, https://doi.org/10.1007/s00410-015-1171-2.

Ketcham, R.A., 2005, Forward and inverse modeling of low-temperature thermochronometry data: Reviews in Mineralogy and Geochemistry, v. 58, no. 1, p. 275–314, https://doi.org/10.2138/rmg.2005.58.11.

Ketcham, R.A., Carter, A., Donelick, R.A., Barbarand, J., and Hurford, A.J., 2007, Improved modeling of fission-track annealing in apatite: The American Mineralogist, v. 92, no. 5–6, p. 799–810, https://doi.org/10.2138/am.2007.2281.

Ketner, K.B., 1984, Recent studies indicate that major structures in northeastern Nevada and the Golconda thrust in north-central Nevada are of Jurassic or Cretaceous age: Geology, v. 12, p. 483–486, https://doi.org/10.1130/0091-7613(1984)12<483:RSITMS>2.0.CO;2.

Ketner, K.B., 2008, The Inskip Formation, the Harmony Formation, and the Havallah Sequence of Northwestern Nevada—An Interrelated Paleozoic Assemblage in the Home of the Sonoma Orogeny: U.S. Geological Survey Professional Paper 1757, 21 p., https://doi.org/10.3133/pp1757.

Ketner, K.B., and Alpha, A.G., 1992, Mesozoic and Tertiary rocks near Elko Nevada—Evidence for Jurassic to Eocene folding and low-angle faulting: U.S. Geological Survey Bulletin 1988-C, p. 13.

Ketner, K.B., Day, W.C., Elrick, M., Vaag, M.K., Zimmerman, R.A., Snee, L.W., Saltus, R.W., Wardlaw, B.R., Taylor, M.E., and Harris, A.G., 1998, An outline of tectonic, igneous, and metamorphic events in the Goshute-Toano range between Silver Zone pass and White Horse pass, Elko county, Nevada: A history of superposed contractional and extensional deformation: U.S. Geological Survey Professional Paper 1593, 12 p.

Kirsch, M., Paterson, S.R., Wobbe, F., Ardila, A.M.M., Clausen, B.L., and Alasino, P.H., 2016, Temporal histories of Cordilleran continental arcs: Testing models for magmatic episodicity: The American Mineralogist, v. 101, no. 10, p. 2133–2154, https://doi.org/10.2138/am-2016-5718.

Koehler, R.D., and Wesnousky, S.G., 2011, Late Pleistocene regional extension rate derived from earthquake geology of late Quaternary faults across the Great Basin, Nevada, between 38.5 N and 40 N latitude: Geological Society of America Bulletin, v. 123, no. 3–4, p. 631–650, https://doi.org/10.1130/B30111.1.

Koehler, S.R., Jackson, M.R., Harp, M.T., Edie, R.J., Whitmer, N.E., Mathewson, D.C., Norby, J.W., and Henry, C., 2015,

Precious and base metal mineralization within a large Eocene, magmato-thermal system, Railroad district, Carlin trend, Nevada: Geological Society of Nevada New Concepts and Discoveries, p. 1229–1242.

Kucks, R.P., Hill, P.L., and Ponce, D.A., 2006, Nevada magnetic and gravity maps and data: A website for the distribution of data: U.S. Geological Survey Data Series 234, https://doi.org/10.3133/ds234.

Kuehn, C.A., and Rose, A.W., 1995, Carlin gold deposits, Nevada; origin in a deep zone of mixing between normally pressured and overpressured fluids: Economic Geology and the Bulletin of the Society of Economic Geologists, v. 90, no. 1, p. 17–36, https://doi.org/10.2113/gsecongeo.90.1.17.

Kuiper, K.F., Deino, A., Hilgen, F.J., Krijgsman, W., Renne, P.R., and Wijbrans, A.J., 2008, Synchronizing rock clocks of Earth history: Science, v. 320, no. 5875, p. 500–504, https://doi.org/10.1126/science.1154339.

Lachenbruch, A.H., 1979, Heat flow in the Basin and Range province and thermal effects of tectonic extension: Geothermics and Geothermal Energy, v. 117, p. 34–50, https://doi.org/10.1007/978-3-0348-6525-8_3.

Latham, J.R., 2016, Mechanisms and patterns of strain related to late Mesozoic tectonic shortening on the Independence Thrust, Pequop Mountains, Elko County Nevada: Keck Geology Consortium Short Contributions, v. 29, 6 p.

Law, R.D., 2014, Deformation thermometry based on quartz c-axis fabrics and recrystallization microstructures: A review: Journal of Structural Geology, v. 66, p. 129–161, https://doi.org/10.1016/j.jsg.2014.05.023.

Lawton, T.F., Cashman, P.H., Trexler, J.H., and Taylor, W.J., 2017, The late Paleozoic southwestern Laurentian borderland: Geology, v. 45, no. 8, p. 675–678, https://doi.org/10.1130/G39071.1.

Lee, S.Y., Barnes, C.G., Snoke, A.W., Howard, K.A., and Frost, C.D., 2003, Petrogenesis of Mesozoic, peraluminous granites in the Lamoille Canyon area, Ruby Mountains, Nevada, USA: Journal of Petrology, v. 44, no. 4, p. 713–732, https://doi.org/10.1093/petrology/44.4.713.

Leonardson, R.W., 2011, Barrick Cortez Gold Acres structure, *in* Steininger, R., and Pennell, B, eds., Great Basin Evolution and Metallogeny: Reno/Sparks, Nevada: Geological Society of Nevada Symposium Volume, p. 17–29.

Levy, D.A., Zuza, A.V., Haproff, P.J., and Odlum, M.L., 2021, Early Permian tectonic evolution of the Last Chance thrust system: An example of induced subduction initiation along a plate boundary transform: Geological Society of America Bulletin, v. 113, p. 1105–1127, https://doi.org/10.1130/B35752.1.

Lewis, C.J., Wernicke, B.P., Selverstone, J., and Bartley, J.M., 1999, Deep burial of the footwall of the northern Snake Range decollement, Nevada: Geological Society of America Bulletin, v. 111, no. 1, p. 39–51, https://doi.org/10.1130/0016-7606(1999)111<0039:DBOTFO>2.3.CO;2.

Li, B., Chen, X., Zuza, A.V., Hu, D., Ding, W., Huang, P., and Xu, S., 2019, Cenozoic cooling history of the North Qilian Shan, northern Tibetan Plateau, and the initiation of the Haiyuan fault: Constraints from apatite-and zircon-fission track thermochronology: Tectonophysics, v. 751, p. 109–124, https://doi.org/10.1016/j.tecto.2018.12.005.

Li, J., Zhang, Y., Dong, S., and Johnston, S.T., 2014, Cretaceous tectonic evolution of South China: A preliminary synthesis: Earth-Science Reviews, v. 134, p. 98–136, https://doi.org/10.1016/j.earscirev.2014.03.008.

Li, J., Dong, S., Cawood, P.A., Zhao, G., Johnston, S.T., Zhang, Y., and Xin, Y., 2018, An Andean-type retro-arc foreland system beneath northwest South China revealed by SINOPROBE profiling: Earth and Planetary Science Letters, v. 490, p. 170–179, https://doi.org/10.1016/j.epsl.2018.03.008.

Li, Z.X., and Li, X.H., 2007, Formation of the 1300-km-wide intracontinental orogen and postorogenic magmatic province in Mesozoic South China: A flat-slab subduction model: Geology, v. 35, no. 2, p. 179–182, https://doi.org/10.1130/G23193A.1.

Livaccari, R.F., Burke, K., and Şengör, A.M.C., 1981, Was the Laramide orogeny related to subduction of an oceanic plateau?: Nature, v. 289, 5795, https://doi.org/10.1038/289276a0.

Long, S.P., 2012, Magnitudes and spatial patterns of erosional exhumation in the Sevier hinterland, eastern Nevada and western Utah, USA: Insights from a Paleogene paleogeologic map: Geosphere, v. 8, no. 4, p. 881–901, https://doi.org/10.1130/GES00783.1.

Long, S.P., 2015, An upper-crustal fold province in the hinterland of the Sevier orogenic belt, eastern Nevada, USA: A Cordilleran Valley and Ridge in the Basin and Range: Geosphere, v. 11, no. 2, p. 404–424, https://doi.org/10.1130/GES01102.1.

Long, S.P., 2018, Geometry and magnitude of extension in the Basin and Range Province (39° N), Utah, Nevada, and California, USA: Constraints from a province-scale cross section: Geological Society of America Bulletin, v. 131, no. 1–2, p. 99–119.

Long, S.P., and Soignard, E., 2016, Shallow-crustal metamorphism during Late Cretaceous anatexis in the Sevier hinterland plateau: Peak temperature conditions from the Grant Range, eastern Nevada, USA: Lithosphere, v. 8, no. 2, p. 150–164, https://doi.org/10.1130/L501.1.

Long, S.P., Henry, C.D., Muntean, J.L., Edmondo, G.P., and Cassel, E.J., 2014, Early Cretaceous construction of a structural culmination, Eureka, Nevada, USA: Implications for out-of-sequence deformation in the Sevier hinterland: Geosphere, v. 10, no. 3, p. 564–584, https://doi.org/10.1130/GES00997.1.

Long, S.P., Thomson, S.N., Reiners, P.W., and Di Fiori, R.V., 2015, Synorogenic extension localized by upper-crustal thickening: An example from the Late Cretaceous Nevadaplano: Geology, v. 43, no. 4, p. 351–354, https://doi.org/10.1130/G36431.1.

Long, S.P., Gordon, S.M., Young, J.P., and Soignard, E., 2016, Temperature and strain gradients through Lesser Himalayan rocks and across the Main Central thrust, south central Bhutan: Implications for transport-parallel stretching and inverted metamorphism: Tectonics, v. 35, no. 8, p. 1863–1891, https://doi.org/10.1002/2016TC004242.

Long, S.P., Heizler, M.T., Thomson, S.N., Reiners, P.W., and Fryxell, J.E., 2018, Rapid Oligocene to early Miocene extension along the Grant Range detachment system, Nevada, USA: Insights from multipart cooling histories of footwall rocks: Tectonics, v. 37, no. 12, p. 4752–4779, https://doi.org/10.1029/2018TC005073.

Long, S.P., Mullady, C.L., Starnes, J.K., Gordon, S.M., Larson, K.P., Pianowski, L.S., Miller, R.B., and Soignard, E., 2019, A structural model for the South Tibetan detachment system in northwestern Bhutan from integration of temperature, fabric, strain, and kinematic data: Lithosphere, v. 11, no. 4, p. 465–487, https://doi.org/10.1130/L1049.1.

Lovera, O.M., Richter, F.M., and Harrison, T.M., 1989, The $^{40}Ar/^{39}Ar$ thermochronometry for slowly cooled samples having a distribution of diffusion domain sizes: Journal of Geophysical Research. Solid Earth, v. 94, no. B12, p. 17,917–17,935, https://doi.org/10.1029/JB094iB12p17917.

Ludwig, K.R., 2003, User's Manual for Isoplot 3.00: A Geochronological Toolkit for Microsoft Excel: Berkeley Geochronology Center Special Publication 4, 74 p.

Lund Snee, J.E., and Miller, E.L., 2020, Cenozoic Magmatism, Migrating Topography, and the Onset of Basin and Range Faulting: Geological Society of Nevada 2020 Symposium Proceedings, p. 1299–1300.

Lund Snee, J.E., Miller, E.L., Grove, M., Hourigan, J.K., and Konstantinou, A., 2016, Cenozoic paleogeographic evolution of the Elko Basin and surrounding region, northeast Nevada: Geosphere, v. 12, no. 2, p. 464–500, https://doi.org/10.1130/GES01198.1.

MacCready, T., 1996, Misalignment of quartz c-axis fabrics and lineations due to oblique final strain increments in the Ruby Mountains core complex, Nevada: Journal of Structural Geology, v. 18, no. 6, p. 765–776, https://doi.org/10.1016/S0191-8141(96)80010-1.

MacCready, T., Snoke, A.W., Wright, J.E., and Howard, K.A., 1997, Mid-crustal flow during Tertiary extension in the Ruby Mountains core complex, Nevada: Geological Society of America Bulletin, v. 109, no. 12, p. 1576–1594, https://doi.org/10.1130/0016-7606(1997)109<1576:MCFDTE>2.3.CO;2.

Malavieille, J., 1987, Extensional shearing deformation and kilometer-scale "a"-type folds in a Cordilleran Metamorphic Core Complex (Raft River Mountains, northwestern Utah): Tectonics, v. 6, no. 4, p. 423–448, https://doi.org/10.1029/TC006i004p00423.

McGrew, A., 2018, Geologic map of the Humboldt Peak quadrangle, Elko County, Nevada: Nevada Bureau of Mines and Geology Map 186, scale 1:24,000, 23 p.

McGrew, A.J., and Snee, L.W., 1994, $^{40}Ar/^{39}Ar$ thermochronologic constraints on the tectonothermal evolution of the northern East Humboldt Range metamorphic core complex, Nevada: Tectonophysics, v. 238, no. 1–4, p. 425–450, https://doi.org/10.1016/0040-1951(94)90067-1.

McGrew, A.J., and Snoke, A.W., 2015, Geologic map of the Welcome quadrangle and an adjacent part of the Wells quadrangle, Elko County, Nevada: Nevada Bureau of Mines and Geology Map 184.

McGrew, A.J., Peters, M.T., and Wright, J.E., 2000, Thermobarometric constraints on the tectonothermal evolution of the East Humboldt Range metamorphic core complex, Nevada: Geological Society of America Bulletin, v. 112, no. 1, p. 45–60, https://doi.org/10.1130/0016-7606(2000)112<45:TCOTTE>2.0.CO;2.

McQuarrie, N., and Wernicke, B.P., 2005, An animated tectonic reconstruction of southwestern North America since 36 Ma: Geosphere, v. 1, no. 3, p. 147–172, https://doi.org/10.1130/GES00016.1.

Means, W.D., 1989, Stretching faults: Geology, v. 17, no. 10, p. 893–896, https://doi.org/10.1130/0091-7613(1989)017<0893:SF>2.3.CO;2.

Metcalf, J.R., McGrew, A.J., Mueller, C., and Meisner, C.B., 2019, The Oligocene-Miocene cooling and exhumation of a Cordillera metamorphic core complex: New apatite, zircon, and titanite (U-Th)/He thermochronology from the Ruby Mountains, Nevada: Geological Society of America Abstracts with Programs, v. 51, no. 5, https://doi.org/10.1130/abs/2019AM-335261.

Miller, D.M., and Hoisch, T.D., 1992, Mesozoic structure, metamorphism, and magmatism in the Pilot and Toano ranges, *in* Wilson, J.R., ed., Field Guide to Geologic Excursions in Utah and Adjacent Areas of Nevada, Idaho, and Wyoming: Geological Society of America and Utah Geological Survey Miscellaneous Publication 92-3, p. 79–92.

Miller, D.M., and Hoisch, T.D., 1995, Jurassic tectonics of northeastern Nevada and northwestern Utah from the perspective of barometric studies, *in* Miller, D.M., and Busby, C., eds., Jurassic Magmatism and Tectonics of the North American Cordillera: Geological Society of America Special Paper 299, p. 267–294, https://doi.org/10.1130/SPE299-p267.

Miller, E.L., and Gans, P.B., 1989, Cretaceous crustal structure and metamorphism in the hinterland of the Sevier thrust belt, western U.S. Cordillera: Geology, v. 17, no. 1, p. 59–62, https://doi.org/10.1130/0091-7613(1989)017<0059:CCSAMI>2.3.CO;2.

Miller, E.L., Gans, P.B., and Garing, J., 1983, The Snake Range decollement: An exhumed mid-Tertiary ductile-brittle transition: Tectonics, v. 2, no. 3, p. 239–263, https://doi.org/10.1029/TC002i003p00239.

Milliard, A.K., Ressel, M.W., Henry, C.D., Ricks, C., and Loptien, G., 2015, Age, Distribution, and Composition of Igneous Rocks of the Pequop Mountains, Northeast Nevada: Association with Carlin-type Gold Deposits: Geological Society of Nevada, 2015 Symposium, p. 895–923.

Min, K., Mundil, R., Renne, P.R., and Ludwig, K.R., 2000, A test for systematic errors in $^{40}Ar/^{39}Ar$ geochronology through comparison with U/Pb analysis of a 1.1-Ga rhyolite: Geochimica et Cosmochimica Acta, v. 64, p. 73–98, https://doi.org/10.1016/S0016-7037(99)00204-5.

Misch, P., and Hazzard, J.C., 1962, Stratigraphy and metamorphism of Late Precambrian rocks in central northeastern Nevada and adjacent Utah: AAPG Bulletin, v. 46, no. 3, p. 289–343.

Mortensen, J.K., Thompson, J.F.H., and Tosdal, R.M., 2000, U-Pb age constraints on magmatism and mineralization in the northern Great Basin, Nevada, *in* Cluer, J.K., Price, J.G., Struhsacker, E.M., Hardyman, R.F., and Morris, C.L., eds., Geology and Ore Deposits: The Great Basin and beyond: Geological Society of Nevada Symposium Proceedings, p. 419–438.

Mueller, C., 2019, Thermochronology of the deep crust in the northern Ruby Mountains, NV [B.S. thesis]: University of Colorado Boulder, 30 p.

Mueller, K.J., 1993, Geologic map of the Windermere Hills, Elko County, Nevada (with cross sections and descriptions of geologic units): Nevada Bureau of Mines and Geology Field Studies Map, no. 4, scale 1:48,000.

Mueller, K.J., and Snoke, A.W., 1993, Progressive overprinting of normal fault systems and their role in Tertiary exhumation of the East Humboldt-Wood Hills Metamorphic Complex northeast Nevada: Tectonics, v. 12, no. 2, p. 361–371, https://doi.org/10.1029/92TC01967.

Mueller, K.J., Cerveny, P.K., Perkins, M.E., and Snee, L.W., 1999, Chronology of polyphase extension in the Windermere Hills, northeast Nevada: Geological Society of America Bulletin, v. 111, p. 11–27, https://doi.org/10.1130/0016-7606(1999)111<0011:COPEIT>2.3.CO;2.

Munroe, J.S., and Laabs, B.J., 2013, Temporal correspondence between pluvial lake highstands in the southwestern US and Heinrich Event 1: Journal of Quaternary Science, v. 28, no. 1, p. 49–58, https://doi.org/10.1002/jqs.2586.

Muntean, J.L., Cline, J.S., Simon, A.C., and Longo, A.A., 2011, Magmatic–hydrothermal origin of Nevada's Carlin-type gold deposits: Nature Geoscience, v. 4, no. 2, p. 122–127, https://doi.org/10.1038/ngeo1064.

Nutt, C.J., and Hofstra, A.H., 2003, Alligator Ridge district, east-central Nevada: Carlin-type gold mineralization at shallow depths: Economic Geology and the Bulletin of the Society of Economic Geologists, v. 98, no. 6, p. 1225–1241, https://doi.org/10.2113/gsecongeo.98.6.1225.

Oldow, J.S., 1984, Evolution of a late Mesozoic back-arcfold and thrust belt, northwestern Great Basin, U.S.A: Tectonophysics, v. 102, p. 245–274, https://doi.org/10.1016/0040-1951(84)90016-7.

Oldow, J.S., Bally, A.W., Avé Lallemant, H.G., and Leeman, W.P., 1989, Phanerozoic evolution of the North American Cordillera; United States and Canada, *in* Bally, A.W., and Palmer, A.R., eds., The Geology of North America—An Overview: Boulder, Colorado, Geological Society of America, Geology of North America, v. A, p. 139–232.

Oversby, B.S., 1972, Thrust sequences in the Windermere Hills, northeastern Elko County, Nevada: Geological Society of America Bulletin, v. 83, p. 2677–2688, https://doi.org/10.1130/0016-7606(1972)83[2677:TSITWH]2.0.CO;2.

Paterson, S.R., and Ducea, M.N., 2015, Arc magmatic tempos: gathering the evidence: Elements, v. 11, no. 2, p. 91–98, https://doi.org/10.2113/gselements.11.2.91.

Pérouse, E., and Wernicke, B.P., 2017, Spatiotemporal evolution of fault slip rates in deforming continents: The case of the Great Basin region, northern Basin and Range province: Geosphere, v. 13, no. 1, p. 112–135, https://doi.org/10.1130/GES01295.1.

Person, M., Banerjee, A., Hofstra, A., Sweetkind, D., and Gao, Y., 2008, Hydrologic models of modern and fossil geothermal systems in the Great Basin: Genetic implications for epithermal Au-Ag and Carlin-type gold deposits: Geosphere, v. 4, p. 888–917, https://doi.org/10.1130/GES00150.1.

Poole, F.G., and Sandberg, C.A., 1977, Mississippian paleogeography and tectonics of the western United State, *in* Stewart, J.H., Stevens, C.H., and Fritsche, A.E., eds., Paleozoic Paleogeography of the Western United States: Society of Economic Paleontologists and Mineralogists, Pacific Section, Pacific Coast Paleogeography Symposium 1, p. 181–215.

Profeta, L., Ducea, M.N., Chapman, J.B., Paterson, S.R., Gonzales, S.M.H., Kirsch, M., Petrescu, L., and DeCelles, P.G., 2015, Quantifying crustal thickness over time in magmatic arcs: Scientific Reports, v. 5, no. 17786, p. 1–7.

Raines, G.L., Sawatzky, D.L., and Connors, K.A., 1996, Great Basin geoscience data base: U.S. Geological Survey Data Series 41.

Reheis, M.C., 1999, Extent of Pleistocene lakes in the western Great Basin: U.S. Geological Survey Miscellaneous Field Studies Map, no 2323.

Ressel, M.W., and Henry, C.D., 2006, Igneous geology of the Carlin trend, Nevada: Development of the Eocene plutonic complex and significance for Carlin-type gold deposits: Economic Geology and the Bulletin of the Society of Economic Geologists, v. 101, no. 2, p. 347–383, https://doi.org/10.2113/gsecongeo.101.2.347.

Rey, P., Vanderhaeghe, O., and Teyssier, C., 2001, Gravitational collapse of the continental crust: Definition, regimes and modes: Tectonophysics, v. 342, no. 3–4, p. 435–449, https://doi.org/10.1016/S0040-1951(01)00174-3.

Rey, P.F., Teyssier, C., and Whitney, D.L., 2009, Extension rates, crustal melting, and core complex dynamics: Geology, v. 37, no. 5, p. 391–394, https://doi.org/10.1130/G25460A.1.

Rhys, D., Valli, F., Burgess, R., Heitt, D., Greisel, G., and Hart, K., 2015, Controls of fault and fold geometry on the distribution of gold mineralization on the Carlin trend, *in* Prennell, W.M., and Garsize, L.J., eds., New concepts and discoveries: Proceedings, Geological Society of Nevada Symposium, v. 1, p. 333–389.

Riva, J., 1970, Thrusted Paleozoic rocks in the northern and central HD Range, northeastern Nevada: Geological Society of America Bulletin, v. 81, p. 2689–2716, https://doi.org/10.1130/0016-7606(1970)81[2689:TPRITN]2.0.CO;2.

Roberts, R.J., Hotz, P.E., Gilluly, J., and Ferguson, H.G., 1958, Paleozoic rocks of north-central Nevada: American Association of Petroleum Geologists Bulletin, v. 42, p. 2813–2857.

Royse, F., Jr., Warner, M.A., and Reese, D.L., 1975, Thrust belt structural geometry and related stratigraphic problems, Wyoming-Idaho–northern Utah: Denver, Rocky Mountain Association of Geologists Symposium Volume, p. 41–54.

Saltus, R.W., and Jachens, R.C., 1995, Gravity and basin-depth maps of the Basin and Range Province, western United States: Geophysical Investigation Map 1012.

Satarugsa, P., and Johnson, R.A., 2000, Cenozoic tectonic evolution of the Ruby Mountains metamorphic core complex and adjacent valleys, northeastern Nevada: Rocky Mountain Geology, v. 35, no. 2, p. 205–230, https://doi.org/10.2113/35.2.205.

Schellart, W.P., Stegman, D.R., Farrington, R.J., Freeman, J., and Moresi, L., 2010, Cenozoic tectonics of western North America controlled by evolving width of Farallon slab: Science, v. 329, no. 5989, p. 316–319, https://doi.org/10.1126/science.1190366.

Schweickert, R.A., 2015, Jurassic evolution of the Western Sierra Nevada metamorphic province, *in* Anderson, T.H., Didenko, A.N., Johnson, C.L., Khanchuk, A.I., and MacDonald, J.H., Jr., eds., Late Jurassic Margin of Laurasia—A Record of Faulting Accommodating Plate Rotation: Late Jurassic Margin of Laurasia—A Record of Faulting Accommodating Plate Rotation: Geological Society of America Special Paper 513, p. 299–358, https://doi.org/10.1130/2015.2513(08).

Schweickert, R.A., Merguerian, C., and Bogen, N.L., 1988, Deformational and metamorphic history of Paleozoic and Mesozoic basement terranes in the western Sierra Nevada metamorphic belt, *in* Ernst, W.G., ed., Metamorphism and Crustal Evolution of the Western United States: Englewood Cliffs, New Jersey, Prentice-Hall, p. 789–820.

Seton, M., Müller, R.D., and Zahirovic, S., 2012, Global continental and ocean basin reconstructions since 200 Ma: Earth-Science Reviews, v. 113, no. 3–4, p. 212–270, https://doi.org/10.1016/j.earscirev.2012.03.002.

Sharma, P.V., 1997, Environmental and Engineering Geophysics: Cambridge University Press, https://doi.org/10.1017/CBO9781139171168.

Sharp, R.P., 1939, The Miocene Humboldt Formation in northeastern Nevada: The Journal of Geology, v. 47, no. 2, p. 133–160, https://doi.org/10.1086/624749.

Shu, L.S., Zhou, X.M., Deng, P., Wang, B., Jiang, S.Y., Yu, J.H., and Zhao, X.X., 2009, Mesozoic tectonic evolution of the Southeast China Block: New insights from basin analysis:

Journal of Asian Earth Sciences, v. 34, no. 3, p. 376–391, https://doi.org/10.1016/j.jseaes.2008.06.004.
Smith, D.L., Wyld, S.J., Miller, E.L., and Wright, J.E., 1993, Progression and timing of Mesozoic crustal shortening in the northern Great Basin, western USA, *in* Dunn, G., and McDougall, L., eds., Mesozoic Paleogeography of the Western United States II: SEPM Book 71, p. 389–406.
Smith, J.F., Jr., Ketner, K.B., Hernandez, G.X., Harris, A.G., and Smith, M.C., 1983, Preliminary geologic map of the southern Snake Mountains, Elko County, Nevada: U.S. Geological Survey Open-File Map 83-303, scale 1:24,000.
Smith, M.E., Cassel, E.J., Jicha, B.R., Singer, B.S., and Canada, A.S., 2017, Hinterland drainage closure and lake formation in response to middle Eocene Farallon slab removal, Nevada, USA: Earth and Planetary Science Letters, v. 479, p. 156–169, https://doi.org/10.1016/j.epsl.2017.09.023.
Smith, M.T., Rhys, D., Ross, K., Lee, C., and Gray, J.N., 2013, The Long Canyon deposit: Anatomy of a new off-trend sedimentary rock-hosted gold discovery in northeastern Nevada: Economic Geology and the Bulletin of the Society of Economic Geologists, v. 108, no. 5, p. 1119–1145, https://doi.org/10.2113/econgeo.108.5.1119.
Snell, K.E., Koch, P.L., Druschke, P., Foreman, B.Z., and Eiler, J.M., 2014, High elevation of the 'Nevadaplano' during the Late Cretaceous: Earth and Planetary Science Letters, v. 386, p. 52–63, https://doi.org/10.1016/j.epsl.2013.10.046.
Snelson, S., 1955, The Geology of the Southern Pequop Mountains, Elko County, northeastern Nevada [M.S. thesis]: Seattle, Washington, University of Washington, 59 p.
Snelson, S., 1957, The geology of the northern Ruby Mountains and eastern Humboldt Range, Elko County, northeastern Nevada [Ph.D. dissertation]: Seattle, Washington, University of Washington, 268 p.
Snoke, A.W., 1980, Transition from infrastructure to suprastructure in the northern Ruby Mountains, Nevada, *in* Crittenden, M.D., Coney, P.J., and Davis, G.H., eds., Cordilleran Metamorphic Core Complexes: Geological Society of America Memoir 153, p. 287-334, https://doi.org/10.1130/MEM153-p287.
Snoke, A.W., McGrew, A.J., Valasek, P.A., and Smithson, S.B., 1990, A crustal cross-section for a terrain of superimposed shortening and extension: Ruby Mountains-East Humboldt Range metamorphic core complex, Nevada, *in* Salisbury, M.H., and Fountain, D.M., eds., Exposed Cross Sections of the Continental Crust: The Netherlands, Kluwer Academic Publishers, p. 103–135, https://doi.org/10.1007/978-94-009-0675-4_5.
Snoke, A.W., Howard, K.A., McGrew, A.J., Burton, B.R., Barnes, C.G., Peters, M.T., and Wright, J.E., 1997, The Grand Tour of the Ruby-East Humboldt Metamorphic Core complex, Northeastern Nevada, *in* Link, P.K., and Kowalis, B.J., eds., Proterozoic to Recent Stratigraphy, Tectonics, and Volcanology, Utah, Nevada, Southern Idaho, and Central Mexico: Brigham Young University Geology Studies, v. 42, Part I, p. 225–269.
Solomon, B.J., McKee, E.H., and Andersen, D.W., 1979, Stratigraphy and Depositional Environments of Paleogene Rocks Near Elko, Nevada, *in* Armentrout, J.M., Cole, M.R., and Ter Best, H., Jr., eds., Cenozoic Paleogeography of the Western United States: Society of Economic Paleontologists and Mineralogists: Pacific Section, Pacific Coast Paleogeography Symposium, v. 3, p. 75–88.
Sonder, L.J., and Jones, C.H., 1999, Western United States extension: How the west was widened: Annual Review of Earth and Planetary Sciences, v. 27, no. 1, p. 417–462, https://doi.org/10.1146/annurev.earth.27.1.417.
Spear, F.S., 1993, Metamorphic Phase Equilibria and Pressure-Temperature-Time Paths: Mineralogical Society of America Monograph 1, 799 p.
Speed, R.C., and Sleep, N.H., 1982, Antler orogeny and foreland basin: A model: Geological Society of America Bulletin, v. 93, no. 9, p. 815–828, https://doi.org/10.1130/0016-7606(1982)93<815:AOAFBA>2.0.CO;2.
Spencer, K.J., Hacker, B.R., Kylander-Clark, A.R.C., Andersen, T.B., Cottle, J.M., Stearns, M.A., Poletti, J.E., and Seward, G.G.E., 2013, Campaign-style titanite U-Pb dating by laser-ablation ICP: Implications for crustal flow, phase transformations and titanite closure: Chemical Geology, v. 341, p. 84–101, https://doi.org/10.1016/j.chemgeo.2012.11.012.
Steiger, R.H., and Jäger, E., 1977, Subcommission on geochronology: Convention on the use of decay constants in geo-and cosmochronology: Earth and Planetary Science Letters, v. 36, no. 3, p. 359–362, https://doi.org/10.1016/0012-821X(77)90060-7.
Stewart, J.A., 1978, Basin-range structure in western North America: A review, *in* Smith, R.B., and Eaton, G.P., eds., Cenozoic Tectonics and Regional Geophysics of the Western Cordillera: Geological Society of America Memoir 152, p. 1–13, https://doi.org/10.1130/MEM152-p1.
Stewart, J.H., 1971, Basin and Range structure—A system of horsts and grabens produced by deep-seated extension: Geological Society of America Bulletin, v. 82, p. 1019–1043, https://doi.org/10.1130/0016-7606(1971)82[1019:BARSAS]2.0.CO;2.
Stewart, J.H., 1972, Initial deposits in the Cordilleran geosyncline: Evidence of a Late Precambrian (<850 m.y.) continental separation: Geological Society of America Bulletin, v. 83, p. 1345–1360, https://doi.org/10.1130/0016-7606(1972)83[1345:IDITCG]2.0.CO;2.
Stewart, J.H., 1980, Geology of Nevada: A discussion to accompany the Geologic Map of Nevada: Nevada Bureau of Mines and Geology Special Publication 4, 136 p.
Stewart, J.H., and Poole, F.G., 1974, Lower Paleozoic and uppermost Precambrian Cordilleran miogeocline, Great Basin, western United States, *in* Dickinson, W.R., ed., Tectonics and Sedimentation: Society of Economic Paleontologists and Mineralogists (SEPM) Special Publication 22, p. 28–57, https://doi.org/10.2110/pec.74.22.0028.
Stipp, M., Stünitz, H., Heilbronner, R., and Schmid, S.M., 2002, Dynamic recrystallization of quartz: Correlation between natural and experimental conditions *in* De Meer, S., et al., eds., Deformation Mechanisms, Rheology and Tectonics: Current Status and Future Perspectives: Geological Society of London, Special Publication 200, p. 171–190, https://doi.org/10.1144/GSL.SP.2001.200.01.11.
Stock, J., and Molnar, P., 1988, Uncertainties and implications of the Late Cretaceous and Tertiary position of North America relative to the Farallon, Kula, and Pacific plates: Tectonics, v. 7, no. 6, p. 1339–1384, https://doi.org/10.1029/TC007i006p01339.
Swenson, R.F., 1991, Analysis of a fault-fold system in the southern Pequop Mountains, Elko County, Nevada (M.S. thesis): Laramie, University of Wyoming, 131 p.
Taylor, W.J., Bartley, J.M., Martin, M.W., Geissman, J.W., Walker, J.D., Armstrong, P.A., and Fryxell, J.E., 2000, Relations between hinterland and foreland shortening: Sevier orogeny, central North American Cordillera: Tectonics, v. 19, p. 1124–1143, https://doi.org/10.1029/1999TC001141.
Thorman, C.H., 1962, Structure and stratigraphy of the Wood Hills and a portion of the northern Pequop Mountains, Elko County, Nevada [Ph.D. dissertation]: Seattle, University of Washington, 218 p.
Thorman, C.H., 1970, Metamorphosed and nonmetamorphosed Paleozoic rocks in the Wood Hills and Pequop Mountains, northeast Nevada: Geological Society of America Bulletin, v. 81, no. 8, p. 2417–2448, https://doi.org/10.1130/0016-7606(1970)81[2417:MANPRI]2.0.CO;2.
Thorman, C.H., 2011a, Some musings regarding structural evolution of NE Nevada–NW Utah from Jurassic to Recent: Geological Society of America, Abstracts with Programs, v. 43, no. 4, p. 3.
Thorman, C.H., 2011b, The Elko orogeny—A major tectonic event in eastern Nevada-western Utah, *in* Sprinkel, D.A., Yonkee, W.A., and Chidsey, T.C., Jr., eds., Sevier Thrust Belt: Northern and Central Utah and Adjacent Areas: Utah Geological Association Publication 40, 13 p.
Thorman, C.H., and Peterson, F., 2003, The Middle Jurassic Elko Orogeny: A major tectonic event in Nevada-Utah: American Association of Petroleum Geologists Annual Meeting Expanded Abstracts, v. 12, p. 169–174.
Thorman, C.H., and Snee, L.W., 1988, Thermochronology of metamorphic rocks in the Wood Hills and Pequop Mountains, northeastern Nevada: Geological Society of America, Abstracts with Programs, v. 20, no. 7, p. A18.
Thorman, C.H., Ketner, K.B., and Peterson, F., 1990, The Elko orogeny—Late Jurassic orogenesis in the Cordilleran miogeocline: Geological Society of America, Abstracts with Programs, v. 22, no. 3, p. 88.
Thorman, C.H., Ketner, K.B., Brooks, W.E., Snee, L.W., and Zimmerman, R.A., 1991, Late Mesozoic-Cenozoic tectonics in northeastern Nevada, *in* Geology and Ore Deposits of the Great Basin: Symposium Proceedings: Reno, Nevada, Geological Society of Nevada, v. 1, p. 25–45.
Thorman, C.H., Ketner, K.B., and Peterson, F., 1992, The Middle to Late Jurassic Elko orogeny in eastern Nevada and western Utah: Geological Society of America, Abstracts with Programs, v. 24, no. 66.
Thorman, C.H., Sandberg, C.A., Henry, C.D., Zuza, A.V., and Ressel, M.W., 2019, Regional tectonics and conodont CAIs indicate normal burial depths, not Mesozoic thickening, in the Pequop Mountains, NE Nevada: Geological Society of America, Abstracts with Programs, v. 51, no. 4, https://doi.org/10.1130/abs/2019CD-329504.
Trexler, J.H., Jr., and Nitchman, S.P., 1990, Sequence stratigraphy and evolution of the Antler foreland basin, east-central Nevada: Geology, v. 18, no. 5, p. 422–425, https://doi.org/10.1130/0091-7613(1990)018<0422:SSAEOT>2.3.CO;2.
Villien, A., and Kligfield, R.M., 1986, Thrusting and synorogenic sedimentation in central Utah, *in* Peterson, J.A., ed., Paleotectonics and Sedimentation in the Rocky Mountain Region, United States: American Association of Petroleum Geologists Memoir 41, p. 281–308, https://doi.org/10.1306/M41456C13.
Wallace, A.R., Perkins, M.E., and Fleck, R.J., 2008, Late Cenozoic paleogeographic evolution of northeastern Nevada: Evidence from the sedimentary basins: Geosphere, v. 4, p. 36–74, https://doi.org/10.1130/GES00114.1.

Wang, C., Gao, R., Yin, A., Wang, H., Zhang, Y., Guo, T., Li, Q., and Li, Y., 2011, A mid-crustal strain-transfer model for continental deformation: A new perspective from high-resolution deep seismic-reflection profiling across NE Tibet: Earth and Planetary Science Letters, v. 306, no. 3–4, p. 279–288, https://doi.org/10.1016/j.epsl.2011.04.010.

Watkins, H., Butler, R.W., Bond, C.E., and Healy, D., 2015, Influence of structural position on fracture networks in the Torridon Group, Achnashellach fold and thrust belt, NW Scotland: Journal of Structural Geology, v. 74, p. 64–80, https://doi.org/10.1016/j.jsg.2015.03.001.

Wells, M.L., Hoisch, T.D., Cruz-Uribe, A.M., and Vervoort, J.D., 2012, Geodynamics of synconvergent extension and tectonic mode switching: Constraints from the Sevier-Laramide orogen: Tectonics, v. 31, no. 1, https://doi.org/10.1029/2011TC002913.

Wesnousky, S.G., and Willoughby, C.H., 2003, Neotectonic note: The Ruby–East Humboldt Range, northeastern Nevada: Bulletin of the Seismological Society of America, v. 93, no. 3, p. 1345–1354, https://doi.org/10.1785/0120020032.

Whitney, D.L., Teyssier, C., Rey, P., and Buck, W.R., 2013, Continental and oceanic core complexes: Geological Society of America Bulletin, v. 125, no. 3–4, p. 273–298, https://doi.org/10.1130/B30754.1.

Wills, M.A., 2014, A metamorphic pressure-temperature time path from the Wood Hills, Elko County, eastern Nevada [M.S. thesis]: Flagstaff, Arizona, Northern Arizona University, 81 p.

Wolfe, F.D., 2016, New constraints on the timing, rate, and style of exhumation of the Wood Hills and Pequop Mountains, Elko County, Nevada [B.S. thesis]: Lexington, Virginia, Washington and Lee University.

Wright, J.E., and Snoke, A.W., 1993, Tertiary magmatism and mylonitization in the Ruby-East Humboldt metamorphic core complex, northeastern Nevada: U-Pb geochronology and Sr, Nd, and Pb isotope geochemistry: Geological Society of America Bulletin, v. 105, no. 7, p. 935–952, https://doi.org/10.1130/0016-7606(1993)105<0935:TMAMIT>2.3.CO;2.

Wyld, S.J., 2000, Triassic evolution of the arc and backarc of northwest Nevada, and evidence for extensional tectonism, *in* Soreghan, M.J., and Gehrels, G.E., eds., Paleozoic and Triassic Paleogeography and Tectonics of Western Nevada and Northern California: Geological Society of America Special Paper 347, p. 185–207, https://doi.org/10.1130/0-8137-2347-7.185.

Wyld, S.J., 2002, Structural evolution of a Mesozoic backarc fold-and-thrust belt in the US Cordillera: New evidence from northern Nevada: Geological Society of America Bulletin, v. 114, no. 11, p. 1452–1468, https://doi.org/10.1130/0016-7606(2002)114<1452:SEOAMB>2.0.CO;2.

Wyld, S.J., and Wright, J.E., 2014, Jurassic back-arc magmatism in the eastern Great Basin: A product of slab-tear due to localized arc collision at the plate boundary: Geological Society of America, Abstracts with Programs, v. 46, no. 5, p. 19.

Wyld, S.J., and Wright, J.E., 2015, Effects of Jurassic slab break-off in the northern Great Basin; Geochemistry and geochronology of magmatism; structural and stratigraphic relations; and possible implications for younger gold mineralization, *in* Pennell, W.M., and Garside, L.J., eds., New Concepts and Discoveries, 2015 Symposium Volume: Reno/Sparks, Nevada, Geological Society of Nevada, p. a10.

Wyld, S.J., Rogers, J.W., and Wright, J.E., 2001, Structural evolution within the Luning-Fencemaker fold-thrust belt, Nevada: Progression from back-arc basin closure to intra-arc shortening: Journal of Structural Geology, v. 23, no .12, p. 1971–1995.

Wyld, S.J., Rogers, J.W., and Copeland, P., 2003, Metamorphic evolution of the Luning-Fencemaker fold-thrust belt, Nevada: Illite crystallinity, metamorphic petrology, and $^{40}Ar/^{39}Ar$ geochronology: The Journal of Geology, v. 111, no. 1, p. 17–38, https://doi.org/10.1086/344663.

Yin, A., 2010, Cenozoic tectonic evolution of Asia: A preliminary synthesis: Tectonophysics, v. 488, no. 1–4, p. 293–325, https://doi.org/10.1016/j.tecto.2009.06.002.

Yonkee, A., 2005, Strain patterns within part of the Willard thrust sheet, Idaho-Utah-Wyoming thrust belt: Journal of Structural Geology, v. 27, no. 7, p. 1315–1343, https://doi.org/10.1016/j.jsg.2004.06.014.

Yonkee, W.A., and Weil, A.B., 2015, Tectonic evolution of the Sevier and Laramide belts within the North American Cordillera orogenic system: Earth-Science Reviews, v. 150, p. 531–593, https://doi.org/10.1016/j.earscirev.2015.08.001.

Yonkee, W.A., Eleogram, B., Wells, M.L.D., Stockli, D.F., Kelley, S., and Barber, D.E., 2019, Fault slip and exhumation history of the Willard thrust sheet, Sevier fold-thrust belt, Utah: Relations to wedge propagation, hinterland uplift, and foreland basin sedimentation: Tectonics, v. 38, https://doi.org/10.1029/2018TC005444.

Zimmerer, M.J., Lafferty, J., and Coble, M.A., 2016, The eruptive and magmatic history of the youngest pulse of volcanism at the Valles caldera: Implications for successfully dating late Quaternary eruptions: Journal of Volcanology and Geothermal Research, v. 310, p. 50–57, https://doi.org/10.1016/j.jvolgeores.2015.11.021.

Zuza, A.V., Cheng, X., and Yin, A., 2016, Testing models of Tibetan Plateau formation with Cenozoic shortening estimates across the Qilian Shan–Nan Shan thrust belt: Geosphere, v. 12, no. 2, p. 501–532, https://doi.org/10.1130/GES01254.1.

Zuza, A.V., Henry, C.D., Ressel, M.W., Thorman, C.H., Dee, S., and Blackmon, J.E., 2018, Preliminary geologic map of the Independence Valley NE quadrangle, Elko County, Nevada: Nevada Bureau of Mines and Geology Open-File Report 18-4, scale 1:24,000, 12 p.

Zuza, A.V., Dee, S., Henry, C.D., Ressel, M.W., and Thorman, C.H., 2019a, Preliminary geologic map of the Independence Valley NW quadrangle, Elko County, Nevada: Nevada Bureau of Mines and Geology Open-File Report 19-3, scale 1:24,000, 18 p.

Zuza, A.V., Wu, C., Wang, Z., Levy, D.A., Li, B., Xiong, X., and Chen, X., 2019b, Underthrusting and duplexing beneath the northern Tibetan Plateau and the evolution of the Himalayan-Tibetan orogen: Lithosphere, v. 11, no. 2, p. 209–231, https://doi.org/10.1130/L1042.1.

Zuza, A.V., Thorman, C.H., Henry, C.D., Levy, D.A., Dee, S., Long, S.P., Sandberg, C.A., and Soignard, E., 2020a, Pulsed Mesozoic deformation in the Cordilleran hinterland and evolution of the Nevadaplano: Insights from the Pequop Mountains, NE Nevada: Lithosphere, v. 2020, https://doi.org/10.2113/2020/8850336.

Zuza, A.V., Dee, D., and Laabs, B., 2020b, Geologic map of the north half of the Tent Mountain quadrangle, Elko County, Nevada: Nevada Bureau of Mines and Geology Open-File Report 20-03, scale 1:24,000, 16 p.